US 20130333814A1

(19) **United States**

(12) **Patent Application Publication**

FLEURY et al.

(10) **Pub. No.: US 2013/0333814 A1**

(43) **Pub. Date: Dec. 19, 2013**

(54) **TITANIUM-BASED BULK AMORPHOUS MATRIX COMPOSITE AND METHOD OF FABRICATING THEREOF**

(76) Inventors: **Eric FLEURY**, Seoul (KR); **Jin-Yoo SUH**, Seoul (KR); **Yu-Chan KIM**, Seoul (KR); **Mukta Rani DEBNATH**, Seoul (KR); **Min-Hyun KIM**, Seoul (KR); **Tristan GEILLER**, Seoul (KR)

(21) Appl. No.: **13/526,975**

(22) Filed: **Jun. 19, 2012**

(30) **Foreign Application Priority Data**

Jun. 19, 2012 (KR) 10-2012-0065705

Publication Classification

(51) **Int. Cl.**

C22C 45/10	(2006.01)
C22F 1/18	(2006.01)
B22D 18/06	(2006.01)

(52) **U.S. Cl.**

USPC **148/561**; 148/403; 164/61

(57) **ABSTRACT**

A Ti-based bulk amorphous matrix composite including a composition represented by Formula 1, in at %:

$$Ti_aZr_bBe_cCu_dNi_eM_fI_g \quad \text{Formula 1}$$

where M is at least one of Nb and Ta, I is an impurity, and a, b, c, d, e, and f vary within the ranges $38 \le a \le 50$, $11 \le b \le 18$, $12 \le c \le 20$, $6 \le d \le 10$, $6 \le e \le 9$, $1 \le f \le 20$ and $0.01 \le g \le 0.5$, with $a+b+c+d+e+f+g=100$.

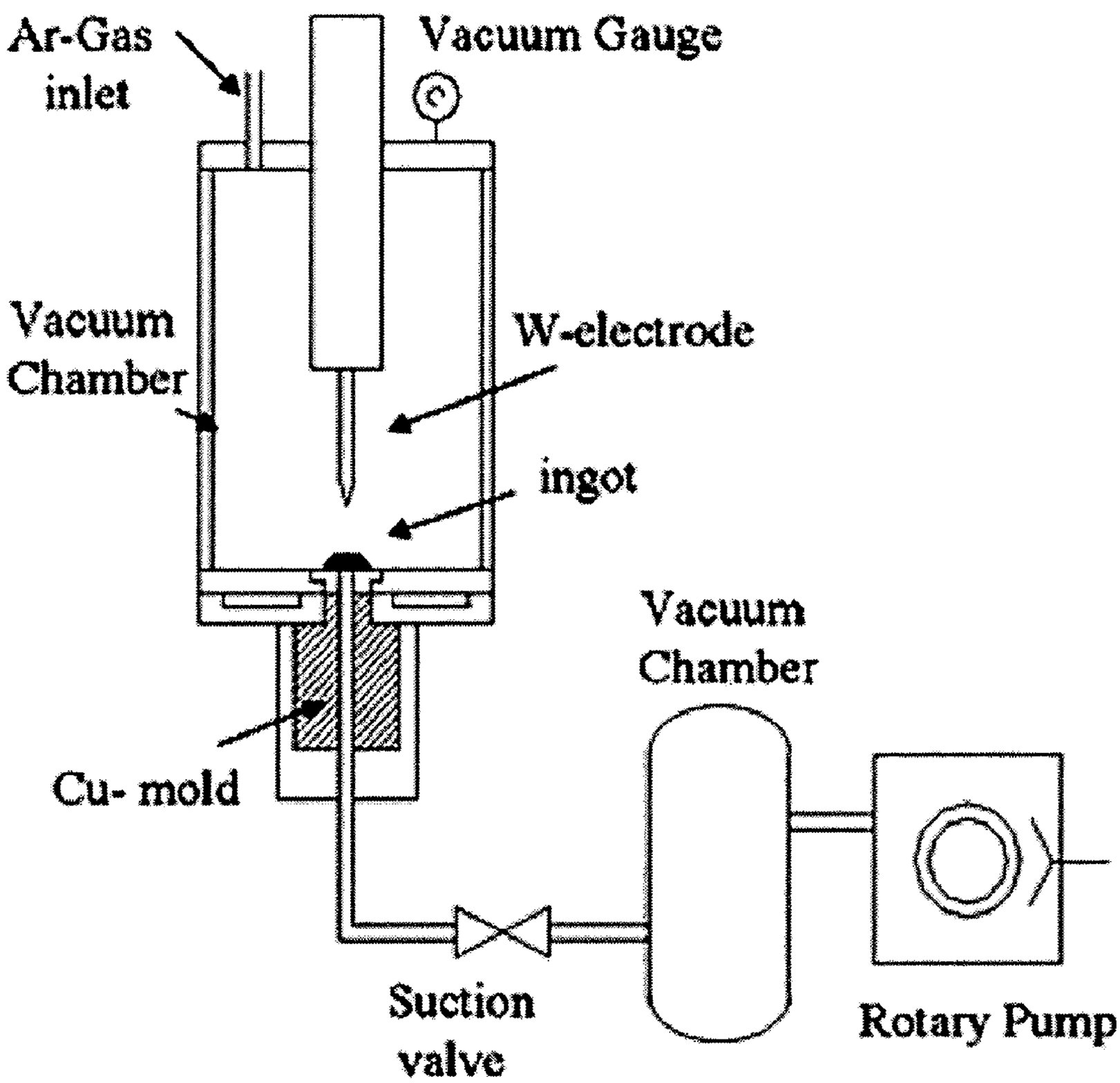

FIG. 1A

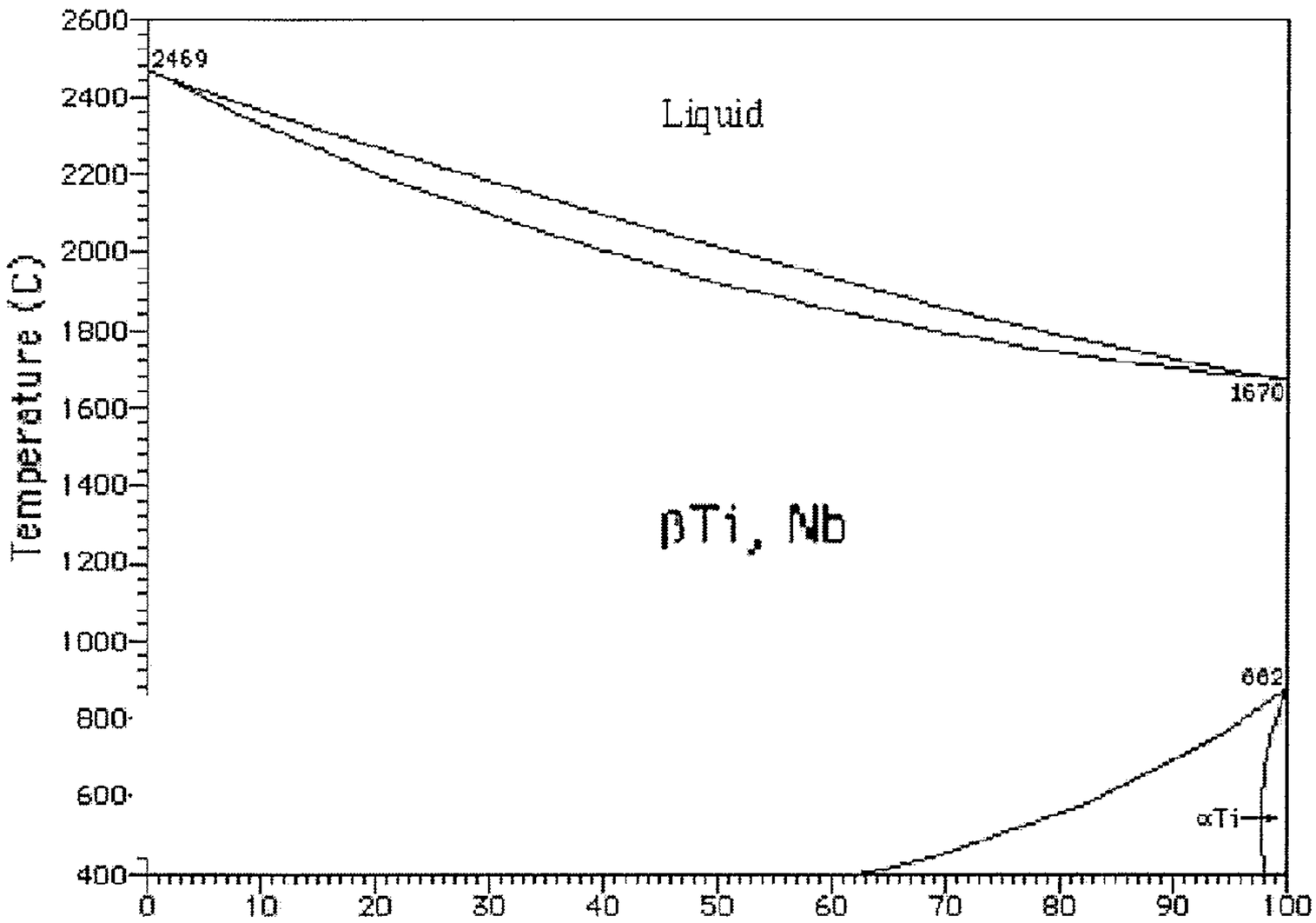
2600
2400
2200
2000
1800
1600
1400
1200
1000
800
600
400
Temperature (C)
2469
Liquid
1670
βTi, Nb
662
αTi
0
10
20
30
40
50
60
70
80
90
100
Nb
Atomic Percent Ti
Ti

FIG. 1B

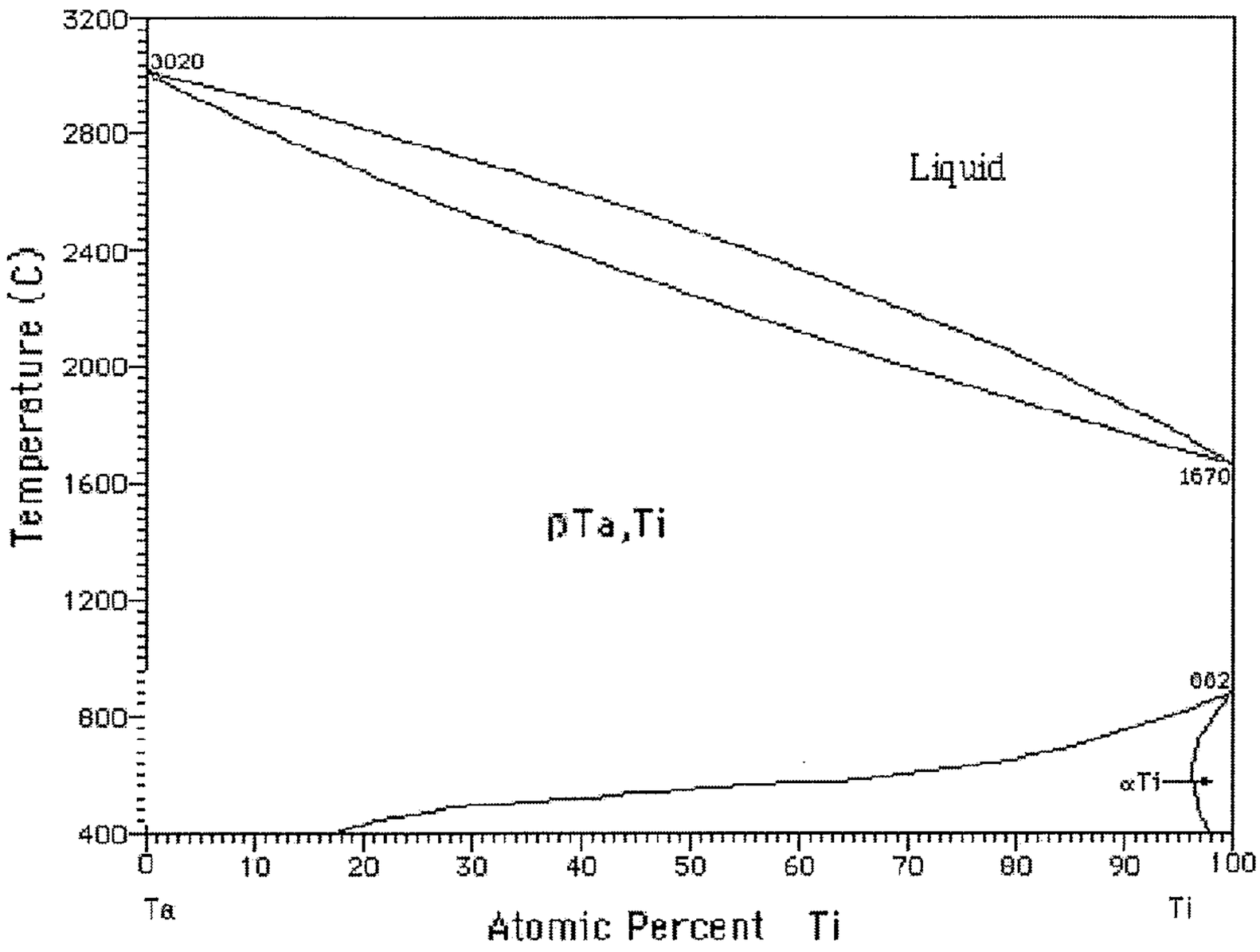
3200
2800
2400
2000
1600
1200
800
400
Temperature (C)
3020
Liquid
1670
βTa,Ti
882
αTi
0
10
20
30
40
50
60
70
80
90
100
Ta
Atomic Percent Ti
Ti

FIG. 1C

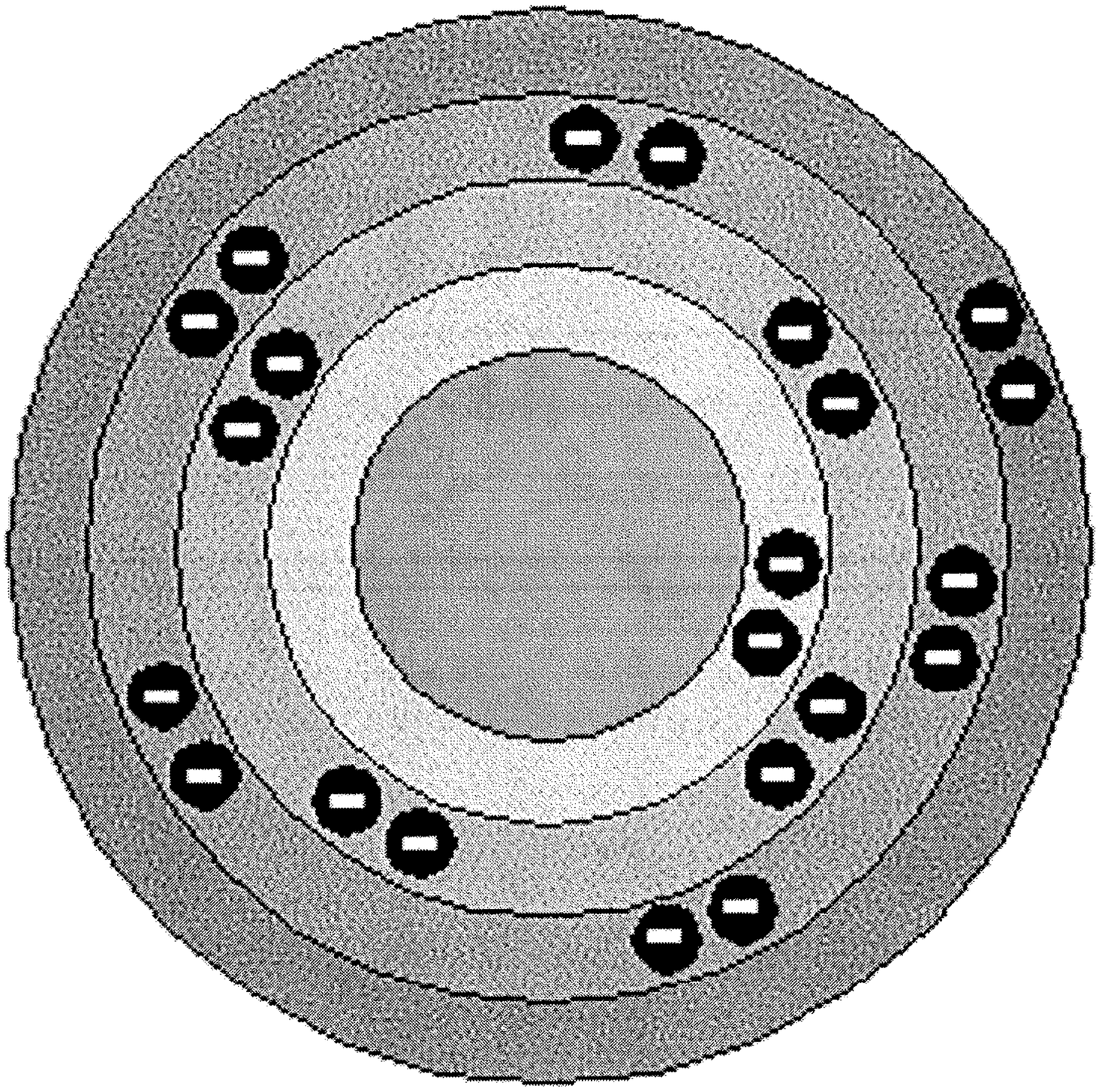

FIG. 1D

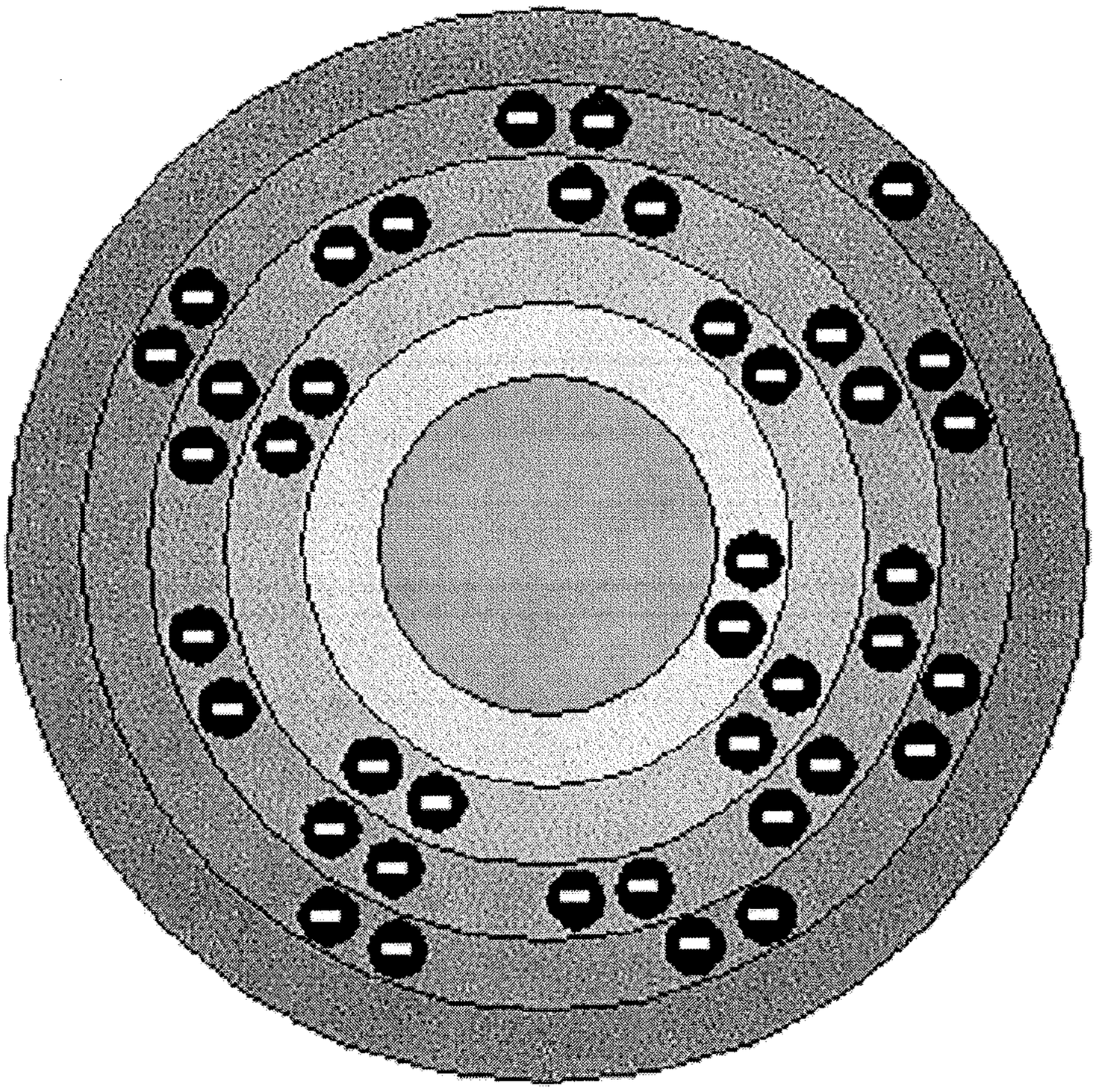

FIG. 1E

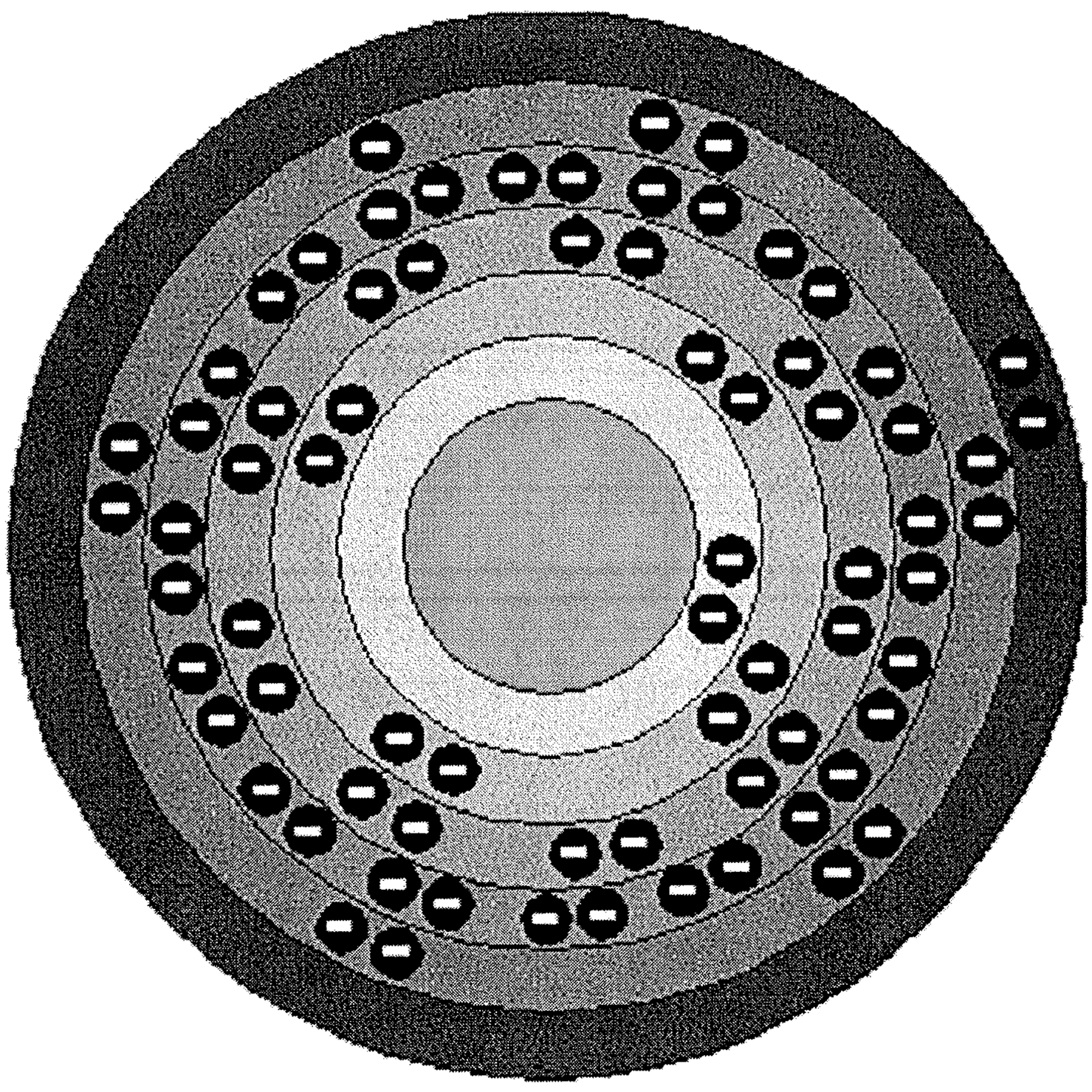

FIG. 1F

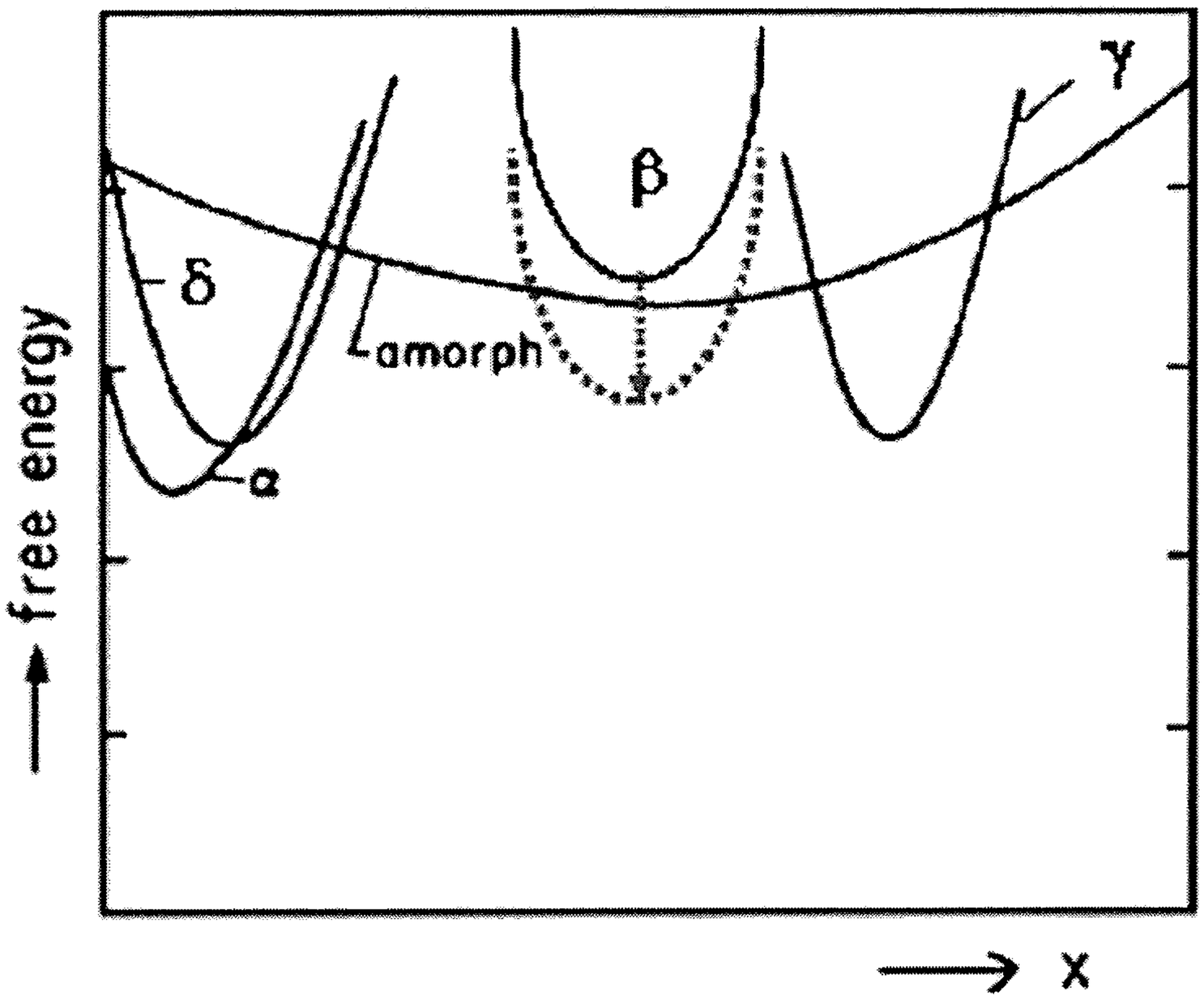

FIG. 2A

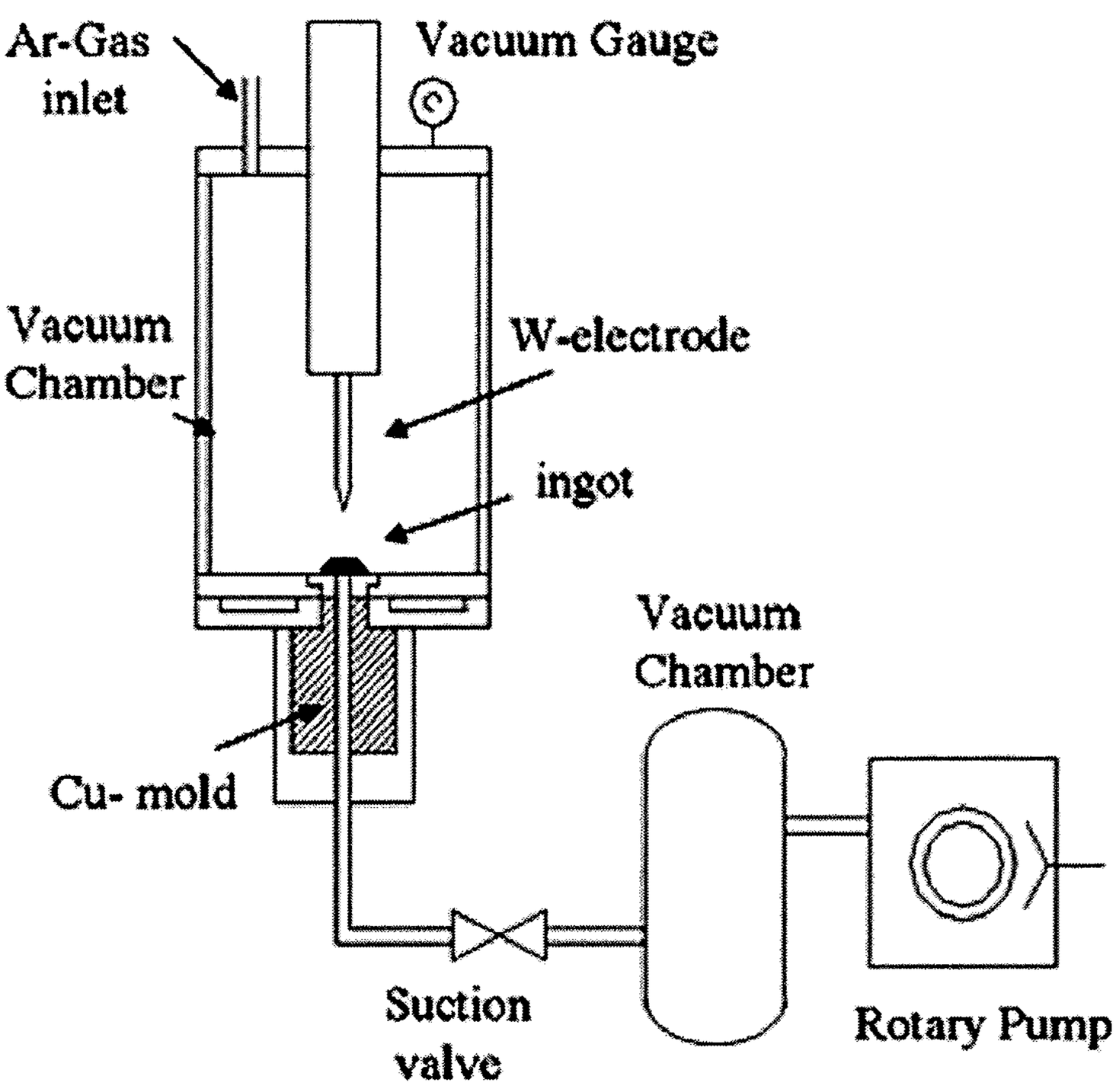
Ar-Gas inlet
Vacuum Gauge
Vacuum Chamber
W-electrode
ingot
Cu- mold
Vacuum Chamber
Suction valve
Rotary Pump

FIG. 2B

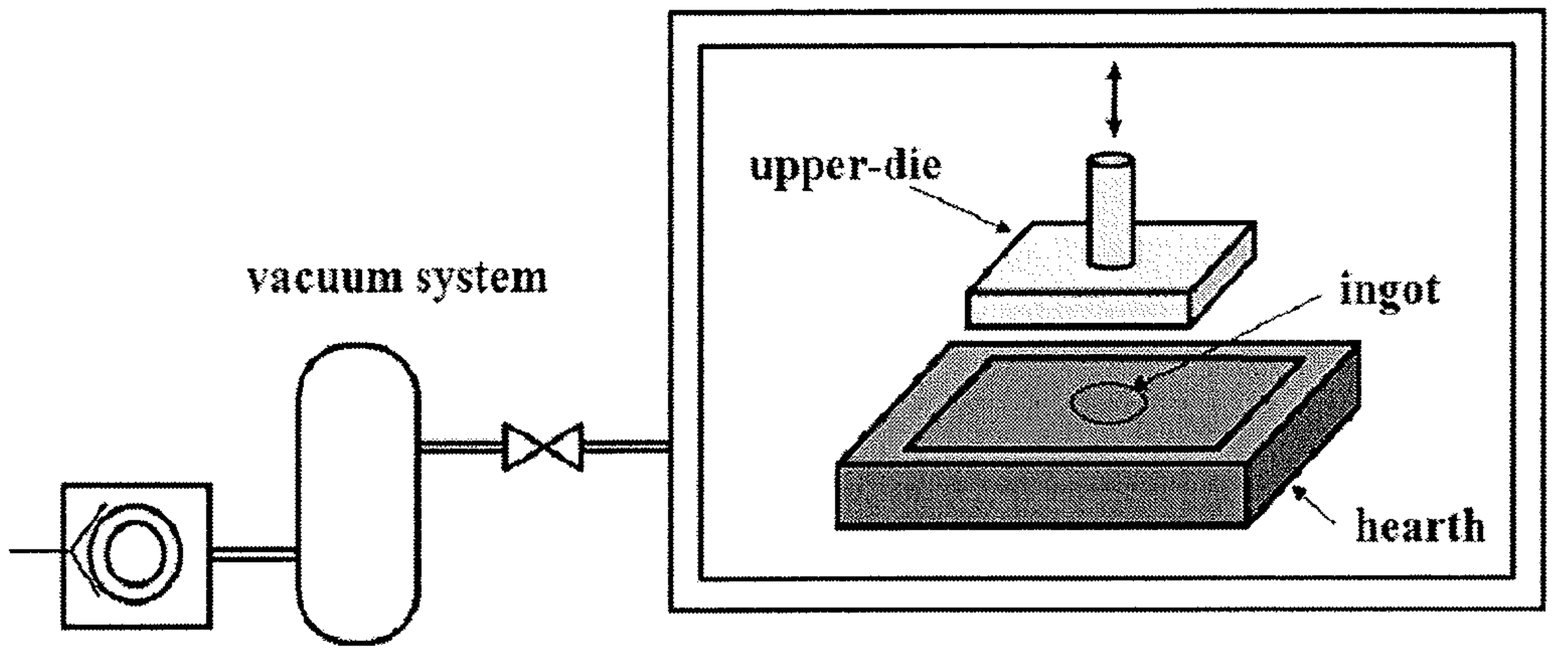

FIG. 3A

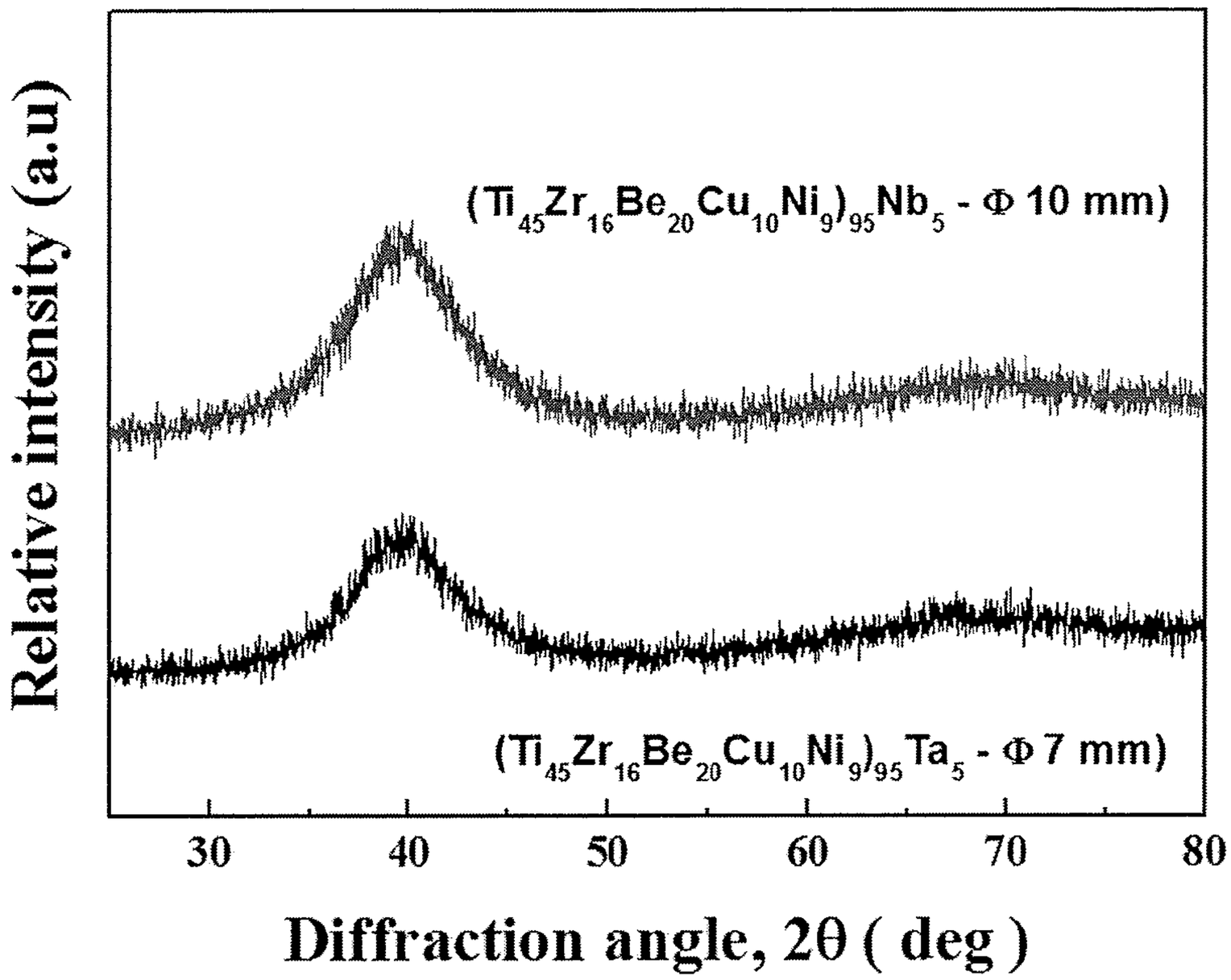
Relative intensity (a.u)
(Ti45Zr16Be20Cu10Ni9)95Nb5 - Φ 10 mm)
(Ti45Zr16Be20Cu10Ni9)95Ta5 - Φ 7 mm)
30
40
50
60
70
80
Diffraction angle, 2θ (deg)

FIG. 3B

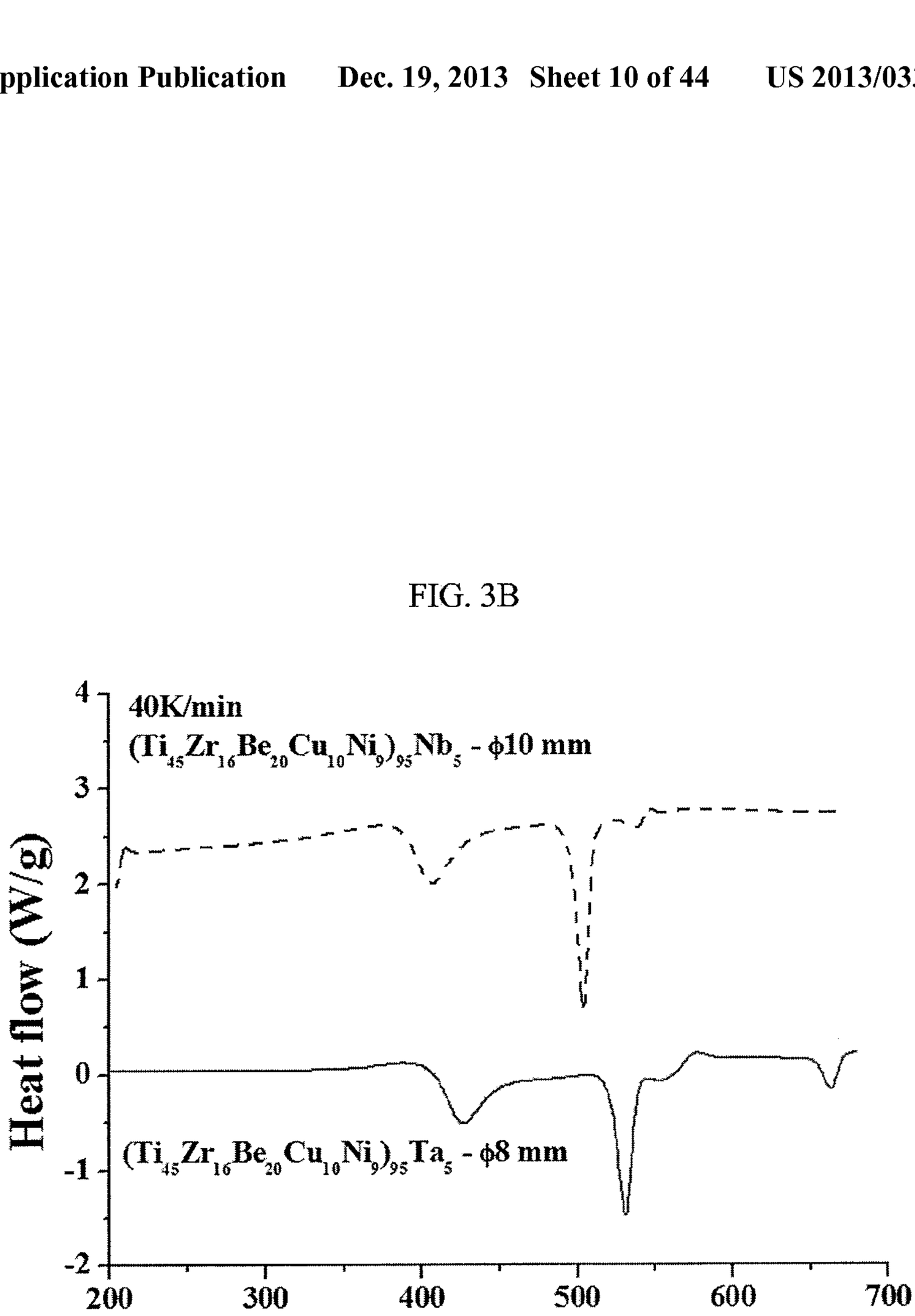
40K/min
(Ti45Zr16Be20Cu10Ni9)95Nb5 - ϕ10 mm
(Ti45Zr16Be20Cu10Ni9)95Ta5 - ϕ8 mm
Heat flow (W/g)
4
3
2
1
0
-1
-2
200
300
400
500
600
700
Temperature (C)

FIG. 3C

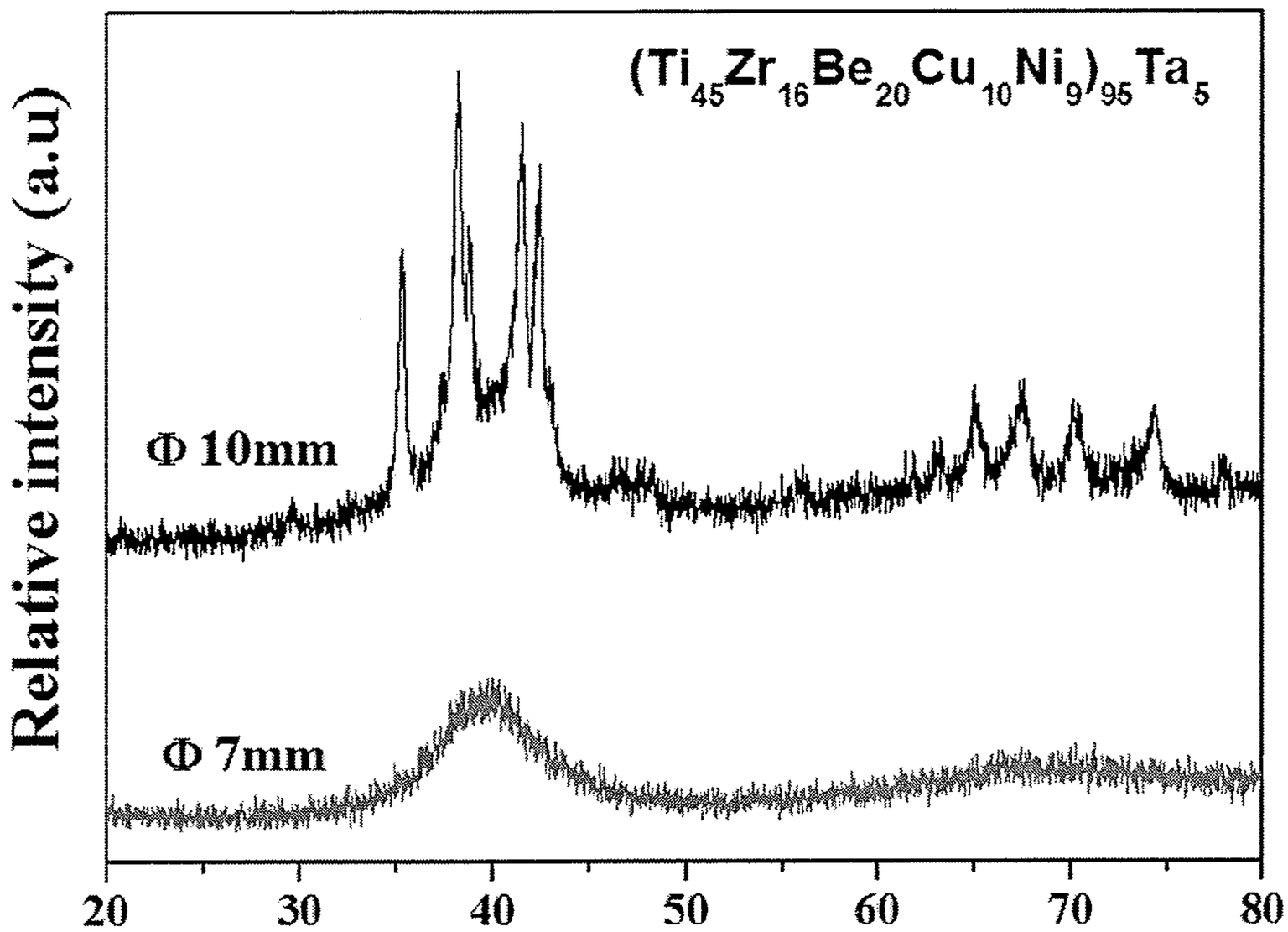
$(Ti_{45}Zr_{16}Be_{20}Cu_{10}Ni_9)_{95}Ta_5$
Φ 10mm
Φ 7mm
Relative intensity (a.u)
20
30
40
50
60
70
80
Diffraction angle, 2θ (deg)

FIG. 3D

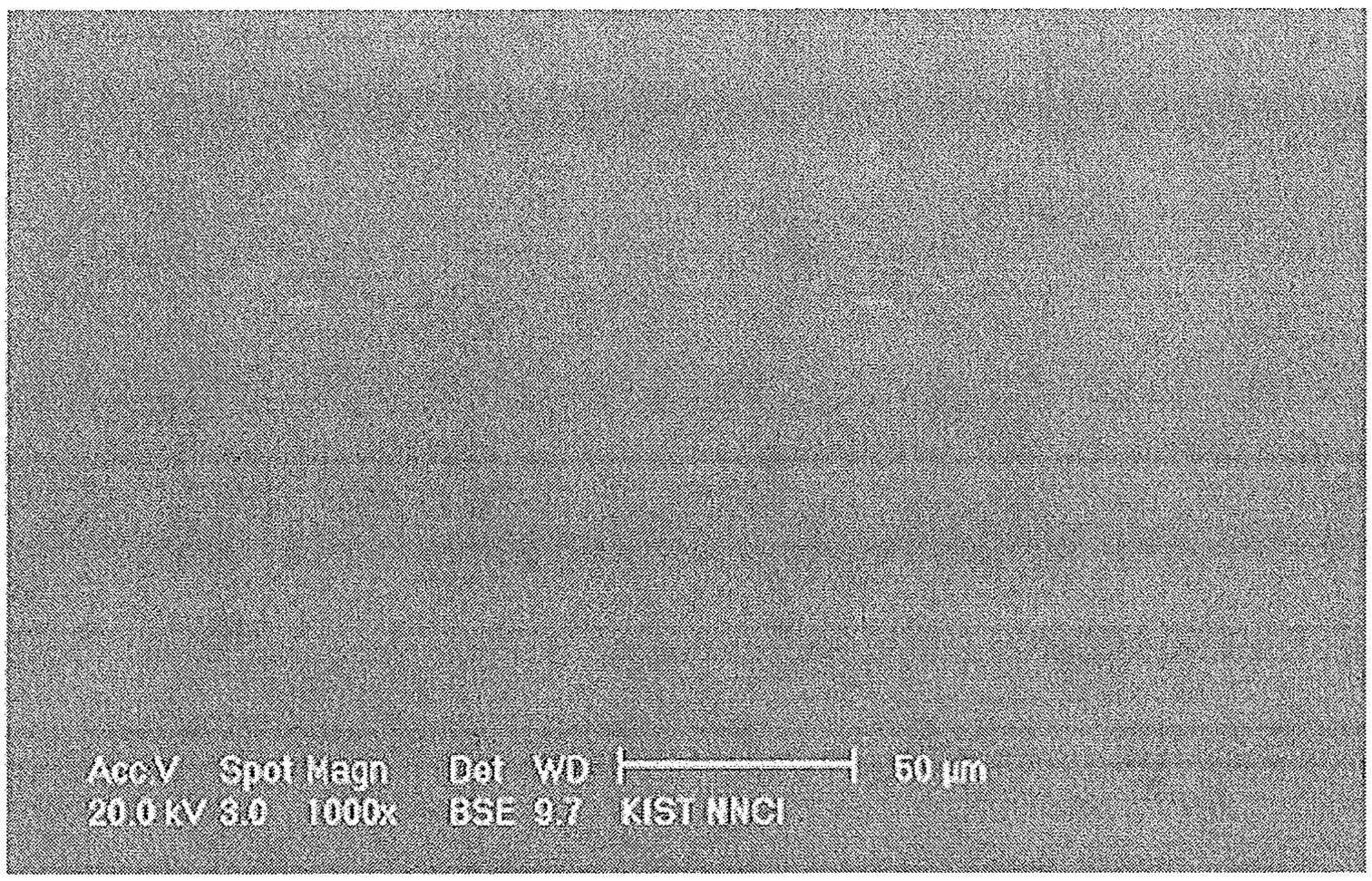

FIG. 3E

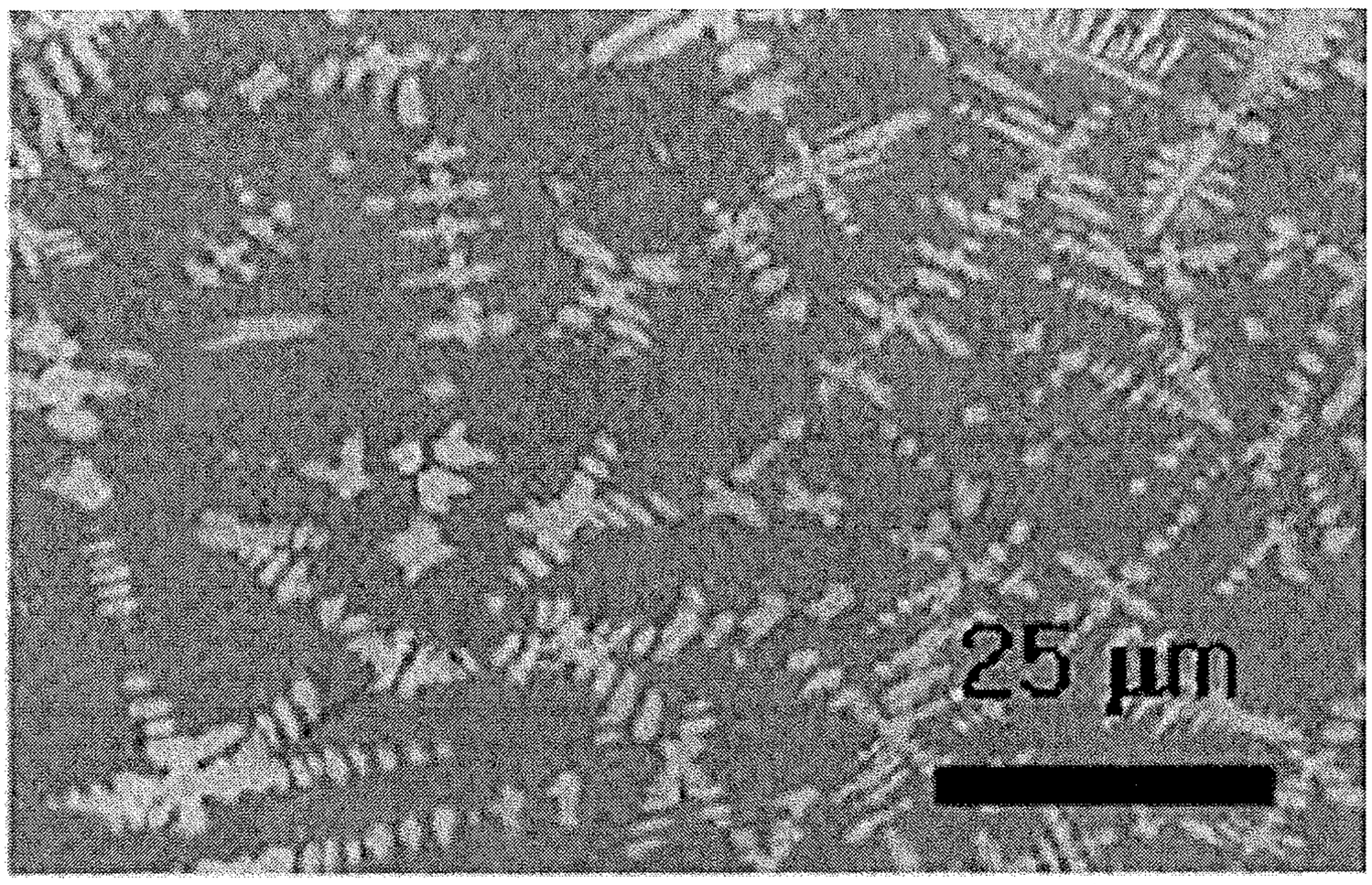

FIG. 4A

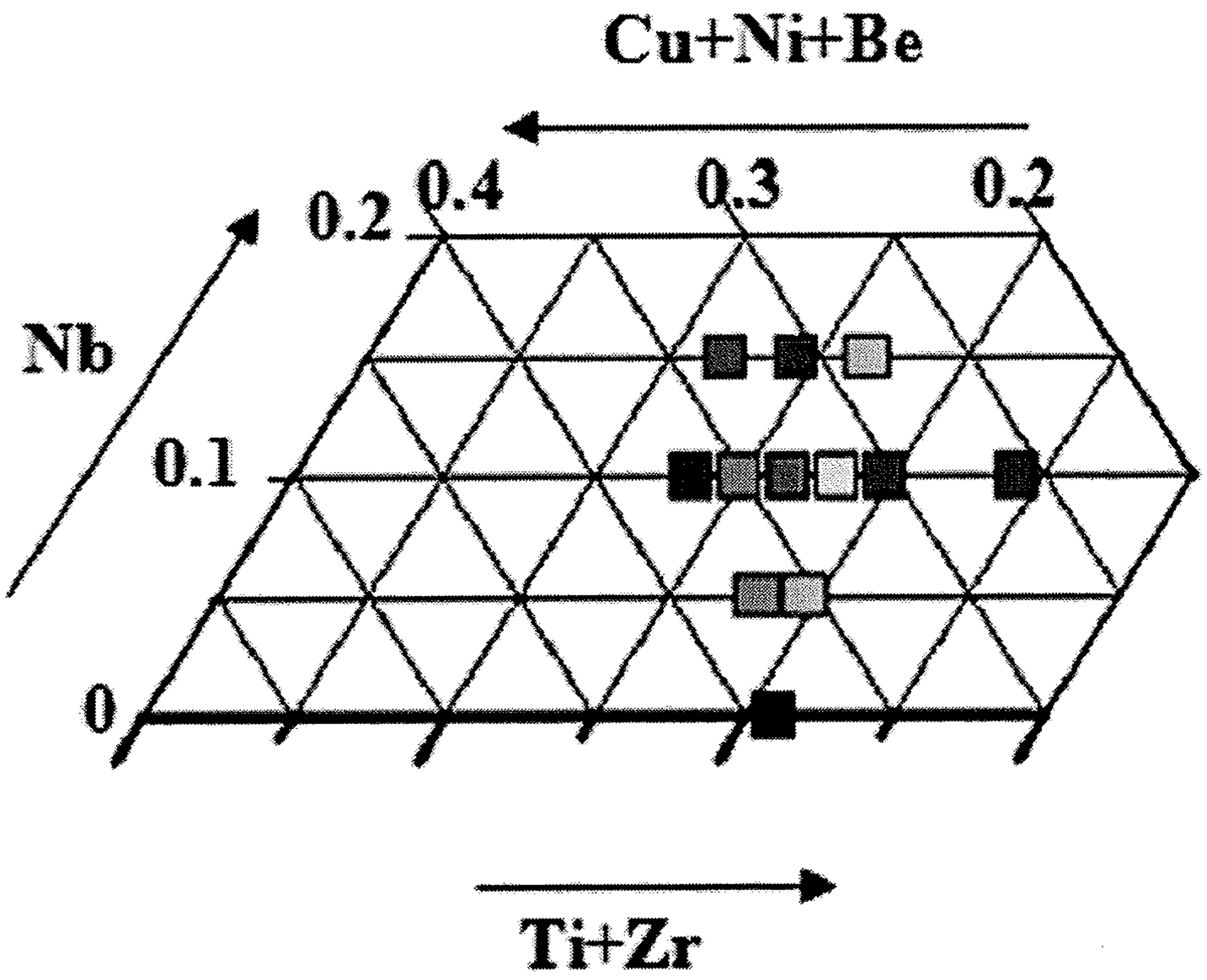

FIG. 4B

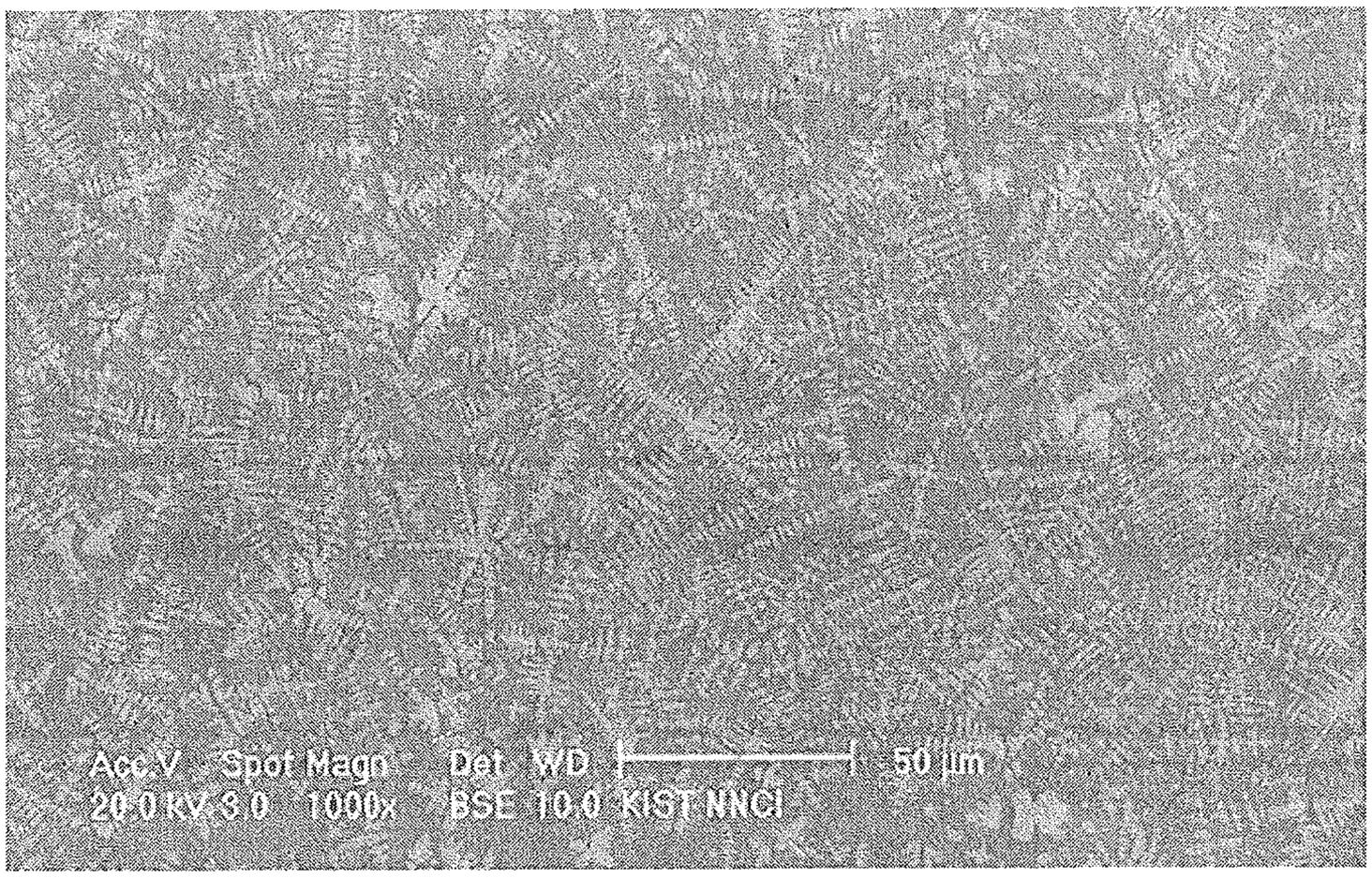

FIG. 4C

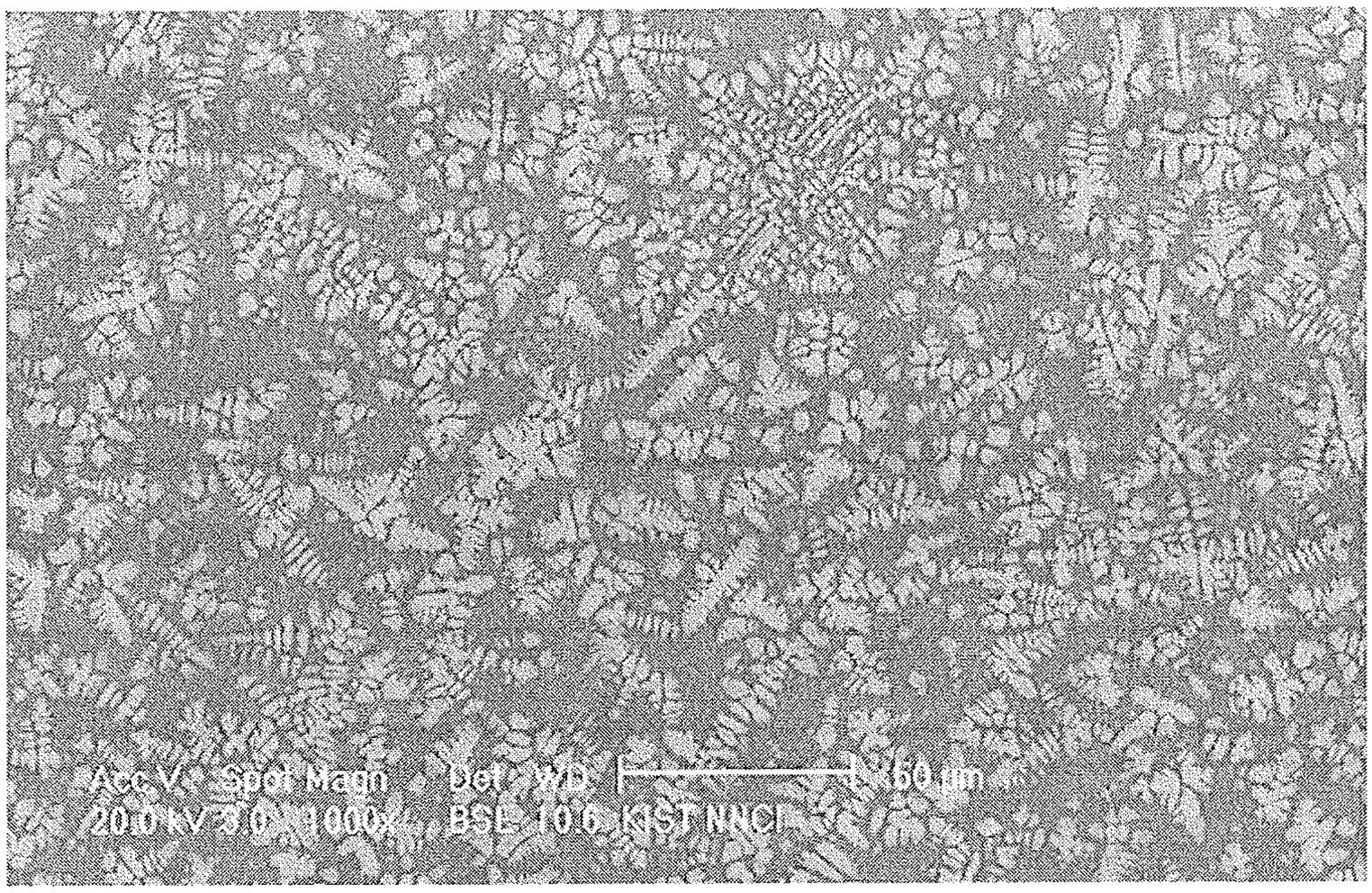

FIG. 4D

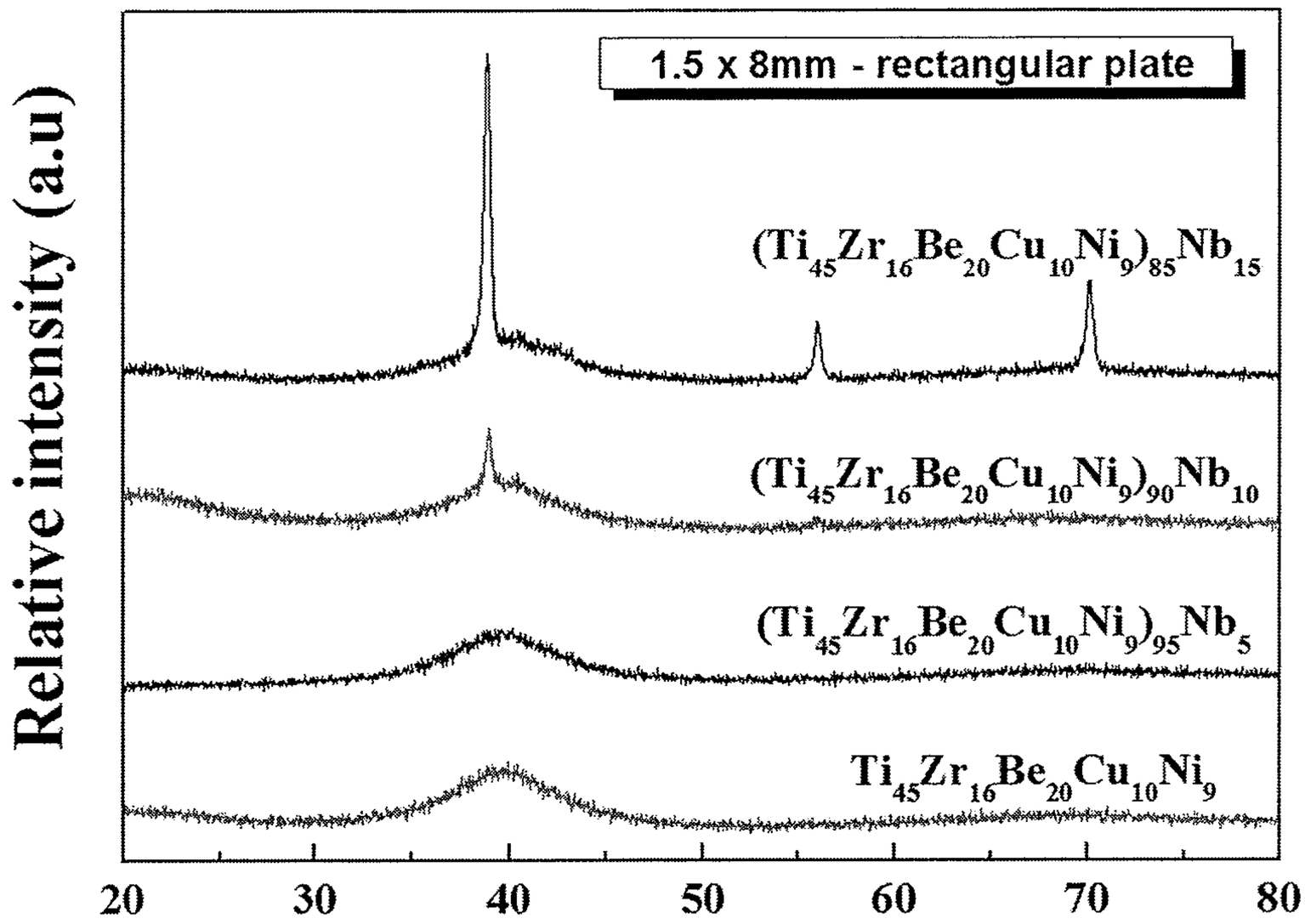
1.5 x 8mm - rectangular plate
(Ti45Zr16Be20Cu10Ni9)85Nb15
(Ti45Zr16Be20Cu10Ni9)90Nb10
(Ti45Zr16Be20Cu10Ni9)95Nb5
Ti45Zr16Be20Cu10Ni9
Relative intensity (a.u)
20
30
40
50
60
70
80
Diffraction angle, 2θ (deg)

FIG. 4E

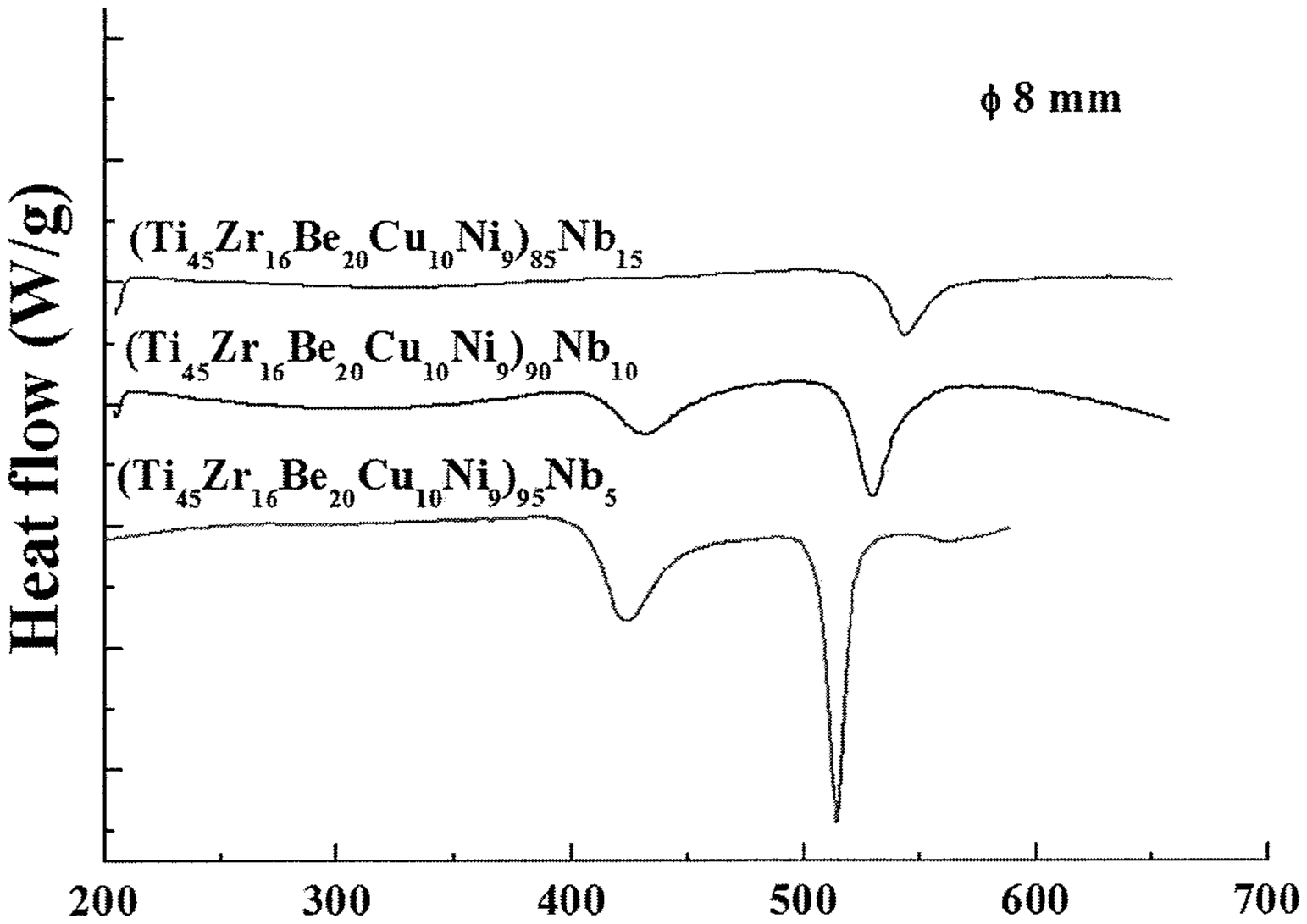
ϕ 8 mm
$(Ti_{45}Zr_{16}Be_{20}Cu_{10}Ni_9)_{85}Nb_{15}$
$(Ti_{45}Zr_{16}Be_{20}Cu_{10}Ni_9)_{90}Nb_{10}$
$(Ti_{45}Zr_{16}Be_{20}Cu_{10}Ni_9)_{95}Nb_5$
Heat flow (W/g)
200
300
400
500
600
700
Temperature (°C)

FIG. 4F

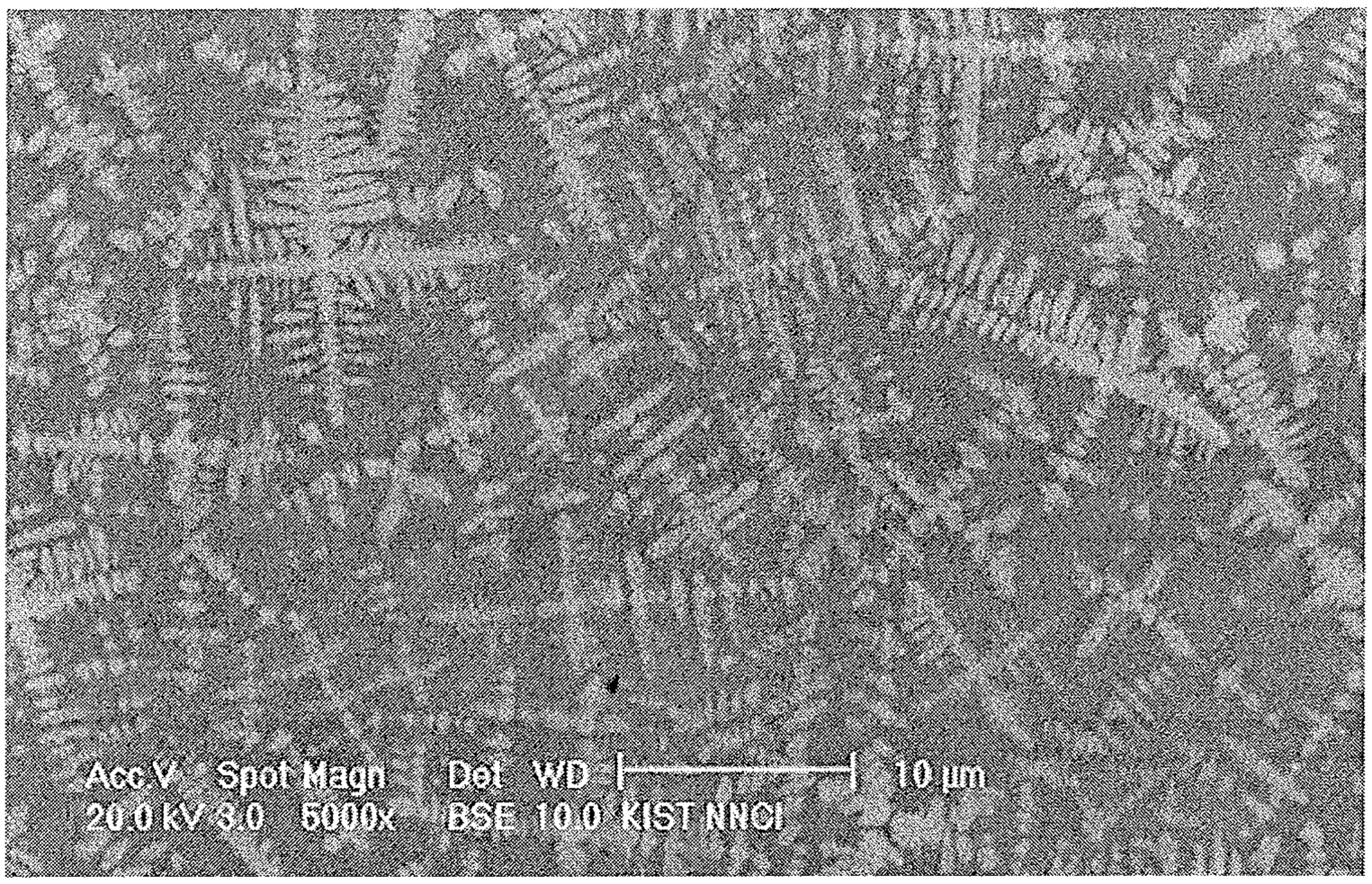

FIG. 4G

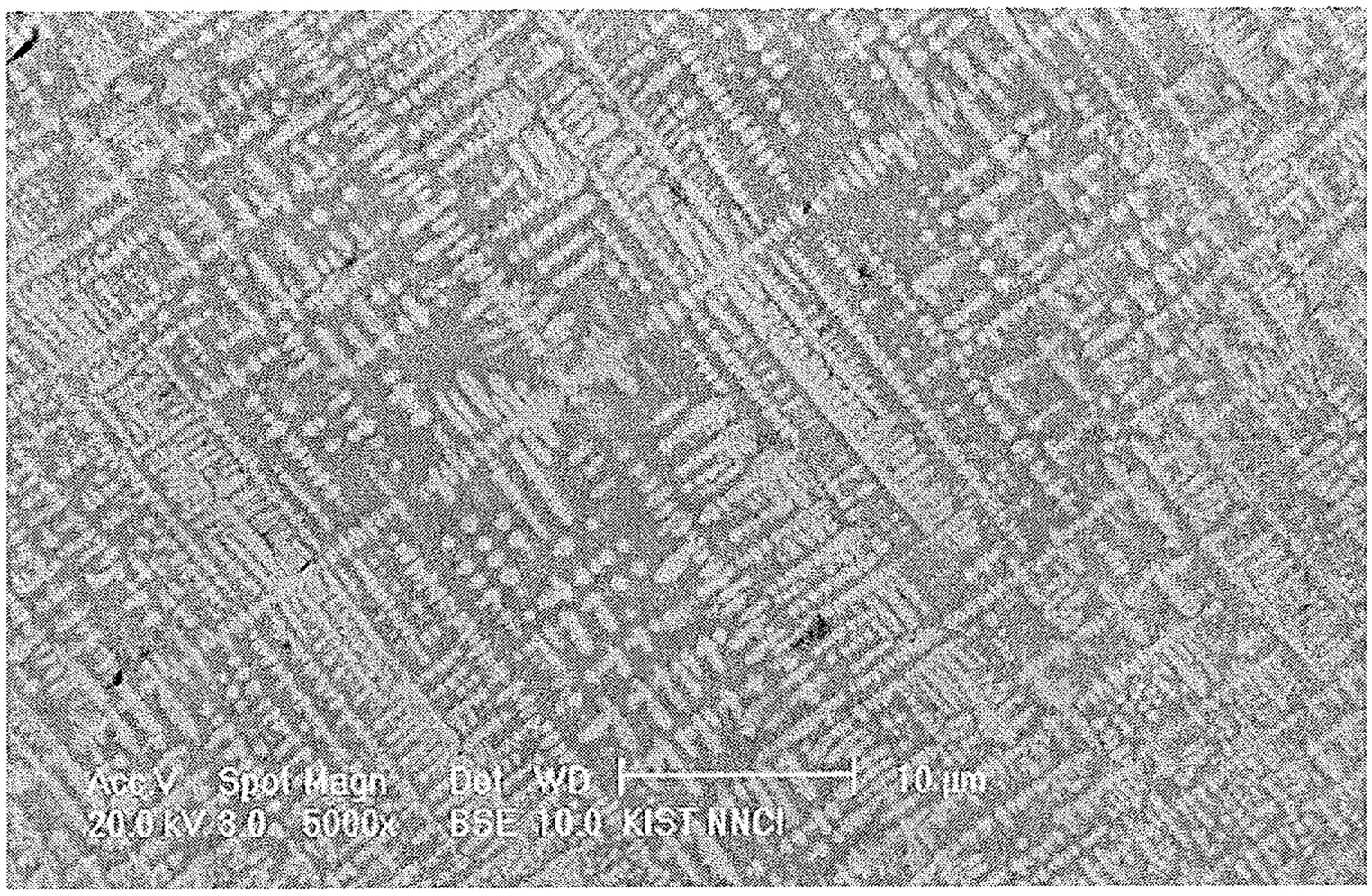

FIG. 5A

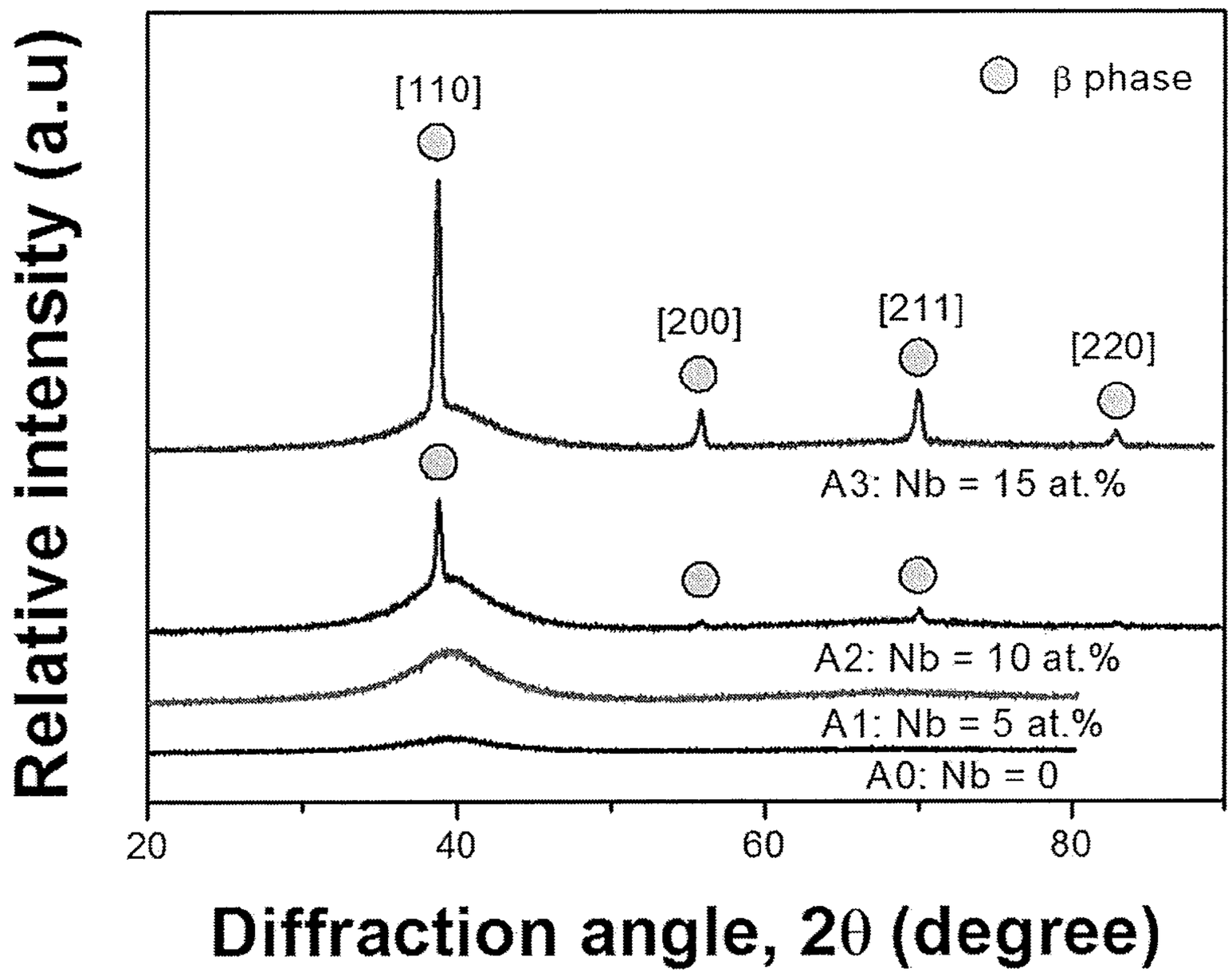
Relative intensity (a.u)
β phase
[110]
[200]
[211]
[220]
A3: Nb = 15 at.%
A2: Nb = 10 at.%
A1: Nb = 5 at.%
A0: Nb = 0
20
40
60
80
Diffraction angle, 2θ (degree)

FIG. 5B

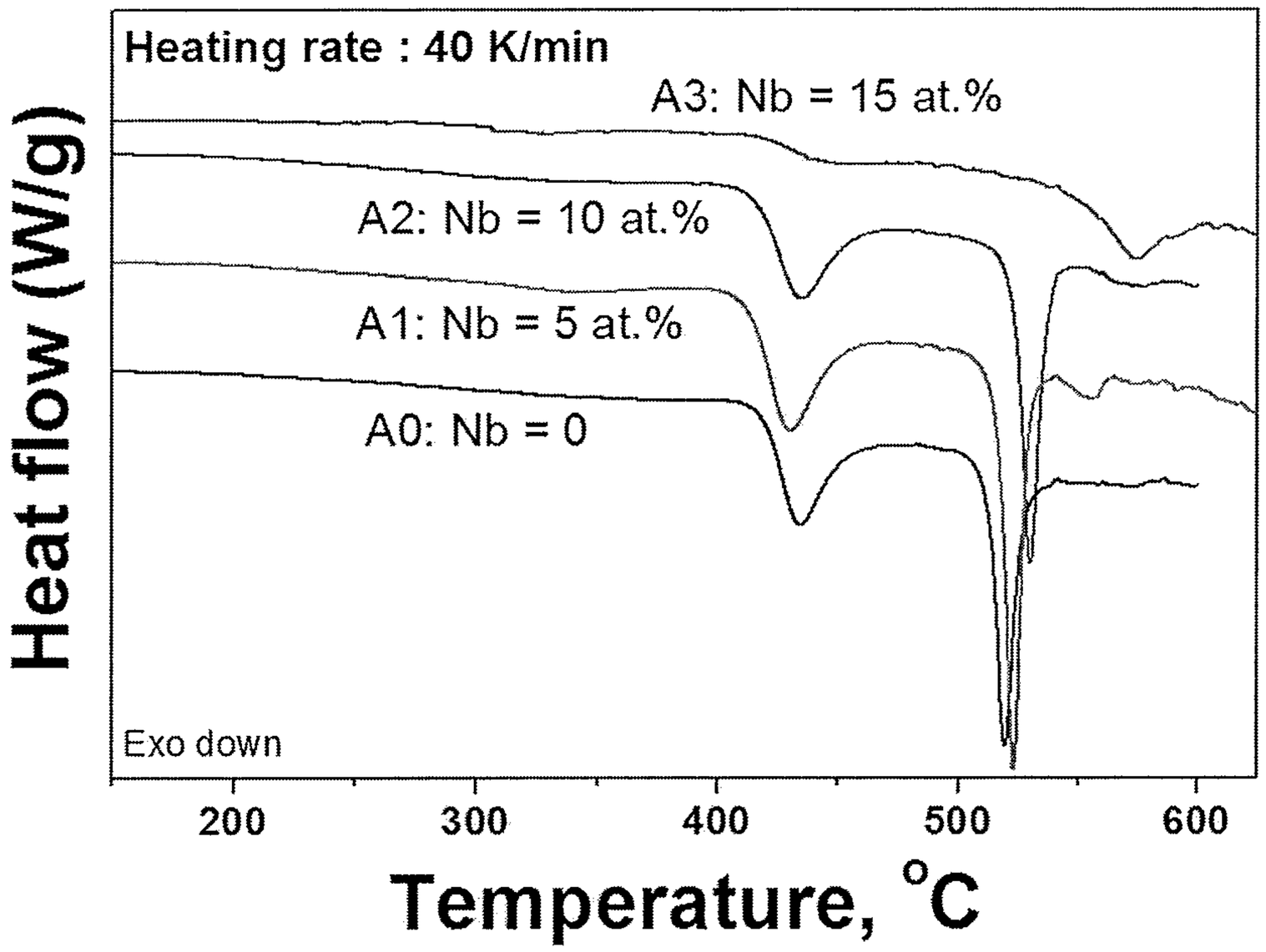
Heating rate : 40 K/min
A3: Nb = 15 at.%
A2: Nb = 10 at.%
A1: Nb = 5 at.%
A0: Nb = 0
Exo down
Heat flow (W/g)
200
300
400
500
600
Temperature, °C

FIG. 5C

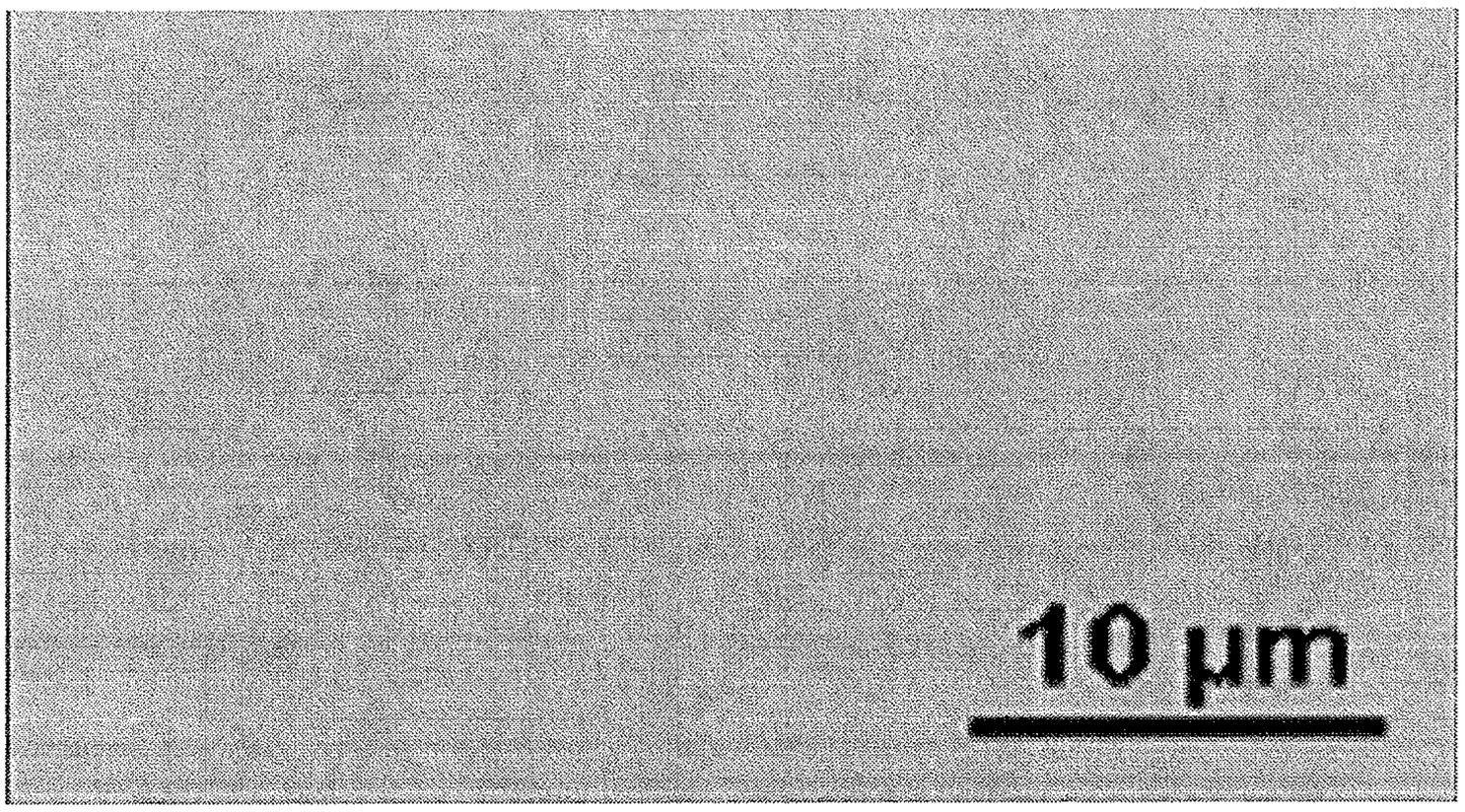

FIG. 5D

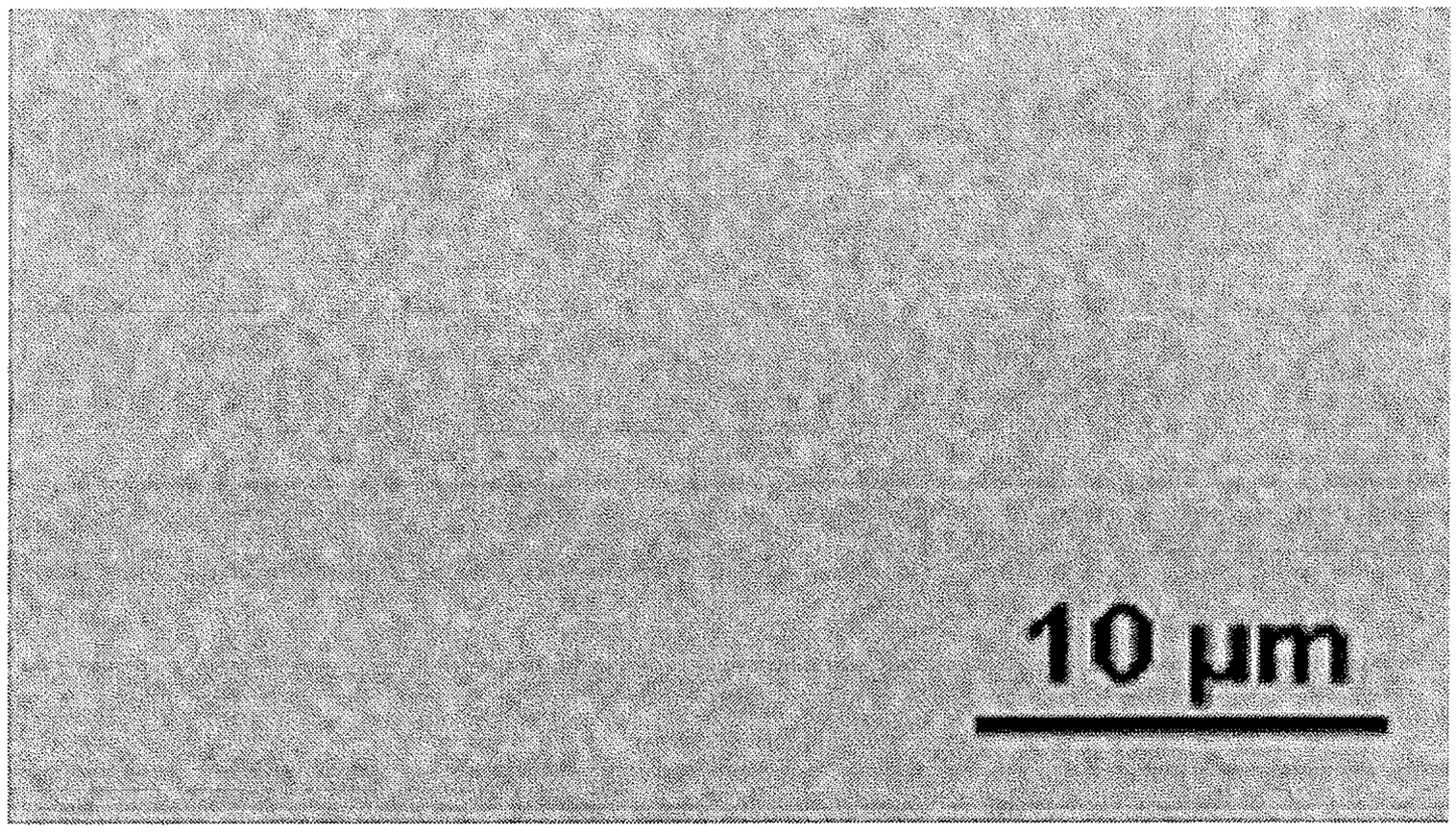

FIG. 5E

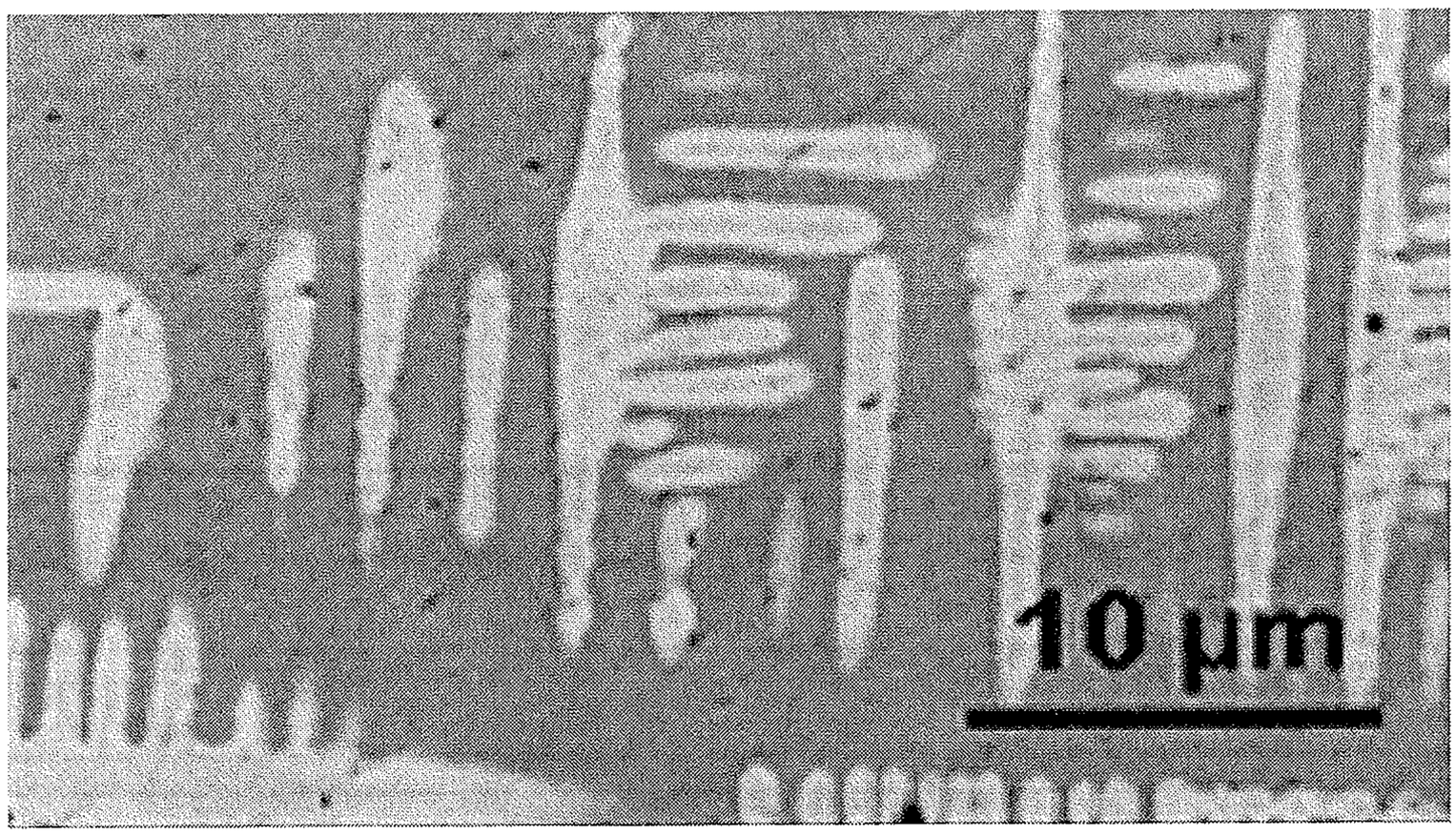

FIG. 5F

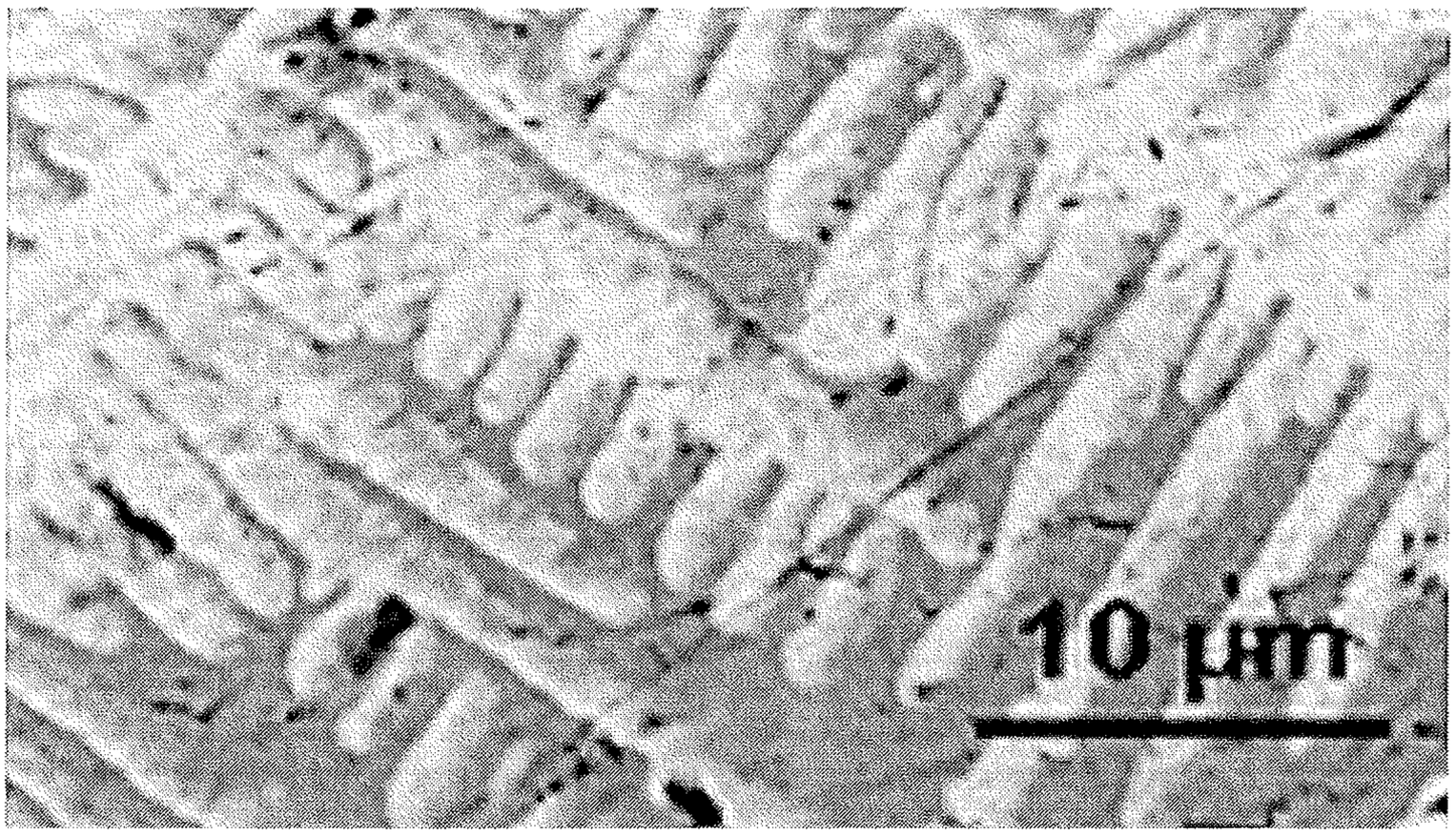

FIG. 6A

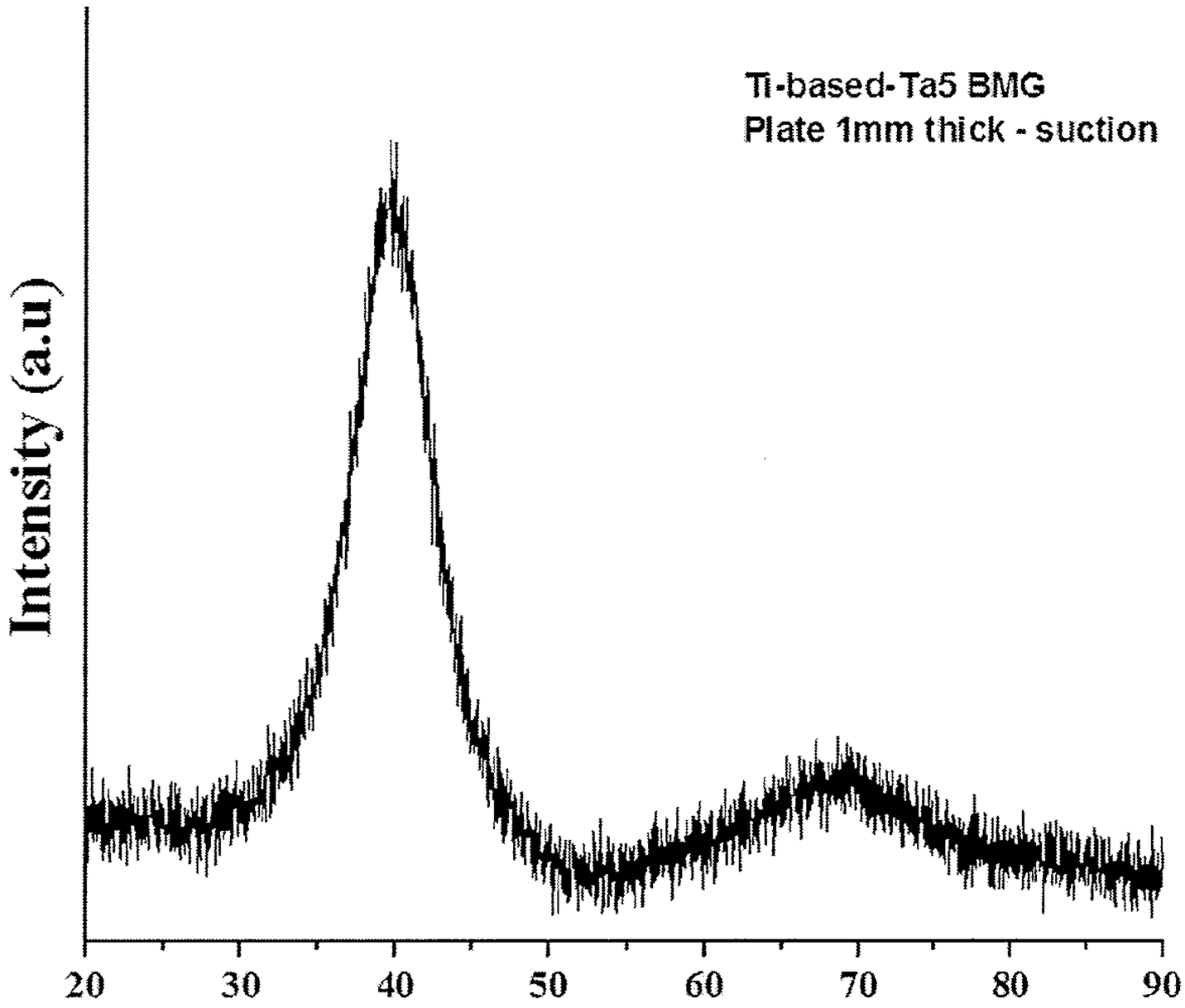
Ti-based-Ta5 BMG
Plate 1mm thick - suction
Intensity (a.u)
20
30
40
50
60
70
80
90
Diffraction angle, 2θ (degree)

FIG. 6B

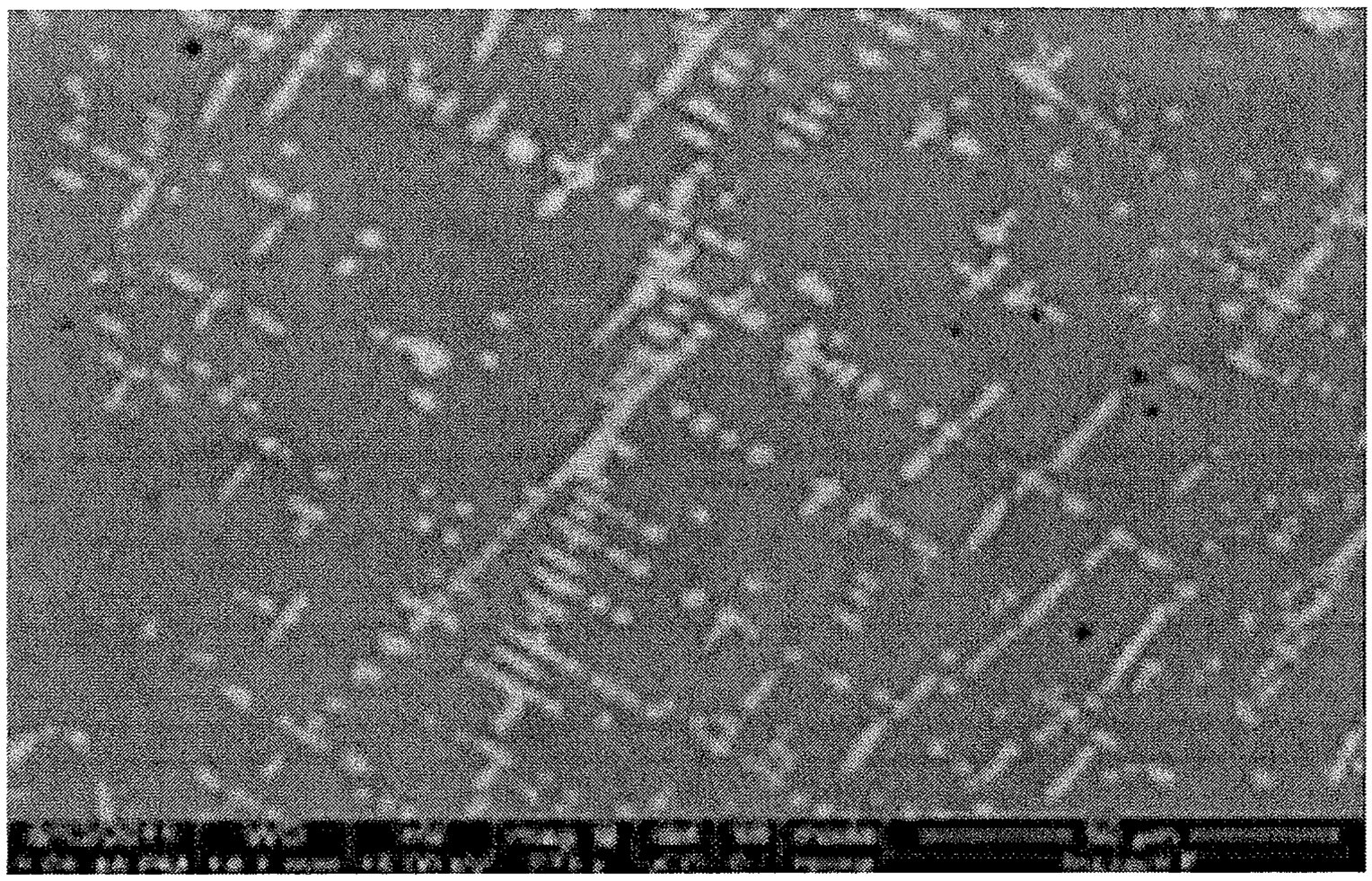

FIG. 6C

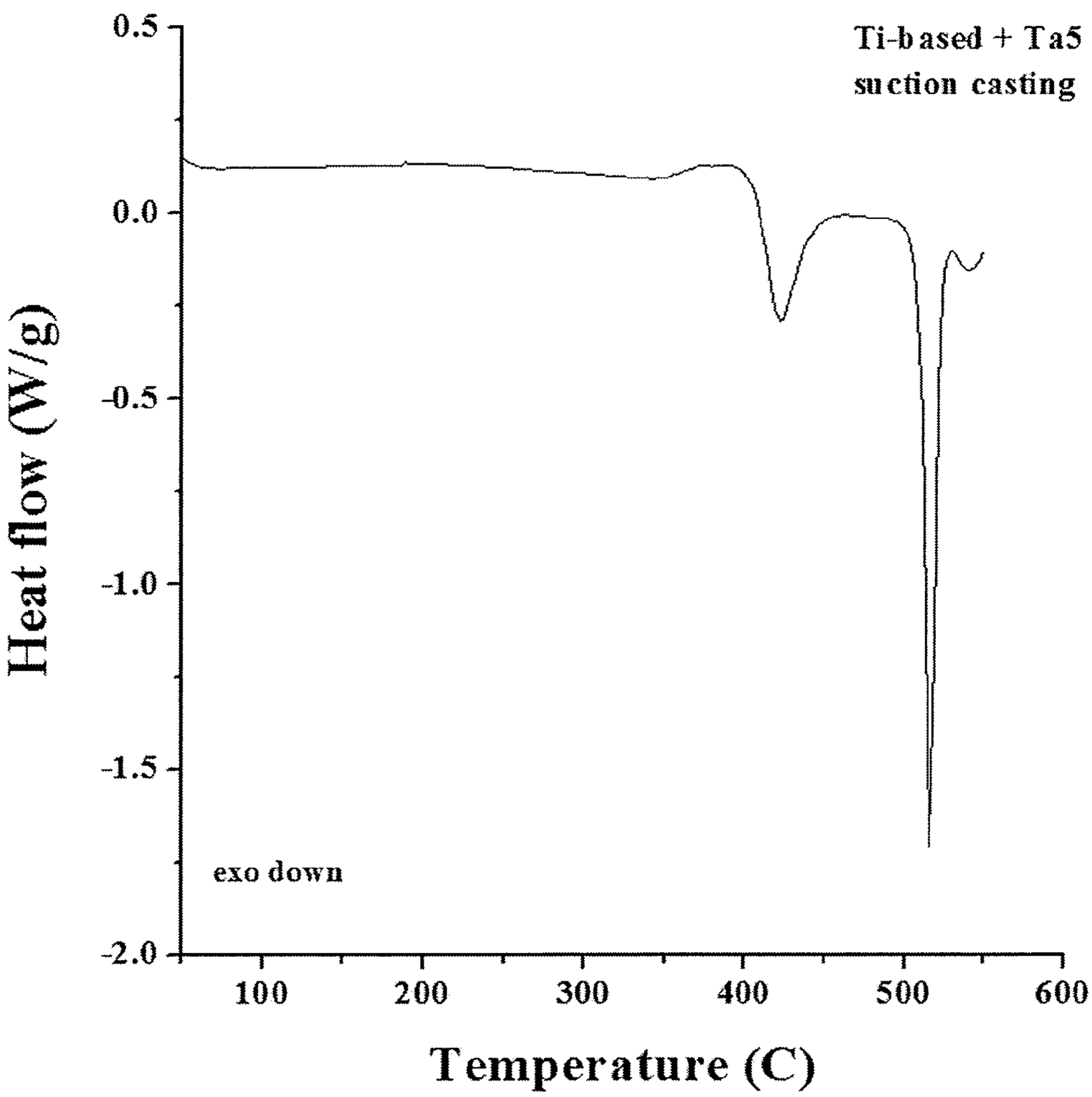
Ti-based + Ta5
suction casting
0.5
0.0
-0.5
-1.0
-1.5
-2.0
Heat flow (W/g)
exo down
100
200
300
400
500
600
Temperature (C)

FIG. 7A

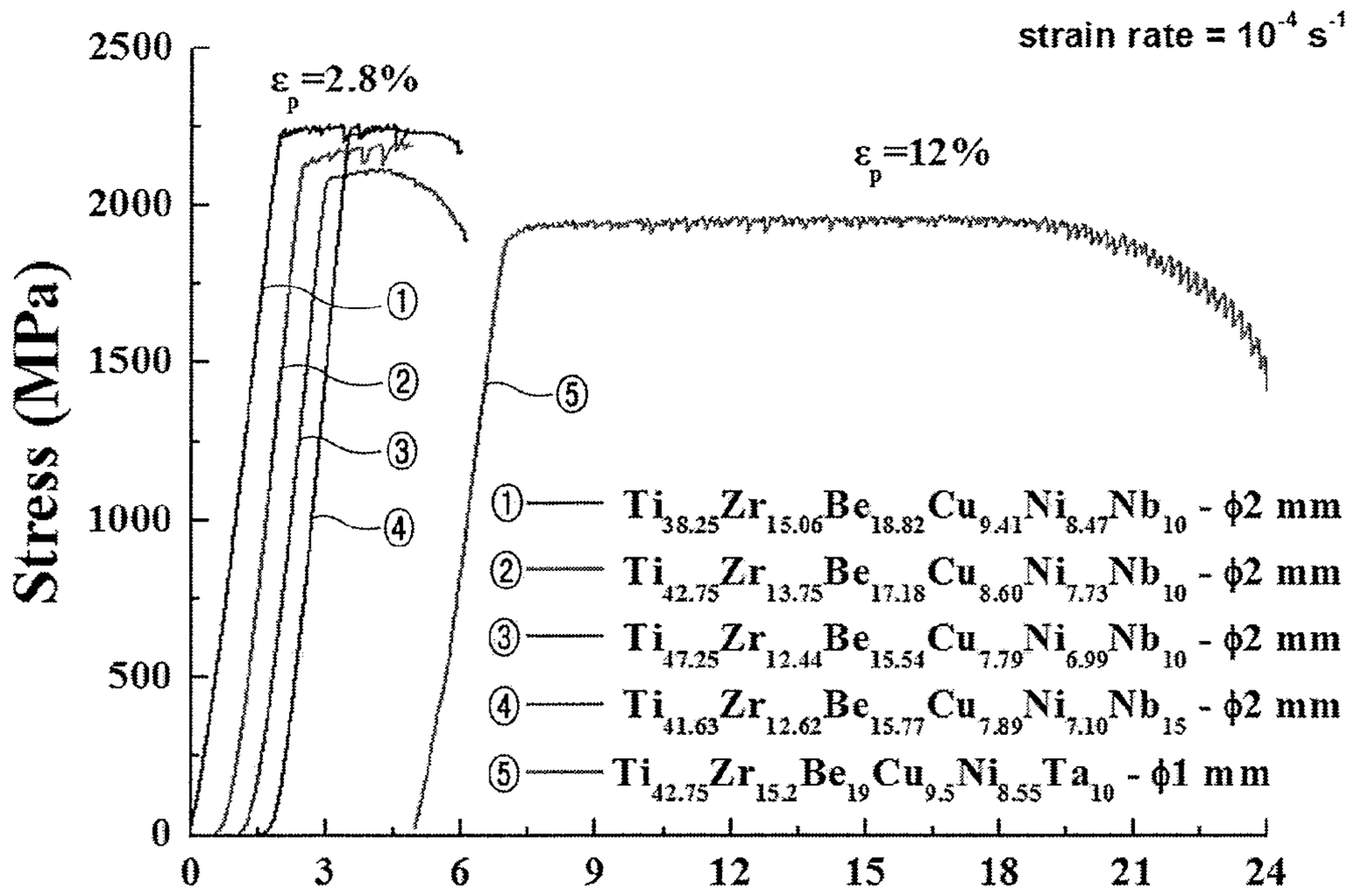
strain rate = 10^{-4} s^{-1}
ε_p=2.8%
ε_p=12%
Stress (MPa)
2500
2000
1500
1000
500
0
0
3
6
9
12
15
18
21
24
Strain
① $Ti_{38.25}Zr_{15.06}Be_{18.82}Cu_{9.41}Ni_{8.47}Nb_{10}$ - ϕ2 mm
② $Ti_{42.75}Zr_{13.75}Be_{17.18}Cu_{8.60}Ni_{7.73}Nb_{10}$ - ϕ2 mm
③ $Ti_{47.25}Zr_{12.44}Be_{15.54}Cu_{7.79}Ni_{6.99}Nb_{10}$ - ϕ2 mm
④ $Ti_{41.63}Zr_{12.62}Be_{15.77}Cu_{7.89}Ni_{7.10}Nb_{15}$ - ϕ2 mm
⑤ $Ti_{42.75}Zr_{15.2}Be_{19}Cu_{9.5}Ni_{8.55}Ta_{10}$ - ϕ1 mm

FIG. 7B

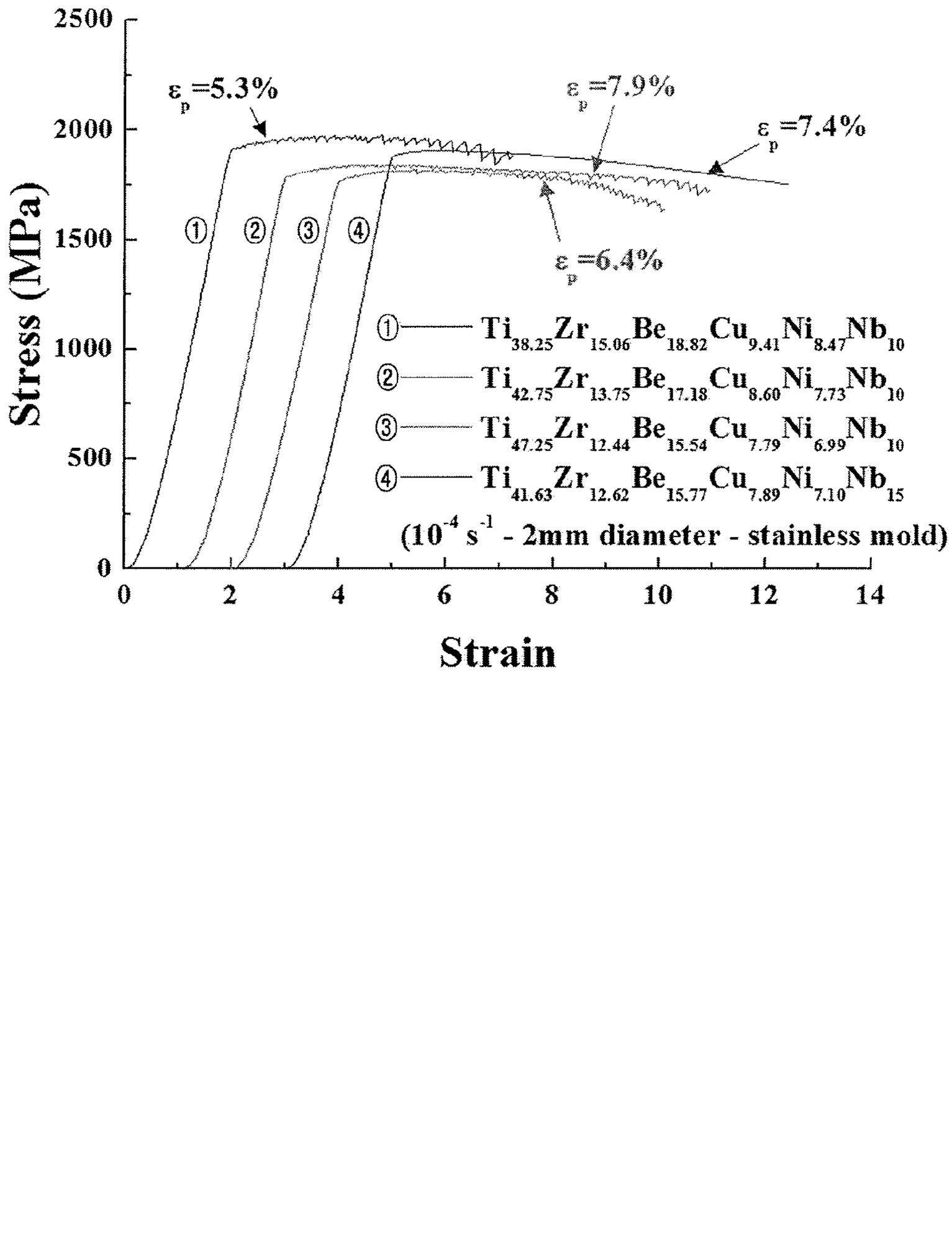
2500
2000
1500
1000
500
0
Stress (MPa)
0
2
4
6
8
10
12
14
Strain
ε_p=5.3%
ε_p=7.9%
ε_p=7.4%
ε_p=6.4%
①
②
③
④
① $Ti_{38.25}Zr_{15.06}Be_{18.82}Cu_{9.41}Ni_{8.47}Nb_{10}$
② $Ti_{42.75}Zr_{13.75}Be_{17.18}Cu_{8.60}Ni_{7.73}Nb_{10}$
③ $Ti_{47.25}Zr_{12.44}Be_{15.54}Cu_{7.79}Ni_{6.99}Nb_{10}$
④ $Ti_{41.63}Zr_{12.62}Be_{15.77}Cu_{7.89}Ni_{7.10}Nb_{15}$
(10^{-4} s^{-1} - 2mm diameter - stainless mold)

FIG. 7C

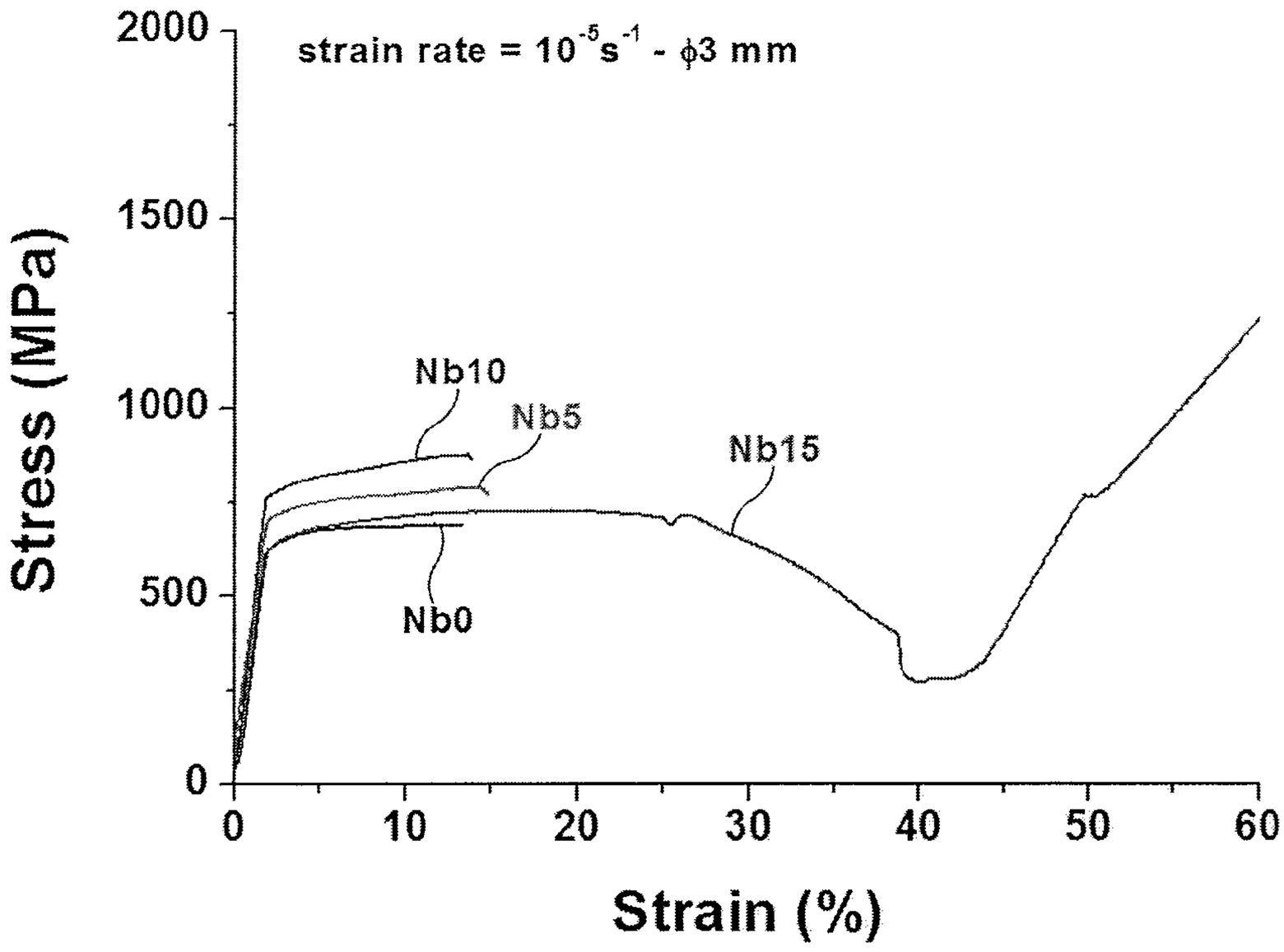
strain rate = 10-5s-1 - ϕ3 mm
Stress (MPa)
2000
1500
1000
500
0
Nb10
Nb5
Nb15
Nb0
0
10
20
30
40
50
60
Strain (%)

FIG. 7D

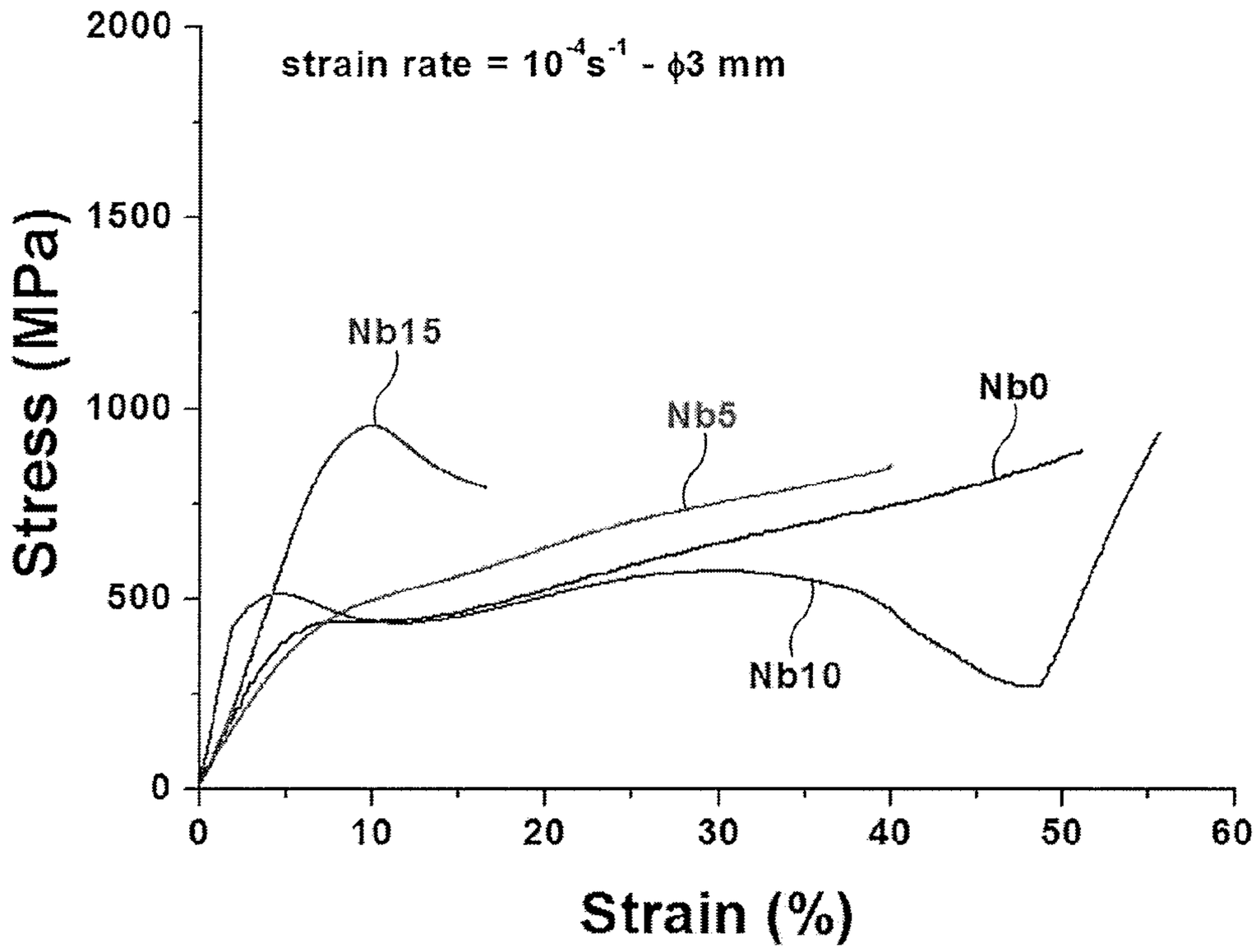
strain rate = $10^{-4}s^{-1}$ - ϕ3 mm
Stress (MPa)
2000
1500
1000
500
0
Nb15
Nb5
Nb0
Nb10
0
10
20
30
40
50
60
Strain (%)

FIG. 7E

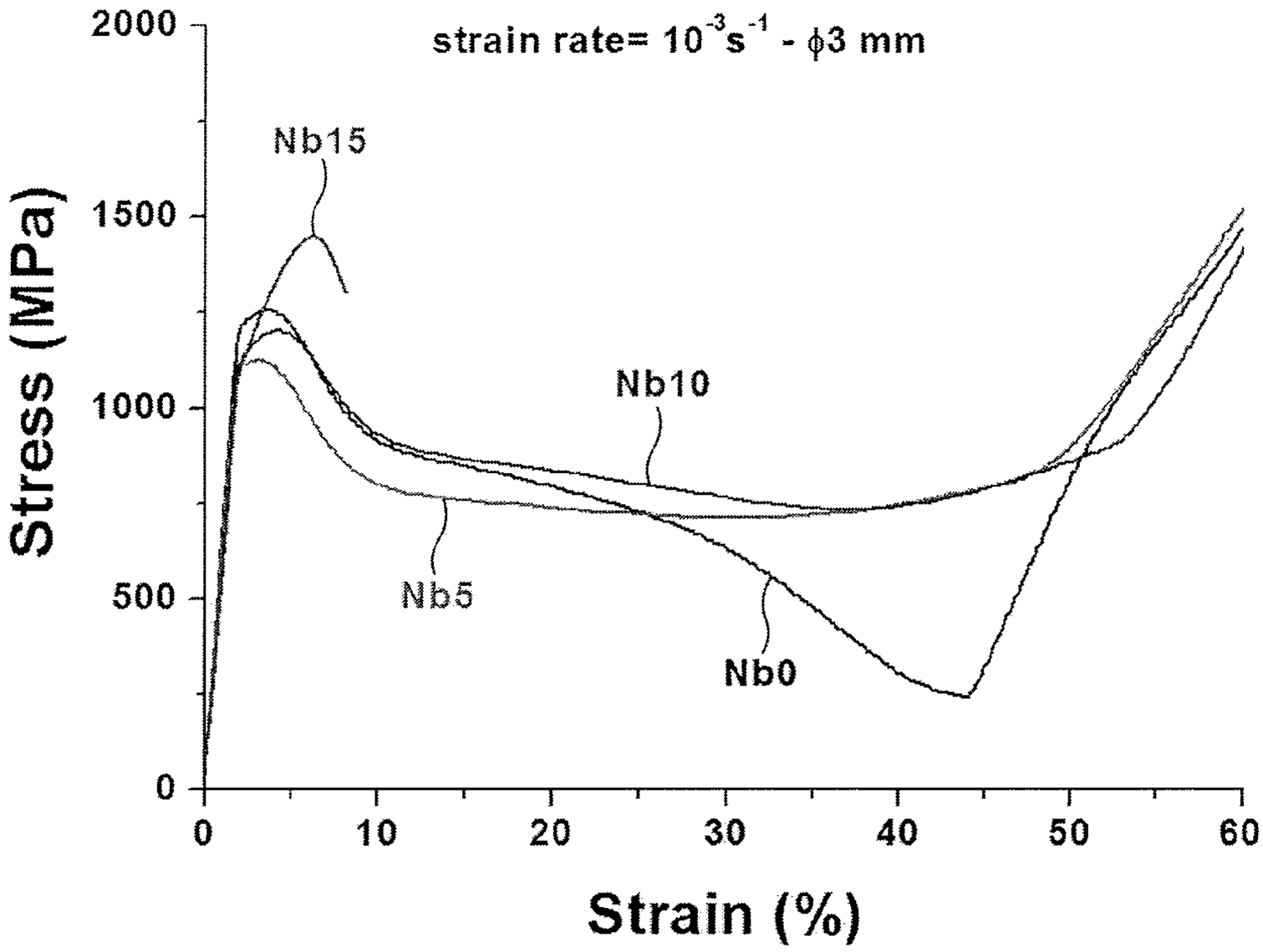
strain rate= 10-3s-1 - ϕ3 mm
Stress (MPa)
2000
1500
1000
500
0
Nb15
Nb10
Nb5
Nb0
0
10
20
30
40
50
60
Strain (%)

FIG. 7F

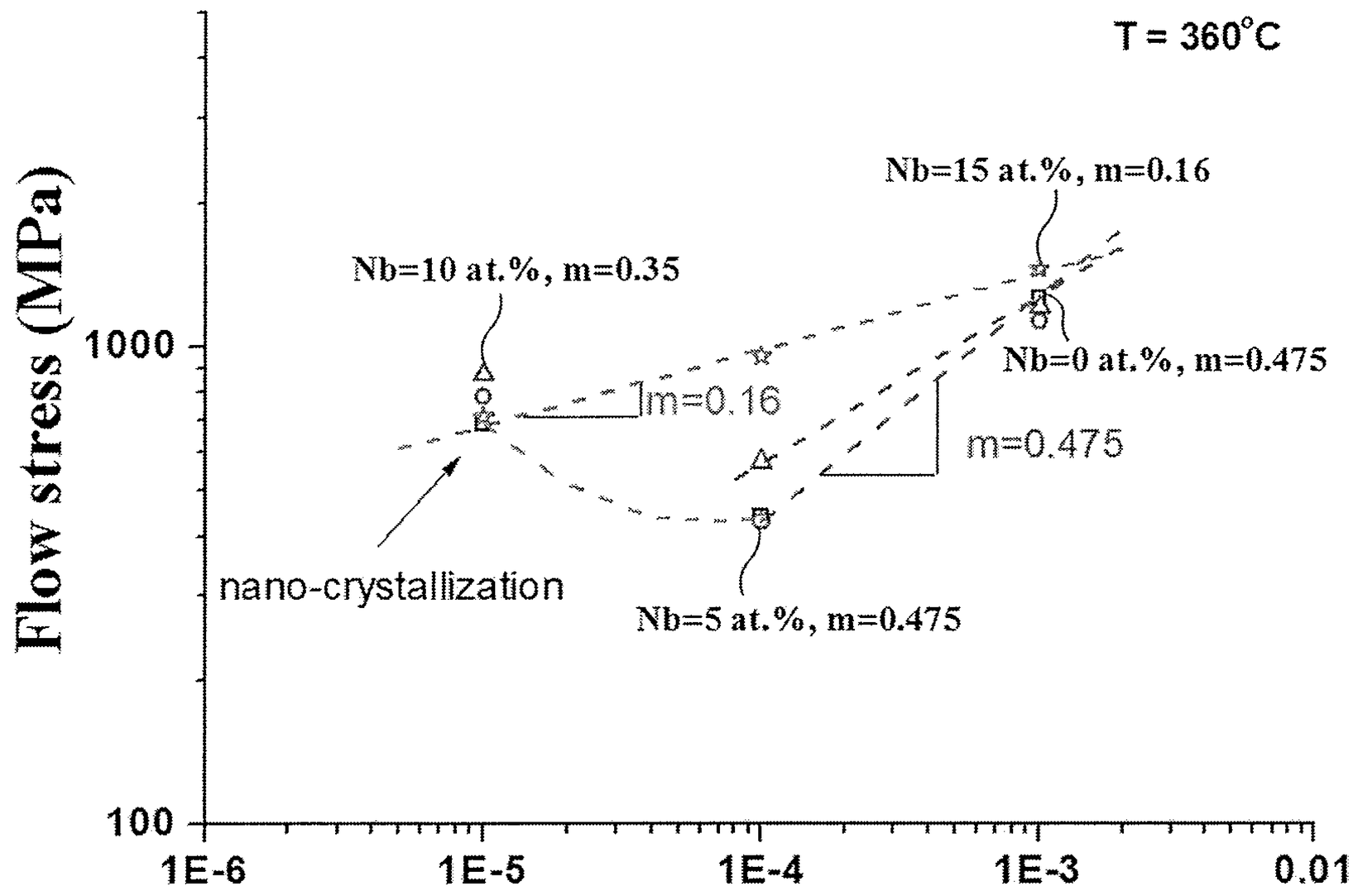
T = 360°C
Nb=15 at.%, m=0.16
Nb=10 at.%, m=0.35
Nb=0 at.%, m=0.475
m=0.16
m=0.475
nano-crystallization
Nb=5 at.%, m=0.475
Flow stress (MPa)
1000
100
1E-6
1E-5
1E-4
1E-3
0.01
Strain rate

FIG. 8A

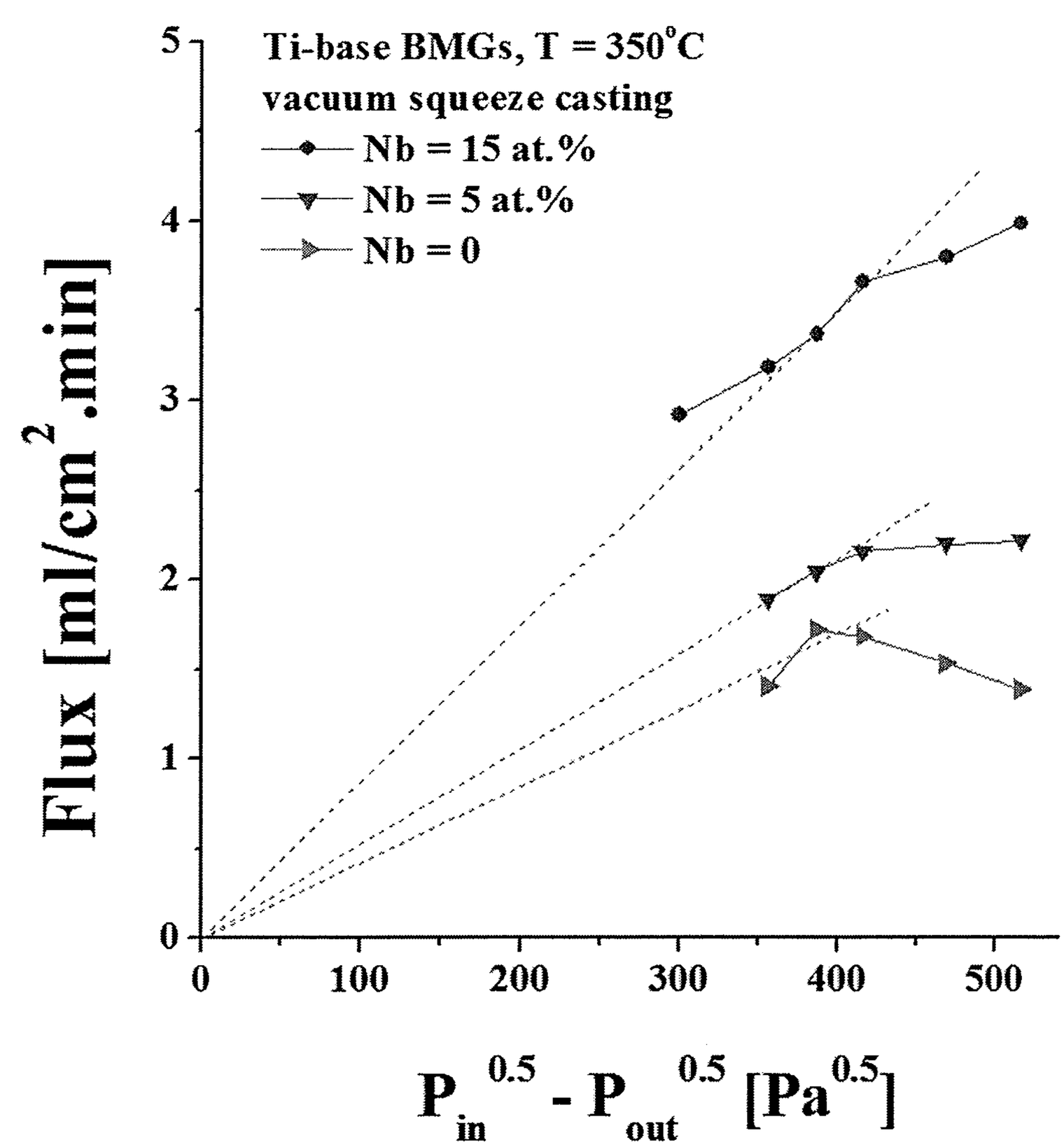
Ti-base BMGs, T = 350°C
vacuum squeeze casting
Nb = 15 at.%
Nb = 5 at.%
Nb = 0
Flux [ml/cm2.min]
0
1
2
3
4
5
0
100
200
300
400
500
P in 0.5 - P out 0.5 [Pa 0.5]

FIG. 8B

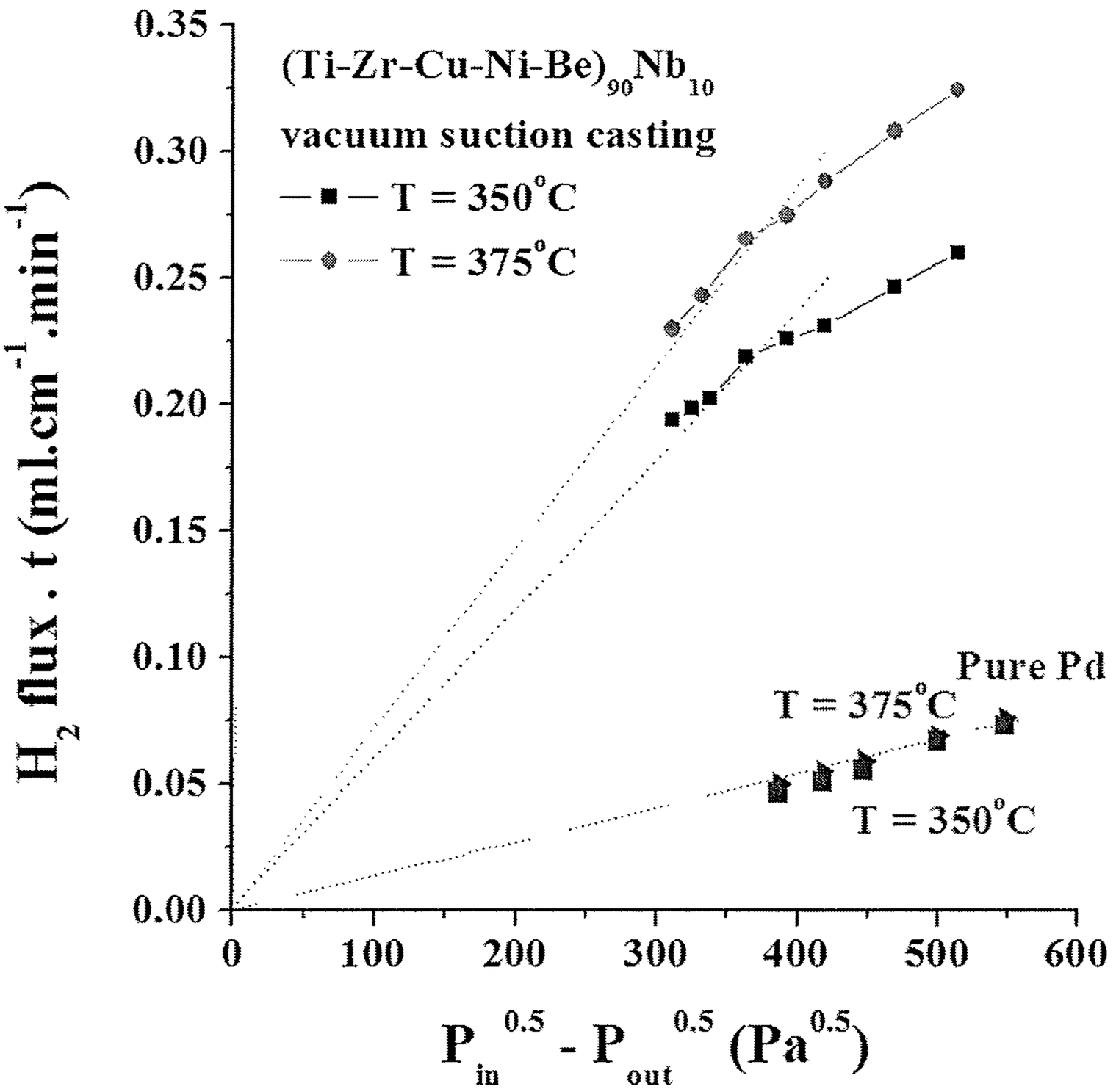
(Ti-Zr-Cu-Ni-Be)90Nb10
vacuum suction casting
T = 350°C
T = 375°C
Pure Pd
T = 375°C
T = 350°C
H2 flux . t (ml.cm-1.min-1)
0.35
0.30
0.25
0.20
0.15
0.10
0.05
0.00
0
100
200
300
400
500
600
P in 0.5 - P out 0.5 (Pa0.5)

FIG. 8C

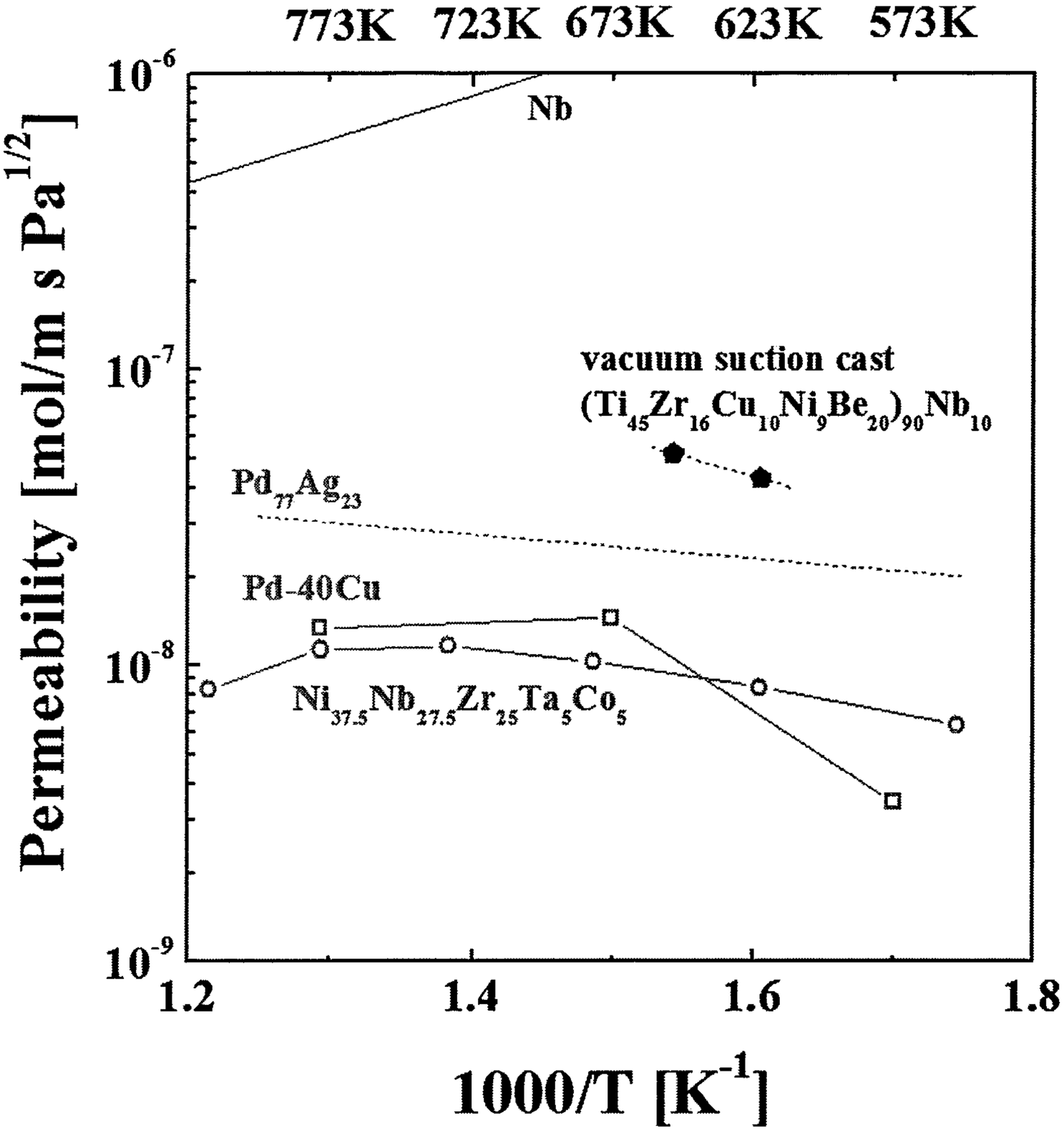
773K 723K 673K 623K 573K
Permeability [mol/m s Pa^1/2]
10^-6
10^-7
10^-8
10^-9
Nb
vacuum suction cast
(Ti45Zr16Cu10Ni9Be20)90Nb10
Pd77Ag23
Pd-40Cu
Ni37.5Nb27.5Zr25Ta5Co5
1.2
1.4
1.6
1.8
1000/T [K^-1]

FIG. 8D

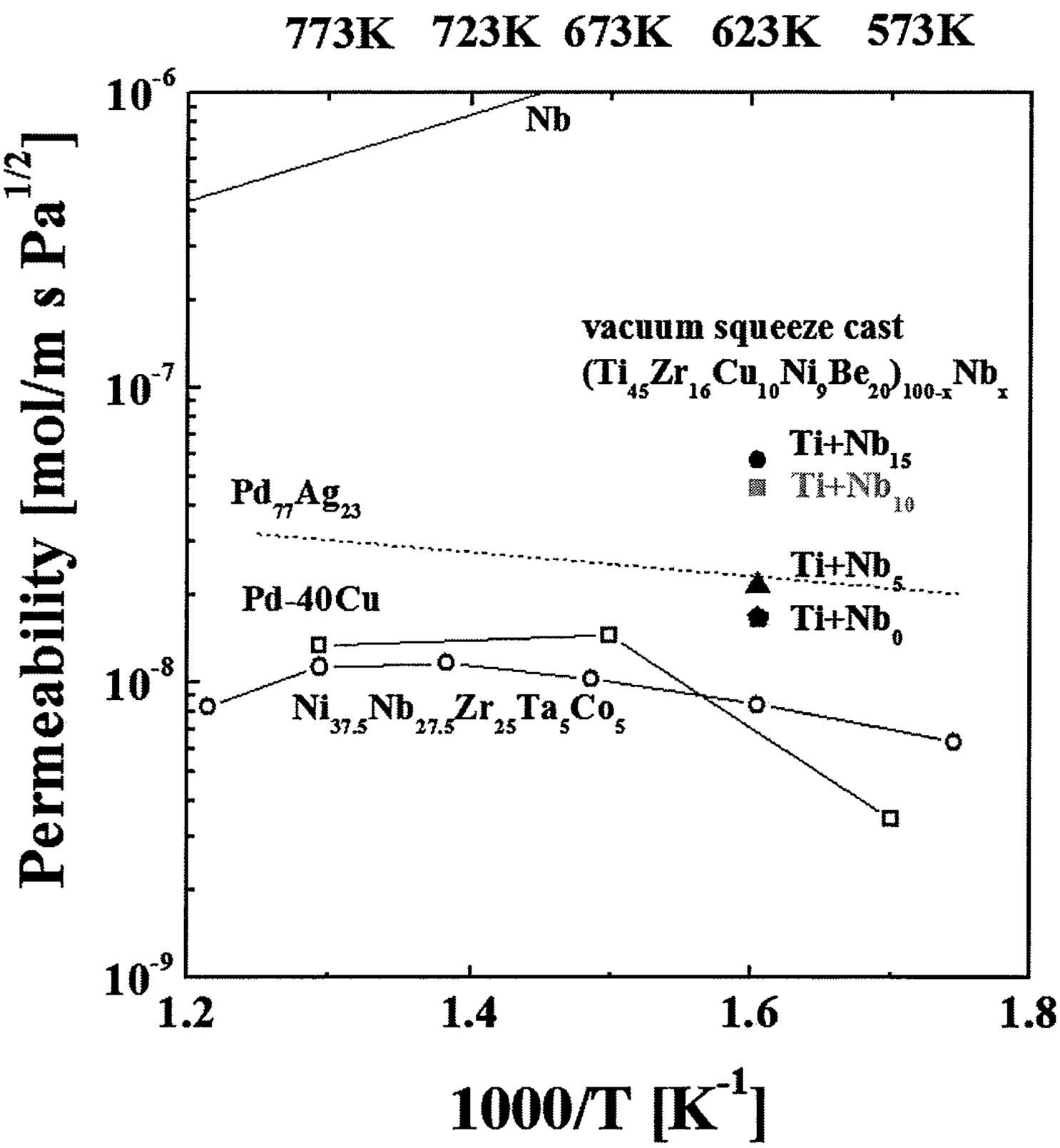
773K 723K 673K 623K 573K
Permeability [mol/m s Pa^1/2]
10^-6
10^-7
10^-8
10^-9
Nb
vacuum squeeze cast
(Ti45Zr16Cu10Ni9Be20)100-xNbx
Ti+Nb15
Ti+Nb10
Pd77Ag23
Ti+Nb5
Pd-40Cu
Ti+Nb0
Ni37.5Nb27.5Zr25Ta5Co5
1.2
1.4
1.6
1.8
1000/T [K^-1]

FIG. 8E

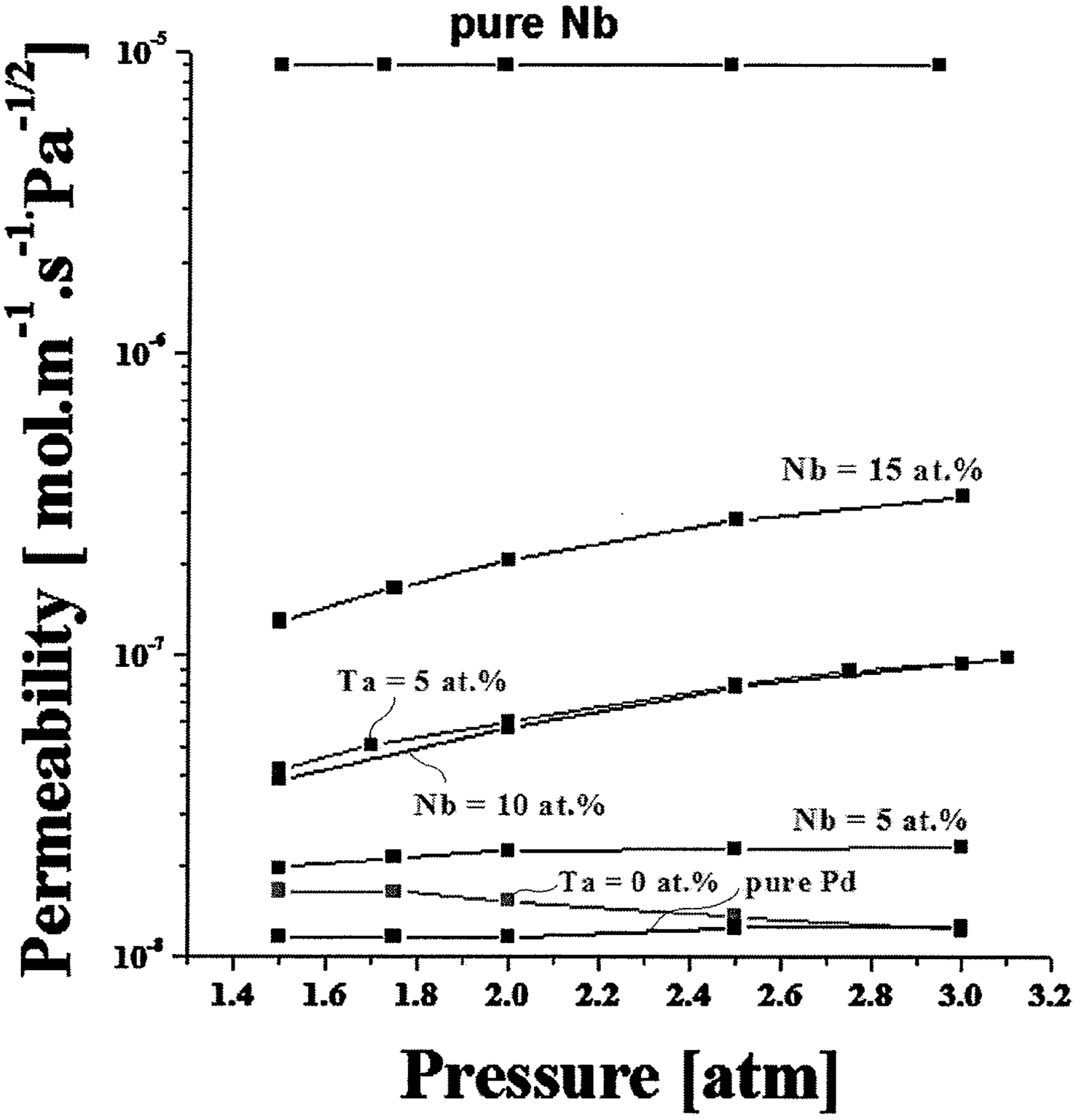
pure Nb
Nb = 15 at.%
Ta = 5 at.%
Nb = 10 at.%
Nb = 5 at.%
Ta = 0 at.%
pure Pd
Permeability [mol.m-1.s-1.Pa-1/2]
10-5
10-6
10-7
10-8
1.4
1.6
1.8
2.0
2.2
2.4
2.6
2.8
3.0
3.2
Pressure [atm]

FIG. 8F

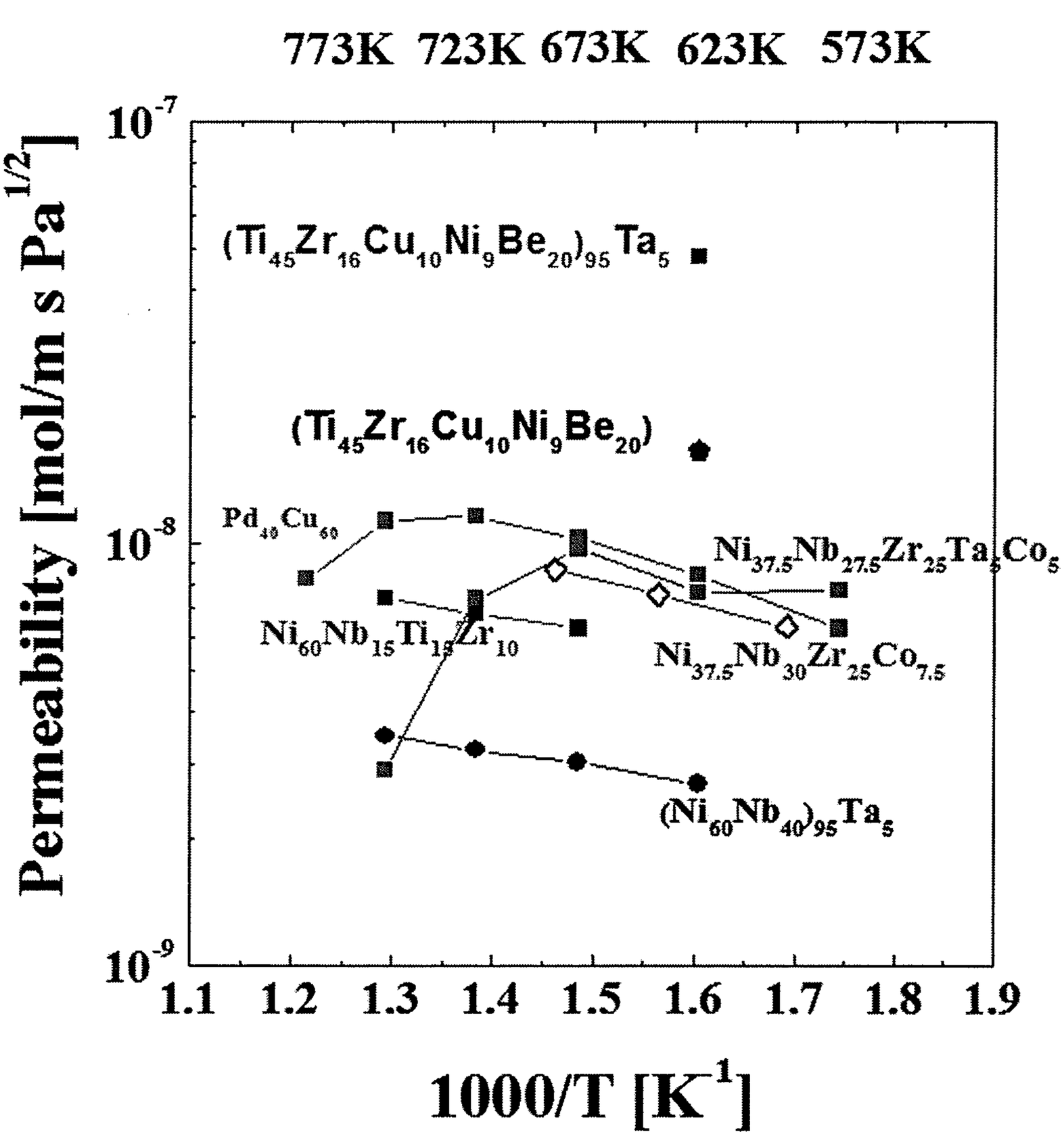
773K 723K 673K 623K 573K
Permeability [mol/m s Pa^1/2]
10^-7
10^-8
10^-9
(Ti45Zr16Cu10Ni9Be20)95Ta5
(Ti45Zr16Cu10Ni9Be20)
Pd40Cu60
Ni37.5Nb27.5Zr25Ta5Co5
Ni60Nb15Ti15Zr10
Ni37.5Nb30Zr25Co7.5
(Ni60Nb40)95Ta5
1.1 1.2 1.3 1.4 1.5 1.6 1.7 1.8 1.9
1000/T [K^-1]

FIG. 9A

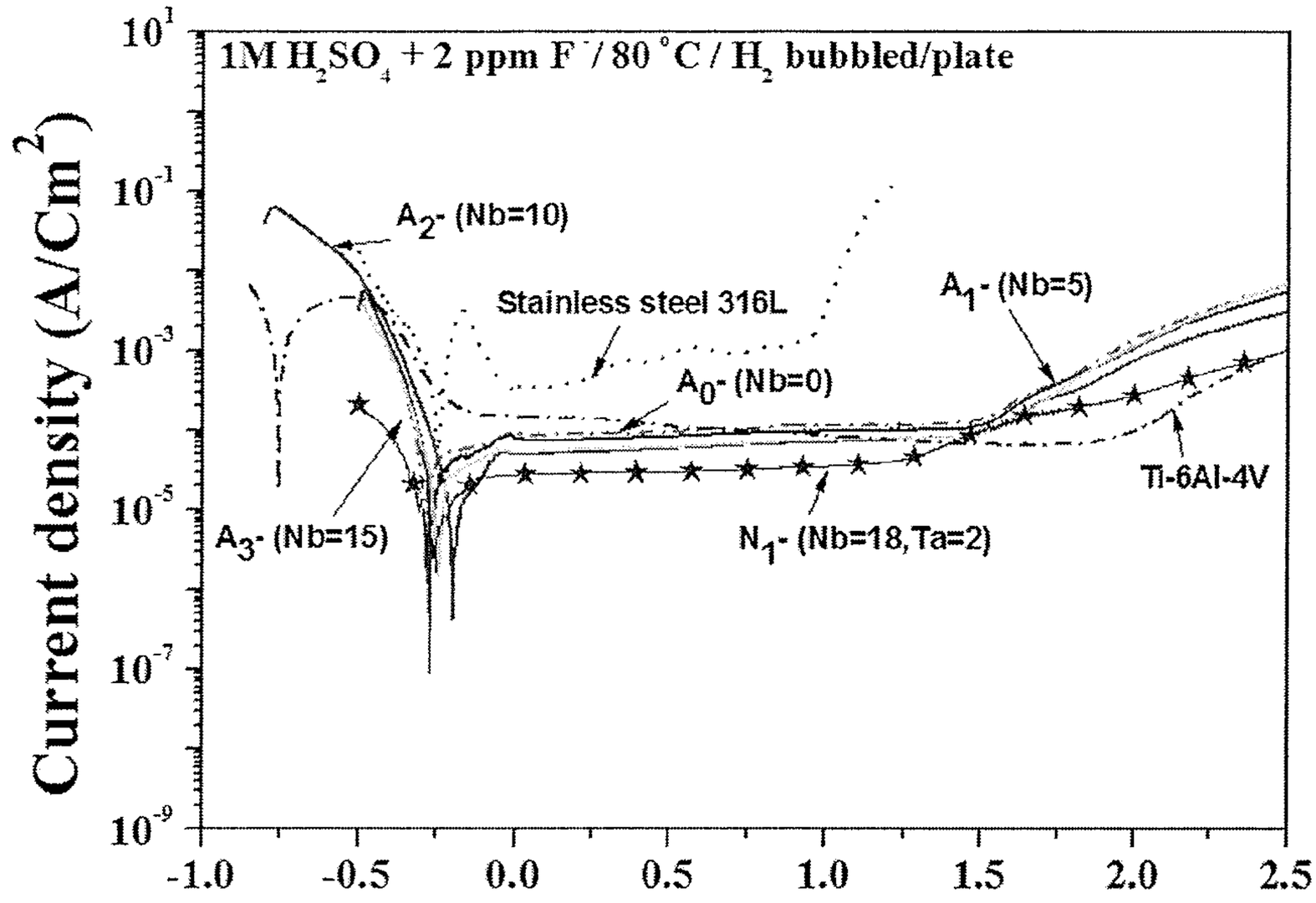
1M H2SO4 + 2 ppm F- / 80 °C / H2 bubbled/plate
Current density (A/Cm2)
Potential (V vs Ag/AgCl)
A2- (Nb=10)
Stainless steel 316L
A1- (Nb=5)
A0- (Nb=0)
A3- (Nb=15)
N1- (Nb=18,Ta=2)
Ti-6Al-4V
10^1
10^-1
10^-3
10^-5
10^-7
10^-9
-1.0
-0.5
0.0
0.5
1.0
1.5
2.0
2.5

FIG. 9B

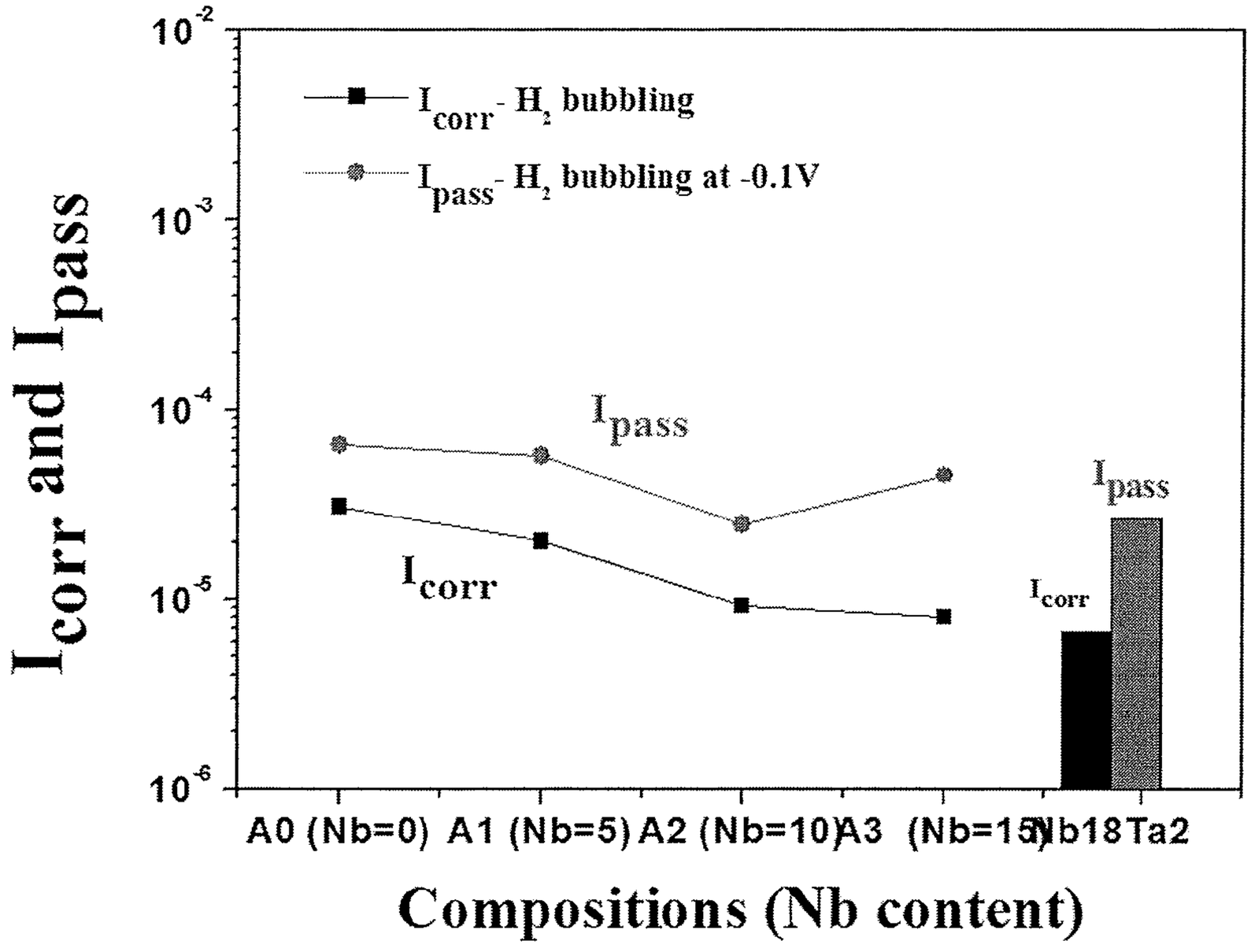
10^{-2}
10^{-3}
10^{-4}
10^{-5}
10^{-6}
I_{corr} and I_{pass}
I_{corr} - H_2 bubbling
I_{pass} - H_2 bubbling at -0.1V
I_{pass}
I_{corr}
I_{pass}
I_{corr}
A0 (Nb=0)
A1 (Nb=5)
A2 (Nb=10)
A3 (Nb=15)
Nb18Ta2
Compositions (Nb content)

FIG. 9C

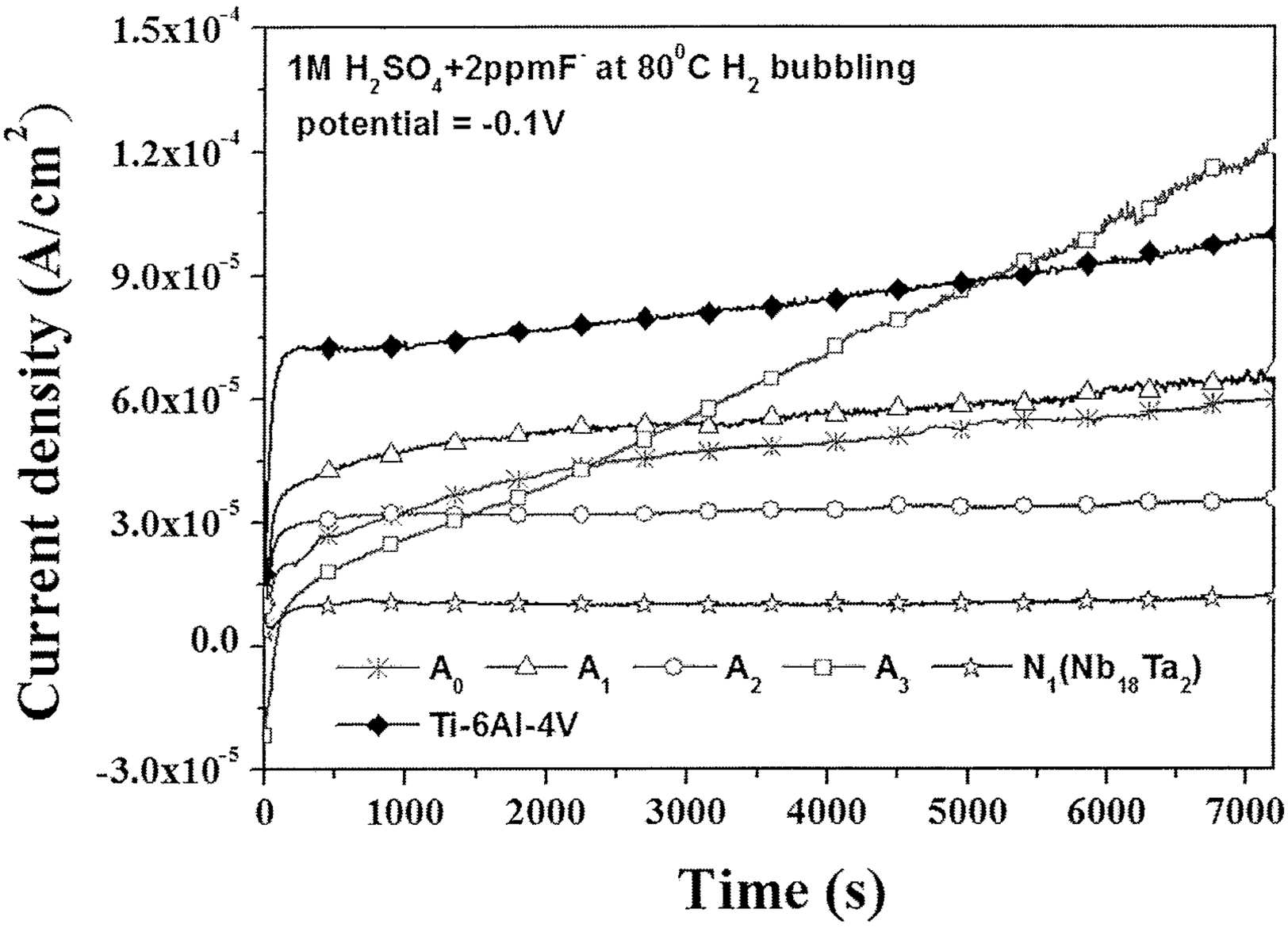
1M H_2SO_4+2ppmF^- at 80^{0}C H_2 bubbling
potential = -0.1V
Current density (A/cm^2)
1.5x10^{-4}
1.2x10^{-4}
9.0x10^{-5}
6.0x10^{-5}
3.0x10^{-5}
0.0
-3.0x10^{-5}
A_0
A_1
A_2
A_3
$N_1(Nb_{18}Ta_2)$
Ti-6Al-4V
0
1000
2000
3000
4000
5000
6000
7000
Time (s)

TITANIUM-BASED BULK AMORPHOUS MATRIX COMPOSITE AND METHOD OF FABRICATING THEREOF

[0001] This application claims priority to and the benefit of Korean Patent Application No. 10-2012-0065705, filed on Jun. 19, 2012, and all the benefits accruing therefrom under 35 U.S.C. §119, the content of which in its entirety is herein incorporated by reference.

BACKGROUND OF THE INVENTION

[0002] (a) Field of the Invention

[0003] A titanium-based bulk amorphous matrix composite and method of fabricating thereof are provided.

[0004] (b) Description of the Related Art

[0005] Concerns about the reduction of natural resources and global warming have encouraged the development of alternative energies. Among possible candidate sustainable and clean energies, hydrogen-related energy such as fuel cell is expected to grow rapidly in the coming years owing to abundance of hydrogen. Before being used as fuel, hydrogen should be extracted from other gasses or compounds. Although several techniques may be applied for this purpose such as chemical or electrolytic methods, the permeation through a solid metallic membrane is expected to become the dominant production route of high purity hydrogen owing to the high selectivity, the high production rate, the compactness and the simplicity of this technique.

[0006] The principle of hydrogen permeation consists in heating a mixed gas, such as CO+H_2 that is produced from steam reforming of methane gas at 400□, to dissociate on the surface of the membrane the hydrogen gas molecules into hydrogen protons that need to diffuse through the atomic structure of the membrane that will recombine into hydrogen molecules on the permeate side. Thus, the permeation of hydrogen through a solid membrane obeys the Fick's first law of diffusion:

$$J = D\frac{\partial C}{\partial x}$$

[0007] where J is the flux, the amount of hydrogen transferred per unit area per unit time, D is the hydrogen diffusion coefficient, and ∂C/∂x is the concentration gradient between the permeate and the retentate side of the membrane.

[0008] This equation is written:

$$J = -D\frac{\Delta C}{t}$$

[0009] where ΔC is the difference of hydrogen concentration between the permeate and retentate side of the membrane of thickness, t. From this equation, it is thus deduced that high values of the hydrogen flux, i.e., high production rate of pure hydrogen, may be achieved for membranes as thin as possible. However that thickness should be sufficient to support the applied hydrogen pressure at the inlet side.

[0010] Under equilibrium, the concentration of hydrogen in a solid membrane depends on the hydrogen pressure that is usually expressed by the Sievert's law:

$$C = K_s P_{H_2}^{0.5}$$

[0011] where K_s is a material constant and P_{H2} is the hydrogen partial pressure.

[0012] The expression of the hydrogen flux thus becomes:

$$J = \frac{D \cdot K_s}{t}(P_{in}^{0.5} - P_{out}^{0.5})$$

[0013] The hydrogen flux depends on the difference of pressure between the retentate and permeate side of the membrane, the diffusivity and solubility of hydrogen and the thickness of the membrane.

[0014] Among candidate materials, Pd and its alloys, particularly the Pd—Ag alloys, demonstrate the best properties in term of hydrogen permeation, durability and tolerance to H_2O, CO, CO_2 and H_2S, and they have already been used as a hydrogen membrane and a gas separation apparatus commercialized in the United States. However, the scarcity and price of Pd element is encouraging the development of alternative alloys for the commercialization of H_2 separation membranes.

[0015] A large number of alloys with either a crystalline or amorphous structure have been proposed to replace Pd. The first metallic glass with amorphous structure was produced nearly 50 years ago by researchers at Caltech using an original technique now known as the melt spinning technique. In contrast to non-metallic amorphous solids such as ceramic glasses, metallic alloys exhibit pronounced characteristics in their mechanical properties in the amorphous state. The aperiodic arrangement of the atoms in the amorphous structure provides remarkable physical, chemical and mechanical properties which make this type of materials attractive for a wide range of applications. In respect to elasticity, the stiffness is usually 30% lower than that of crystalline state while the yield strength is about 2 to 3 times greater than that of crystalline alloys, providing to metallic glasses the possibility of deforming with large elastic strain. However, the first industrial applications in the 70's took advantage of the soft magnetic properties of the Fe-6.0 wt % P-1.7 wt % C metallic glasses, developed in 1967 also by the Caltech group, to enhance the efficiency of transformer, the resolution of magnetic head, etc. Continuous progress in this class of materials enabled the production of metallic glass from vacuum casting technique in the bulk form, i.e., with lower cooling rate. Progressively, new alloys were developed and nowadays bulk specimens with size of at least 1 cm diameter may be produced in all alloy systems from Mg, Ca, Zr, Pd, Ti, Cu, Fe, Co, Ni including RE (rear earth elements), but with the exception of Al which may only be produced so far in the form of rod of diameter less than 1 mm. Despite the remarkable combination of physical, chemical and mechanical properties achieved by these various alloy systems, the range of applications of metallic glasses have not been extended for several reasons. Firstly, the metallic glasses suffer from the lack of reliability and reproducibility of the properties because alloys developed till now are sensitive to impurities, particularly oxygen, which generally led to severe embrittlement. Secondly, these alloys as for oxide glasses are intrinsically brittle, i.e., they may not be deformed plastically at ambient temperature under tensile mode.

[0016] As research in this field is quickly progressing and as the next generation of metallic glasses will likely exhibit ductile behavior, new applications may be expected. Several applications have already been proposed for corrosion-resistant coatings, MEMS, biomedical applications but may also be extended to ship hulls, automobile parts, bicycles, and recreational equipments such as tennis rackets and golf clubs.

[0017] In comparison to crystalline alloys, the science of metallic glass is still in infancy and the exact mechanisms controlling some properties, as for example the plastic deformation, are not clear. At low temperature, the plastic deformation occurred by localized atomic flow in thin shear bands as the stress exceeds the yield stress. Recent experimental investigations indicate that the origin of shear bands in metallic glasses is not a thermo-mechanical softening of the material, as during high rate deformation in steels, but rather it arises due to structural softening. Structure appears to be a key element to study in order to understand the deformation mechanism. Although the free-volume model proposed by Spaepen has been rather well accepted, results obtained from Molecular Dynamic simulation tends to give support for the localized shear transformation zone (STZ) mechanism proposed by Argon, which places more emphasis on the analogy to atomic flow in viscous matter. The inelastic deformation in metallic glasses is thus interpreting as the local shearing of clusters of atoms (30~50 atoms) accompanied by an inelastic dilatation producing strain-softening, and then leading to the formation of shear bands. When shear strain increases, one jammed (fully deformed) STZ affects the surrounding material and eventually triggers the generation of thin shear bands (about 10-15 nm thick).

[0018] The mechanism of plastic deformation in metallic glasses is thus fundamentally different from that in crystalline solids because of the lack of long-range order in the atomic structure of these materials. Under tensile mode, the shear bands do not extend but remain localized and unstable. The inconceivably large value of plastic strain in a thin region induced the cumulation of point defects leading to formation of cracks and thus leading to a brittle fracture.

[0019] One way of enhancing the plastic deformation of metallic glasses under tensile loading mode at low temperature is to introduce inhomogeneities in the amorphous structure that will initiate a large number of STZs and play a role of obstacles to the propagation of shear bands. While several types of inhomogeneity may be introduced in an amorphous structure, the dynamic propagation of shear bands requires the obstacles to be close to each other and of large size in comparison to the thickness of the shear bands. Successful approaches to achieve plastic deformation under tensile mode include the production of ex-situ and in-situ bulk metallic glass (BMG) matrix composites. The ex-situ approach enables tensile ductility however at the expense of the strength and makes the preparation of the composites more complicated. The most attractive method consists in producing in-situ composites as did Johnson and his coworkers at Caltech. They could achieve up to 9% plastic deformation for the Zr—Ti—Nb—Cu—Be in-situ BMG matrix composites under tensile mode. It should be noticed that the mechanical behavior is characterized by a strain softening and that the maximum strength of this ductile in-situ BMG composite was reduced by about 15% in comparison to monolithic Zr-based BMGs. The structure of these composites is characterized by the presence of Nb-rich dendritic phase in Zr-based amorphous structure.

[0020] Such type of in-situ BMG matrix composite presents similarity with the crystalline Nb—(Ti,Zr)—Ni two-phase alloys prepared by Aoki's group in Kitami Institute in Japan that are composed of Nb-rich dendrite in Ni—(Ti,Zr) crystalline matrix. The presence of Nb-rich phase is of particular interest because experimental investigations have demonstrated that the permeability of hydrogen in elements of group 5 in the periodic table of elements with a body centered cubic (bcc) atomic structure is much larger than that of Pd that has a face centered cubic (fcc) structure. However, the shortcoming of these bcc metals, such as V, Nb and Ta, is not the insufficient permeability, but the mechanical integrity of these materials under H_2, i.e., hydrogen embrittlement.

[0021] Metallic glasses have already been proposed as materials for hydrogen membranes. Ni—Nb-based or Ni—Zr-based amorphous alloys have demonstrated encouraging performance, with values of hydrogen permeability reported so far similar those of Pd alloys, i.e., about 2×10^{-8} mol/m.s.$Pa^{1/2}$ at 400° C.

[0022] One approach to enhance the hydrogen permeability of amorphous alloys to values significantly larger than those of Pd alloys is to produce a composite structure consisting in the dispersion of a phase rich in these group 5 elements into the amorphous structure. Particularly the dispersion of a continuous crystalline phase would provide a fast diffusion to hydrogen atom, and a role of the amorphous matrix will be to accommodate for the lattice expansion of the dispersed phase induced by hydrogen and to hinder the hydrogen embrittlement.

BRIEF SUMMARY OF THE INVENTION

[0023] An exemplary embodiment relates to the application of in-situ crystalline-reinforced Ti-based bulk amorphous matrix composites (BAMCs) as solid membranes for gas separation technique such as a polymer electrolyte membrane of the fuel cell. The microstructure of the membranes prepared by vacuum casting technique has a bcc crystalline phase with a dendritic morphology embedded in a Ti-based amorphous matrix.

[0024] In an exemplary embodiment, the composites formed in a wide range of composition are relatively easy to prepare owing to the large glass forming ability. For example, the volume fraction and size of the reinforcement, i.e., a bcc crystalline phase, may be varied in the range 1 to 40% and 0.01 to 100 μm, respectively. The dendritic morphology of the reinforcement may be varied from isolated, slender or with directionality depending on the requested properties.

[0025] In an exemplary embodiment, the composites have excellent properties, such as high hydrogen permeability, high mechanical strength and high corrosion resistance. For example, the bcc phase rich in group 5 elements such as Nb and/or Ta provides high values of the hydrogen permeability, less than 6×10^{-8} mol/m.s.$Pa^{1/2}$ in the temperature 325-375□, which are about 2 to 3 times higher that those of Pd-based alloys under identical testing conditions. The hydrogen permeability is necessary for solid membrane materials used for the separation and purification of hydrogen. The composites exhibit also high strength and malleability at room temperature. The composites are also characterized by an excellent corrosion resistance in 1M H_2SO_4 at 80° C. with either H_2 or air bubbling. The presence of the second phase also improves the mechanical strength in the supercooled liquid region. The combination of these remarkable physical, mechanical and chemical properties as well as the relatively low cost place

these in-situ BMG matrix composites as potential candidate materials for the separation and purification of hydrogen.

[0026] In exemplary embodiment, a Ti-based bulk amorphous matrix composite including a composition represented by Formula 1, in at %:

$$Ti_aZr_bBe_cCu_dNi_eM_fI_g \quad \text{Formula 1}$$

[0027] where M is at least one of Nb or Ta, I is an impurity, and a, b, c, d, e, and f vary within the ranges $38 \le a \le 50$, $11 \le b \le 18$, $12 \le c \le 20$, $6 \le d \le 10$, $6 \le e \le 9$, $1 \le f \le 20$ and $0.01 \le g \le 0.5$, with a+b+c+d+e+f+g=100.

BRIEF DESCRIPTION OF THE DRAWINGS

[0028] The above and other aspects, advantages, and features of the invention will become more apparent by describing in further detail exemplary embodiments thereof with reference to the attached drawings, in which:

[0029] FIGS. **1**A and **1**B are binary phase diagrams of Ti—Nb and Ti—Ta, respectively;

[0030] FIGS. **1**C, **1**D and **1**E are schematic representations of the shell structure of Ti, Nb, and Ta elements, respectively;

[0031] FIG. **1**F is a graph showing the principle of the in-situ composite formation;

[0032] FIG. **2**A is a schematic diagram of the vacuum suction casting apparatus;

[0033] FIG. **2**B is a schematic diagram of the vacuum squeeze casting type apparatus;

[0034] FIG. **3**A shows XRD traces of Ø10 mm $(Ti—Zr—Be—Cu—Ni)_{95}Nb_5$ and Ø7 mm $(Ti—Zr—Be—Cu—Ni)_{95}Ta_5$ rods;

[0035] FIG. **3**B shows DSC traces of Ø10 mm $(Ti—Zr—Be—Cu—Ni)_{95}Nb_5$ and Ø8 mm $(Ti—Zr—Be—Cu—Ni)_{95}Ta_5$ rods;

[0036] FIG. **3**C shows XRD traces of Ø7 and Ø10 mm diameter rods of $(Ti—Zr—Be—Cu—Ni)_{95}Ta_5$;

[0037] FIGS. **3**D and **3**E are SEM images of $(Ti_{45}Zr_{16}Be_{20}Cu_{10}Ni_9)_{95}Nb_5$ (Ø8 mm) and $(Ti_{45}Zr_{16}Be_{20}Cu_{10}Ni_9)_{95}Ta_5$ (Ø8 mm), respectively;

[0038] FIG. **4**A is a phase diagram showing the range of formation of the Ti—Zr—Be—Cu—Ni—Nb in-situ metallic glass composite;

[0039] FIGS. **4**B and **4**C are SEM images showing the microstructure of the alloys A**2** and A**3** containing, respectively, 10 at % and 15 at % Nb;

[0040] FIG. **4**D shows XRD traces of the alloys A**0**, A**1**, A**2**, and A**3** containing respectively 0, 5, 10 and 15 at % Nb;

[0041] FIG. **4**E shows DSC traces of the alloys A**1**, A**2** and A**3** containing respectively 5, 10 and 15 at % Nb;

[0042] FIGS. **4**F and **4**G are SEM images showing the microstructure of $Ti_{45}(Zr_{16}Be_{20}Cu_{10}Ni_9)_{45/55}Nb_{10}$, and $Ti_{41.6}Zr_{12.6}Be_{15.8}Cu_{7.9}Ni_{7.1}Nb_{15}$ alloys, respectively;

[0043] FIG. **5**A shows XRD traces of the $(Ti_{45}Zr_{16}Be_{20}Cu_{10}Ni_9)_{100-x}Nb_x$ alloys with x=0, 5, 10 and 15 at %;

[0044] FIG. **5**B shows DSC traces of the $(Ti_{45}Zr_{16}Be_{20}Cu_{10}Ni_9)_{100-x}Nb_x$ alloys with x=0, 5, 10 and 15 at %;

[0045] FIGS. **5**C, **5**D, **5**E and **5**F are SEM images of the $(Ti_{45}Zr_{16}Be_{20}Cu_{10}Ni_9)_{100-x}Nb_x$ alloys with x=0, 5, 10 and 15 at %, respectively;

[0046] FIG. **6**A is a XRD trace of $(Ti_{45}Zr_{16}Be_{20}Cu_{10}Ni_9)_{95}Ta_5$ alloy;

[0047] FIG. **6**B is a SEM image of $(Ti_{45}Zr_{16}Be_{20}Cu_{10}Ni_9)_{95}Ta_5$ alloy;

[0048] FIG. **6**C is a DSC trace of the $(Ti_{45}Zr_{16}Be_{20}Cu_{10}Ni_9)_{95}Ta_5$ alloy;

[0049] FIG. **7**A shows stress-strain curves obtained under compression with a strain rate of 10^{-4} s^{-1} for in-situ Ti-based BMG composites containing Nb and Ta;

[0050] FIG. **7**B shows stress-strain curves obtained under compression with a strain rate of 10^{-4} s^{-1} for various compositions of in-situ Ti-based BMG composites containing Nb;

[0051] FIGS. **7**C, **7**D and **7**E show stress-strain curves obtained for a strain rate of 10^{-5} s^{-1}, 10^{-4} s^{-1}, 10^{-3} s^{-1}, respectively;

[0052] FIG. **7**F shows a variation of the flow stress with the applied strain rate;

[0053] FIG. **8**A shows a variation of the flux at 350° C. for in-situ Ti-based BMG composites containing 5 and 15 at % Nb (prepared by vacuum squeeze casting);

[0054] FIG. **8**B shows a variation of the flux at 350 and 375° C. for in-situ Ti-based BMG composites containing 10 at % Nb (prepared by vacuum suction casting) and comparison with pure Pd;

[0055] FIGS. **8**C and **8**D show hydrogen permeation properties of Ti-BMG composite by vacuum suction casting and Ti-BMG composites prepared by vacuum squeeze casting and comparison with Pd—Cu alloys and Ni-based metallic glass, respectively;

[0056] FIGS. **8**E and **8**F show hydrogen permeation properties of the Ti+Ta-BMG composite prepared by vacuum squeeze casting plotted as a function of the difference of pressure and comparison with Ti+Nb BMG composites, and plotted as a function of the inverse of temperature and comparison with Pd—Cu alloys and Ni-based metallic glass, respectively;

[0057] FIG. **9**A shows a potentio-dynamic graph of in-situ Ti-BMG composites in 1M H_2SO_4+2 ppm F^- at 80° C. with H_2 bubbling and comparison with stainless steel and Ti-6Al-4V;

[0058] FIG. **9**B shows a variation of the corrosion current density and passivation current density as a function of the Nb content (%) for in-situ Ti-BMG composites in 1M H_2SO_4+2 ppm F^- at 80° C. with H_2 bubbling; and

[0059] FIG. **9**C shows a variation of the corrosion current density as a function of time for potentio-static tests performed under an applied potential of −0.1 V in 1M H_2SO_4+2 ppm F^- at 80° C. with H_2 bubbling.

DETAILED DESCRIPTION OF THE INVENTION

[0060] The invention now will be described more fully hereinafter with reference to the accompanying drawings, in which exemplary embodiments of the invention are shown. This invention may, however, be embodied in many different forms and should not be construed as limited to the embodiments set forth herein. Rather, these embodiments are provided so that this disclosure will be thorough and complete, and will fully convey the scope of the invention to those skilled in the art. Like reference numerals refer to like elements throughout. It will be understood that when an element is referred to as being "on" another element, it may be directly on the other element or intervening elements may also be present therebetween. In contrast, when an element is referred to as being "directly on" another element, there are no intervening elements present. As used herein, the term "and/or" includes any and all combinations of one or more of the associated listed items. It will be understood that, although the terms first, second, third etc. may be used herein

to describe various elements, components, regions, layers and/or sections, these elements, components, regions, layers and/or sections should not be limited by these terms. These terms are only used to distinguish one element, component, region, layer or section from another element, component, region, layer or section. Thus, a first element, component, region, layer, or section discussed below could be termed a second element, component, region, layer, or section without departing from the teachings of the present invention. The terminology used herein is for the purpose of describing particular embodiments only and is not intended to be limiting of the invention. As used herein, the singular forms "a," "an," and "the" are intended to include the plural forms as well, unless the context clearly indicates otherwise. It will be further understood that the terms "comprises" and/or "comprising," or "includes" and/or "including" when used in this specification, specify the presence of stated features, regions, integers, steps, operations, elements, and/or components, but do not preclude the presence or addition of one or more other features, regions, integers, steps, operations, elements, components, and/or groups thereof.

[0061] Furthermore, relative terms, such as "lower" or "bottom" and "upper" or "top," may be used herein to describe one element's relationship to another element as illustrated in the figures. It will be understood that relative terms are intended to encompass different orientations of the device in addition to the orientation depicted in the figures. For example, if the device in one of the figures is turned over, elements described as being on the "lower" side of other elements would then be oriented on "upper" sides of the other elements. The exemplary term "lower," may therefore, encompasses both an orientation of "lower" and "upper," depending on the particular orientation of the figure. Similarly, if the device in one of the figures is turned over, elements described as "below" or "beneath" other elements would then be oriented "above" the other elements. The exemplary terms "below" or "beneath" may, therefore, encompass both an orientation of above and below. Unless otherwise defined, all terms (including technical and scientific terms) used herein have the same meaning as commonly understood by one of ordinary skill in the art to which this invention belongs. It will be further understood that terms, such as those defined in commonly used dictionaries, should be interpreted as having a meaning that is consistent with their meaning in the context of the relevant art and the present disclosure, and will not be interpreted in an idealized or overly formal sense unless expressly so defined herein. Exemplary embodiments are described herein with reference to cross section illustrations that are schematic illustrations of idealized embodiments. As such, variations from the shapes of the illustrations as a result, for example, of manufacturing techniques and/or tolerances, are to be expected. Thus, embodiments should not be construed as limited to the particular shapes of regions illustrated herein but are to include deviations in shapes that result, for example, from manufacturing. For example, a region illustrated or described as flat may, typically, have rough and/or nonlinear features. Moreover, sharp angles that are illustrated may be rounded. Thus, the regions illustrated in the figures are schematic in nature and their shapes are not intended to illustrate the precise shape of a region and are not intended to limit the scope of the present invention. All methods described herein may be performed in a suitable order unless otherwise indicated herein or otherwise clearly contradicted by context. The use of any and all examples, or exemplary language (e.g., "such as"), is intended merely to better illustrate the invention and does not pose a limitation on the scope of the invention unless otherwise claimed. No language in the specification should be construed as indicating any non-claimed element as essential to the practice of the invention as used herein.

[0062] Hereinafter, the disclosed embodiments will be described in detail with reference to the accompanying drawings.

[0063] In an exemplary embodiment, in-situ bulk metallic glass composites are proposed as materials for permeable solid membranes used in gas separation technique for the separation and purification of hydrogen. The alloys prepared by vacuum arc melting followed with either vacuum suction casting or vacuum squeeze technique exhibit superior properties in comparison to pure Pd metal and its alloys. In the following paragraphs, the preparation of the membranes, the microstructure characterized by secondary electron microscope (SEM), X-ray diffraction and thermal calorimetry (DSC) will be described before presenting the hydrogen permeation properties, mechanical and chemical properties.

[0064] The formation of the crystalline phase with a dendritic structure in the amorphous matrix and the resulting physical, chemical and mechanical properties of these in-situ bulk metallic glass matrix composites have been intensively studied with the aim of finding the most appropriate industrial applications.

[0065] In the Ti-based metallic glasses, the matrix forms owing to the appropriate balanced of elements with negative heat of mixing ($\Delta H_{Ti—Be}$=−30 kJ/mol, $\Delta H_{Ti—Ni}$=−35 kJ/mol, $\Delta H_{Ti—Cu}$=−9 kJ/mol, $\Delta H_{Zr—Be}$=−43 kJ/mol, $\Delta H_{Ti—Cu}$=−23 kJ/mol, $\Delta H_{Ti—Ni}$=−49 kJ/mol) and atom size ratio (r_{Ti}/r_{Zr}=0.92, r_{Cu}/r_{Ti}=0.87, r_{Be}/r_{Cu}=0.875, r_{Be}/r_{Ni}=0.9). Furthermore, the alloys developed in this work correspond to a composition near the eutectic composition characterized by a low melting point (T_m=1000-1050° C.) [in comparison the melting points of Ti, Zr, Cu, Ni and Be crystalline alloys that are 1660, 1852, 1084, 1453 and 1278° C., respectively]. The amorphous phase is metastable however it may form owing to a relatively low free energy and the high viscosity of the liquid, which prevents the long range diffusion of elements thus hinders the crystallization when the cooling rate is larger than a critical value.

[0066] To develop metallic glass matrix composites for hydrogen membrane application, the formation of a crystalline phase rich in group 5 elements should be promoted. Several approaches may be used for this purpose, but as described in Example 2, the formation of the β-phase was promoted by addition of Nb and/or Ta metal elements into the Ti-based metallic glass.

[0067] In addition to the remarkable hydrogen permeation properties, the in-situ metallic glass matrix composites have the advantage of high strength (between 1.6 to 2 GPa), low density (less than 5.1 to 5.5 g/cm^3), high formability and high corrosion resistance.

[0068] In exemplary embodiment, Ti-based in-situ bulk amorphous matrix composites have chemical compositions represented by formula 1, in at %:

$$Ti_aZr_bBe_cCu_dNi_eM_fI_g$$

[0069] with M at least one element among Nb or Ta, I=impurities such oxygen and carbon, and where a, b, c, d, e

& f vary within the ranges $38 \le a \le 50$, $11 \le b \le 18$, $12 \le c \le 20$, $6 \le d \le 10$, $6 \le e \le 9$, $1 \le f \le 20$ and $0.01 \le g \le 0.5$, with $a+b+c+d+e+f+g=100$.

[0070] In exemplary embodiment, the composite may have a structure composed of a crystalline phase with a dendritic morphology and of a size varying from a few nanometer to about 100 μm embedded in an amorphous matrix.

[0071] In exemplary embodiment, elements for the formation of the amorphous phase may be titanium, zirconium, beryllium, copper and nickel.

[0072] In exemplary embodiment, elements for the formation of the beta bcc crystalline phase may be titanium, zirconium, niobium and/or tantalum.

[0073] In exemplary embodiment, the optimized composition for the formation of the amorphous structure may be defined according to the atomic ratio Ti/Zr less than about 2.8, Ti/Be less than about 2.25 and Ti/(Cu+Ni) less than about 2.37.

[0074] In exemplary embodiment, the optimized composition for the composite formation may be about 5 at %<Nb<about 20 at % and about 2 at %<Ta<about 8 at %.

[0075] In exemplary embodiment, the composite may have a mechanical strength of about 1600 MPa to about 2200 MPa at room temperature and a density between about 6.1 g/cm^3 to about 8.0 g/cm^3.

[0076] In exemplary embodiment, in the as-cast condition, the composite may have a high value of hydrogen permeability between about 2×10^{-8} mol/m.s.Pa$^{0.5}$ to about 6×10^{-8} mol/m.s.Pa$^{0.5}$ at about 350° C., depending on the composition, i.e., the volume fraction of bcc phase. These values may be larger than those of pure Pd metal and Pd alloys tested under identical conditions.

[0077] In exemplary embodiment, the composite may have a high corrosion resistance under hydrogen environment. The corrosion current density at about 80° C. with H_2 bubbling may be several orders of magnitude lower than that of SUS-316L stainless steel and Ti-6Al-4V alloy (for example, the corrosion current density=about 9.6×10^{-3} mA/cm^2 for the $Ti_{45}Zr_{13.1}Be_{16.4}Cu_{8.2}Ni_{7.3}Nb_{10}$ tested in 1M H_2SO_4+2 ppm F^- at 80° C. with H_2 bubbling, while the corrosion current density is about 1.5 mA/cm^2 and about 0.9 mA/cm^2 for SUS-316L and Ti-6Al-4V under identical conditions).

[0078] In exemplary embodiment, a method of fabricating a Ti-based bulk amorphous matrix composite includes a vacuum suction casting technique with either copper or steel molds of up to about 12 mm diameter and a vacuum squeeze casting technique.

[0079] In exemplary embodiment, the method may includes annealing at temperature about 0.6 Tg to about 0.8 Tg, (Tg is the glass transition temperature expressed in Kelvin) for a relatively short time (less than 1 hour) to release the eventual residual stresses.

[0080] In exemplary embodiment, the composite may be deformed under complex shapes in the supercooled liquid region under a neutral and vacuum environment (the supercooled liquid region, ΔT_x, is defined as the temperature range between the glass transition, T_g, and the crystallization temperatures, T_x, $\Delta T_x=T_x-T_g$). For example, hydrogen membranes may be manufactured by stamping technique within the temperature range about 350° C. to about 400° C. by application of a low load for a few minutes.

[0081] Next, the disclosed embodiments are further described in an exemplary embodiment, however the below exemplary embodiment is only an exemplary embodiment and the present invention is not limited thereto.

Exemplary Embodiment 1

[0082] Amorphous Composite Formation

[0083] The amorphous structure may be formed in several compositions of Ti-alloys such as the binary Ti—Cu and Ti—Ni, ternary Ti—Cu—Zr, Ti—Zr—Ni and Ti—Zr—Be, quaternary Ti—Zr—Cu—Ni and quinary Ti—Zr—Be—Cu—Ni. For the latter, the range of glass formation is quite extended and the maximum size reported so far was about 10 mm diameter. Furthermore, these alloys exhibit interesting properties such as high strength (between about 1.6-2 GPa) and may be deformed with up to about 10% plastic deformation under compression mode at room temperature. The mechanical properties may be further enhanced by the introduction of small sized crystalline phase. The formation of in-situ crystalline phase in the amorphous phase may be achieved by several approaches: the partial crystallization owing to a short-time annealing beyond Tx, phase separation resulting from the immiscibility between two elements, or phase partitioning during cooling. The latter has been applied in this exemplary embodiment.

[0084] The competitive phases in the Ti—Zr—Be—Cu—Ni alloy system are the icosahedral quasicrystalline phase, $TiZrCu_2$ or TiZrNi-type Laves phase, α(Ti) and β(Ti)-phases. The icosahedral and Laves phases are intermetallic phases and are usually avoided because of their brittleness. The β(Ti)-phase has a bcc (body centered cubic) structure more ductile than the hexagonal α(Ti)-phase. This β(Ti)-phase is common to Ti and Zr as well as the group 5 metals (i.e., V, Nb and Ta). In the phase diagrams shown FIGS. **1**A and **1**B, it may be seen that the β(Ti)-phase is a high temperature phase existing in the whole range of composition. Although the α-phase is the most stable phase at room temperature, its formation is usually sluggish particularly in these multi-component alloys. Also a long annealing treatment at low temperature is commonly applied to ensure the control of the volume fraction of α-phase. Nb and Ta stabilized the β(Ti) phase however the α-phase may still form at low temperature for a wide range of composition in Ti—Ta alloy. Owing to the range of cooling rate encountered in vacuum casting technique (more than 1 K/s), the most likely phase to form during solidification is the β-phase.

[0085] Consequently, the addition of one or several of these group 5 elements would be expected to promote the formation of (3-phase by decreasing its free energy. Nb and Ta are characterized by atomic radius of about 0.146 and 0.147 nm, respectively, as well as electronic properties [Kr] 4d4 5s1 (2.8.18.12.1 and electron-to-atom ratio, e/a=5.4) and [Xe] 4f14 5d3 6s2 (2.8.18.32.11.2 and e/a=5.5), respectively (FIGS. **1**C, **1**D, and **1**E). Nb and Ta have thus atomic radius similar to that of Ti, which might promotes moderately the glass formation owing to a principle known as the confusion principle.

[0086] Another important parameter is the heat of mixing, and the values with the major elements have been summarized in Table 1. The heat of mixing of Nb and Ta with the major elements such as Ti, Zr and Cu are near zero, while they are negative with Be and Ni.

[0087] Although Nb and Ta elements are added to promote the formation of the β(Ti,Zr) by a reduction of the free energy as schematically shown in FIG. **1**F, the physical, electronic and thermodynamic properties of these elements are not

likely to deteriorate significantly the glass formation in Ti-based metallic glasses thus ensuring a matrix with amorphous structure. Table 1 is showing values of heat of mixing (in kJ/mol).

TABLE 1

	Ti	Zr	Be	Cu	Ni
Ti	—	0	−30	−9	−35
Zr	0	—	−43	−23	−49
Be	−30	−43	—	0	−4
Cu	−9	−23	0	—	4
Ni	−35	−49	−4	4	—
Nb	2	4	−25	3	−30
Ta	1	3	−24	2	−42

Exemplary Embodiment 2

[0088] Preparation of the Membrane Alloys

[0089] The bulk metallic glasses and in-situ BMG matrix composites developed for this exemplary embodiment may be prepared by two different techniques: vacuum suction casting and vacuum squeeze casting type techniques.

[0090] Vacuum Suction Casting Technique

[0091] The suction casting technique was used to produce cylinder type rods. FIG. **2**A shows a schematic diagram of suction casting apparatus. Pieces of samples were placed on the water cooled copper mold with a small nozzle. The chamber was evacuated and back-filled with a high purity Ar gas. The samples were then remelted and cast into water-cooled copper molds having cylindrical cavities of 10 mm diameter and 50 mm in length or in the form of 12 mm wide, 2 mm thick and 50 mm long plates. Membranes of about 0.5 mm thick were sliced by wire cutting.

[0092] Vacuum Squeeze Casting Technique

[0093] In-situ BMG matrix composite samples were also prepared by vacuum squeeze casting type technique as shown in FIG. **2**B. In this technique, the ingot is first melted then the upper-die is rapidly moved down to press the melted ingot against the hearth. Materials for the upper-die and hearth may be either Cu or stainless steel. The size and geometry of the sample may be defined by the size of the cavity in the hearth, which is cooled by a cooling system to ensure high cooling rate. By controlling the vertical motion of the upper-die, it is possible to adjust the thickness of the samples. For the preparation of sample with composite structure, the motion of the upper-die may be retarded to allow for the growth of the crystalline phase.

Exemplary Embodiment 3

[0094] Structure of Ti—Zr—Be—Cu—Ni—Nb and Ti—Zr—Be—Cu—Ni—Ta Composites

[0095] FIG. **3**A shows the XRD traces obtained for the compositions $(Ti_{45}Zr_{16}Be_{20}Cu_{10}Ni_9)_{95}Nb_5$ and $(Ti_{45}Zr_{16}Be_{20}Cu_{10}Ni_9)_{95}Ta_5$ alloys prepared by suction casting technique in the form of rod of 10 and 7 mm diameter, respectively. The halo peaks indicated that these $(Ti_{45}Zr_{16}Be_{20}Cu_{10}Ni_9)_{95}Nb_5$ and $(Ti_{45}Zr_{16}Be_{20}Cu_{10}Ni_9)_{95}Ta_5$ rods are fully amorphous in the as-cast state. DSC curves for these compositions are shown in FIG. **3**B. Both 10 and 8 mm diameter rods of $(Ti_{45}Zr_{16}Be_{20}Cu_{10}Ni_9)_{95}Nb_5$ and $(Ti_{45}Zr_{16}Be_{20}Cu_{10}Ni_9)_{95}Ta_5$ compositions exhibit two exothermal peaks about 425 and 525° C., which are corresponding to the amorphous to a metastable crystalline phase and amorphous+metastable phase to Laves phase transformations, respectively.

[0096] These structural and thermal properties of bulk alloy with composition $(Ti_{45}Zr_{16}Be_{20}Cu_{10}Ni_9)_{95}Nb_5$ indicated that for this concentration, Nb has little effect on the glass forming ability of the Ti-based alloy. In contrast, the XRD trace of 10 mm diameter rod of $(Ti_{45}Zr_{16}Be_{20}Cu_{10}Ni_9)_{95}Ta_5$ alloy composition revealed the presence of crystalline peaks, indicating that Ta reduced more significantly the formation of amorphous structure by promoting the formation of the Laves crystalline phase, as it is shown in FIG. **3**C.

[0097] The structure of the cast rods is confirmed by the SEM images shown in FIGS. **3**D and **3**E. While the image of the Ø8 mm rods of composition $(Ti_{45}Zr_{16}Be_{20}Cu_{10}Ni_9)_{95}Ta_5$ (FIG. **3**E) clearly shows the dendritic structure of the β-Ti crystalline phase in the amorphous matrix, the micrograph of the Ø8 mm rod of composition $(Ti_{45}Zr_{16}Be_{20}Cu_{10}Ni_9)_{95}Nb_5$ (FIG. **3**D) does not reveal any second phase. The fully amorphous structure of this alloy was confirmed by TEM observation.

[0098] An important thermal characteristic of metallic glass is the existence of supercooled liquid region, ΔTx, defined as the difference between the crystallization, Tx, and glass transition temperature, Tg, such as ΔTx=Tx−Tg. The larger is the supercooled liquid region, the easier is the forming of amorphous alloy. For these Ti-based alloys, Tg is difficult to detect and the supercooled liquid region may hardly been defined using calorimetry technique.

Exemplary Embodiment 4

[0099] Range of Formation of the Ti—Zr—Be—Cu—Ni—Nb In-Situ Metallic Glass Matrix Composites Prepared by Vacuum Suction Casting Technique

[0100] It was shown above that the in-situ metallic glass matrix composites may be obtained with size up to Ø10 mm for the $(Ti_{45}Zr_{16}Be_{20}Cu_{10}Ni_9)_{95}Nb_5$ alloy prepared by vacuum suction casting technique. These alloys containing Nb were thus explored in more details. The formation of the metallic glass matrix composites was investigated in the range of composition shown in FIG. **4**A, and the compositions of the corresponding alloys are given in Table 2. The Ti content could be varied from about 38 at % to about 50 at %. Beyond about 50 at %, the glass forming ability decreased drastically and the amorphous structure could not be achieved in large size specimens. This indicates that values of the Ti/Zr ratio should be kept between about 2.8 and about 4.2 and those of Ti/(Cu+Ni) between about 2 and about 3.8. The other important element controlling the glass forming ability is Be. As the Be content is reduced, the formation of the amorphous matrix necessitates higher cooling rate. Consequently, the values of the Ti/Be ratio should be kept between about 2.0 and about 4.0. Table 2 shows compositions of Nb-added in-situ Ti-based metallic glass matrix composites (at %).

TABLE 2

	Series	Ti	Zr	Be	Cu	Ni	Nb
A	A1	42.75	15.2	19.0	9.5	8.55	5.0
	A2	40.5	14.4	18.0	9.0	8.1	10.0
	A3	38.25	13.6	17.0	8.5	7.65	15.0
B	B1	45.0	14.55	18.18	9.09	8.18	5.0
	B2	45.0	13.09	16.36	8.19	7.36	10.0
	B3	45.0	11.64	14.54	7.28	6.54	15.0

TABLE 2-continued

	Series	Ti	Zr	Be	Cu	Ni	Nb
C	C1	38.25	15.055	18.82	9.405	8.47	10.0
	C2	42.75	13.745	17.18	8.595	7.73	10.0
	C3	47.25	12.435	15.54	7.785	6.99	10.0
	C4	41.625	12.62	15.77	7.89	7.095	15.0
B	M1	50.0	14.09	12.36	6.19	7.36	10.0
	M2	47.5	14.0	14.0	8.2	6.3	10.0
	M3	46.12	15.1	17.0	9.6	7.18	5.0

[0101] Beyond 5 atomic percent, the addition of Nb reduced the free energy of the bcc phase, and consequently promotes the nucleation of this crystalline phase in the liquid. The volume fraction and size of the bcc crystalline phase increased as the concentration of Nb is increased as it is clearly observed in FIGS. **4**B and **4**C. This is also illustrated by the increase of the peak intensity of the bcc phase in the XRD traces as shown in FIG. **4**D.

[0102] The effect of Nb on the microstructure may also be observed in the DSC traces shown in FIG. **4**E. This is illustrated by the reduction of the first and second exothermal peaks corresponding to the amorphous-to-metastable phase, and amorphous+metastable phase to the crystalline phase, respectively. It should be remarked that the first exothermal peak vanished for Nb=15 at %, indicating that the amorphous matrix will transform directly into the crystalline phase.

[0103] The β-phase grows in the liquid with a dendritic structure indicating that the growth is favored along certain crystallographic directions. However the morphology of the β-phase depends strongly on the alloy composition. FIGS. **4**F and **4**G show different morphologies with, for example, numerous small dendrites resulting from a large number of nucleation sites for the $Ti_{45}(Zr_{16}Be_{20}Cu_{10}Ni_9)_{45/55}Nb_{10}$ alloy, while the uninterrupted morphology of the dendrites in the $Ti_{41.6}Zr_{12.6}Be_{15.8}Cu_{7.9}Ni_{7.1}Nb_{15}$ alloy shown in FIG. **4**G suggests the growth of the β-phase from a unique nucleation site. These differences of morphology are expected to have significant effect on the properties. Table 3 shows compositional analyses of the matrix and dendrite by EDS (in at %).

TABLE 3

		A2	B1	B2	B3	C3	C4
matrix	Ti	41.5	52.6	48.0	47.5	49.4	48.8
	Zr	25.5	17.8	19.7	18.2	18.2	19.0
	Nb	9.5	8.2	6.5	7.6	9.0	6.7
	Cu	12.0	10.5	14.1	13.9	11.8	13.2
	Ni	11.5	10.9	11.8	12.8	11.6	12.3
dendrite	Ti	51.3	—	58.5	51.1	60.3	51.1
	Zr	9.4	—	6.8	5.6	—	—
	Nb	36.3	—	34.7	43.3	39.7	48.9
	Cu	—	—	—	—	—	—
	Ni	—	—	—	—	—	—

[0104] The composition of the matrix and dendrite was measured by means of energy disperse spectroscopy (EDS) technique (Table 3). It appeared that the 6-phase is essentially rich in Ti, Nb and Zr, and does not contain Cu and Ni (Be cannot be detected by EDS analysis technique). Furthermore, as the nominal content of Nb increased, the Ti and Zr content in the dendrite decreased while the Nb content in the matrix decreased. In parallel, the Ti content in the matrix decreased while the Cu and Ni content increased.

Exemplary Embodiment 5

[0105] Formation of the Ti—Zr—Be—Cu—Ni—Nb In-Situ Metallic Glass Matrix Composites Prepared by Vacuum Squeeze Casting Technique

[0106] The alloys of composition $Ti_{45}Zr_{16}Be_{20}Cu_{10}Ni_9$, $(Ti_{45}Zr_{16}Be_{20}Cu_{10}Ni_9)_{95}Nb_5$, $(Ti_{45}Zr_{16}Be_{20}Cu_{10}Ni_9)_{90}Nb_{10}$ and $(Ti_{45}Zr_{16}Be_{20}Cu_{10}Ni_9)_{85}Nb_{15}$ were also prepared by vacuum squeeze casting technique in the form of plates of about 2-3 mm thick. The XRD and DSC traces of the samples are shown in FIGS. **5**A and **5**B. For the same alloy composition, the structure appeared to be similar to that obtained for samples prepared by vacuum suction casting technique.

[0107] The observation of the samples by SEM, shown in FIGS. **5**C, **5**D, **5**E, and **5**F, confirmed the composites structure for the alloys containing a concentration of Nb larger than 10 at %.

Exemplary Embodiment 6

[0108] Formation of the Ti—Zr—Be—Cu—Ni—Ta In-Situ Metallic Glass Matrix Composites Prepared by Vacuum Suction Casting Technique

[0109] The alloy of composition $(Ti_{45}Zr_{16}Be_{20}Cu_{10}Ni_9)_{95}Ta_5$ has been prepared by vacuum suction casting in the form of 1 mm thick plate. For this alloy system, the addition of only 5 at % induced the formation of β-Ti, as shown from the XRD trace and SEM micrograph shown in FIGS. **6**A and **6**B, respectively. The morphology of the dendritic β-phase in the Ta-containing in-situ Ti-based BMG matrix composite is similar to that of the Nb-containing in-situ Ti-based BMGs. However the addition of a lower Ta content is more efficient than Nb to induce the formation of the β-Ti phase in the amorphous matrix. The volume of the β-phase in the Ti+5 at % Ta BMG matrix composite was found to be equivalent Ti+10 at % Nb BMG matrix composite.

[0110] The amorphous nature of the matrix was confirmed by DSC analyses, as shown in FIG. **6**C. Positions of the peaks as well as values of the heat of crystallization are similar to those of the Nb-containing in-situ Ti-based BMG matrix composites.

Exemplary Embodiment 7

[0111] Mechanical Properties of the In-Situ Ti-Based BMG Composites

[0112] Amorphous materials are characterized by a high value of the microhardness and high strength with Vickers microhardness larger than 300 kgf/mm^2 (3 GPa) and strength near or beyond 2000 MPa (2 GPa) depending on the composition (Table 4). These properties are extremely important for application such as micro-gear and bipolar plates since for the former it may reduce the wear and for the latter the high strength will allow a significant reduction of the sheet plate thickness and thus provide gain on the weight and volume of the fuel cell.

[0113] The stress-strain curves of the Ti-based composites containing Nb and Ta are shown in FIG. **7**A. Though compression tests were performed on samples with different diameter, both Nb and Ta may display some malleability at room temperature. The variation in the value of plastic deformation from one alloy to another may be explained by the difference in volume fraction, size and properties of the crystalline dendritic phase. Table 4 shows microhardness values of various Ti-based BMGs and BMG composites.

TABLE 4

	$Ti_{45}Zr_{16}Be_{20}Cu_{10}Ni_9$	$(Ti_{45}Zr_{16}Be_{20}Cu_{10}Ni_9)_{95}Nb_5$	$(Ti_{45}Zr_{16}Be_{20}Cu_{10}Ni_9)_{95}Ta_5$
Hv	366 ± 22	344 ± 24	414 ± 42
	$(Ti_{45}Zr_{16}Be_{20}Cu_{10}Ni_9)_{95}Nb_5$	$(Ti_{45}Zr_{16}Be_{20}Cu_{10}Ni_9)_{90}Nb_{10}$	$(Ti_{45}Zr_{16}Be_{20}Cu_{10}Ni_9)_{85}Nb_{15}$
Hv	344 ± 24	375 ± 37	366 ± 14

[0114] Samples of in-situ Ti-based BMG composites containing Nb were also prepared using stainless steel mold instead of Cu in order to reduce the cooling and increase the volume fraction of bcc phase. It may be seen in FIG. **7**B, that the modification of the sample preparation modifies the mechanical behavior under compression mode for these alloys. Values of the plastic deformation from about 5 to 8% were achieved instead of ~about 2 to 3% (FIG. **7**A) as the volume fraction of bcc phase has been increased.

[0115] In order to be applied as membrane materials for hydrogen separation and purification, the in-situ Ti-BMG composites should have a somewhat high strength in the temperature range of the membrane application, i.e., about 300-400° C. Characteristics of this class of materials are the existence of a supercooled liquid region, ΔTx, found between the glass transition, Tg, and the crystallization temperature, Tx. In that range of temperature, BMG may be deformed with a superplastic behavior, characterized by high strain rate sensitivity.

[0116] FIGS. **7**C, **7**D, and **7**E show the stress-strain behavior of in-situ Ti-based BMG composites with 5, 10 and 15 at % Nb tested at 360° C. for strain rate of, respectively, 10^{-5}, 10^{-4} and 10^{-3} s^{-1}. In contrast to tests performed at room temperature as shown FIGS. **7**A and **7**B, these composites may be deformed with large plastic deformation at high temperature while retaining a high strength.

[0117] The strain rate sensitivity may be determined by plotting the variation of the flow stress with the strain rate. As shown in FIG. **7**F, Nb-free alloy as well as alloy containing 5 at %, which are both monolithic BMG alloys, exhibit a high strain rate sensitivity with a value of the slope, m, near 0.5 ($m=(\delta \log \sigma)/(\delta \log \epsilon)$) for in the strain rate range 10^{-4}-10^{-5} s^{-1}. For in-situ BMG composites, those structures are composed of bcc crystalline phase embedded in an amorphous matrix, the value of the slope decreased as the higher Nb content increased. This behavior could be attributed to the presence of β-phase in the amorphous matrix, which has a lower strain rate sensitivity in comparison to the amorphous structure.

Exemplary Embodiment 8

[0118] Hydrogen Permeation Tests on In-Situ Ti—Zr—Be—Cu—Ni+Nb BMG Composites

[0119] Hydrogen permeation tests were performed on samples with a diameter of about 12 mm and a thickness of approximately 0.5 mm. These membranes were machined from plates prepared from two different methods: vacuum squeeze casting type and vacuum suction casting techniques. Tests were performed between 350° and 375° C. for hydrogen pressure varying from 1.1 to 3 bars.

[0120] For samples prepared by vacuum squeeze casting, FIG. **8**A indicates that the hydrogen flux at 350° C. increased as the Nb content increased, which may be attributed to the presence of the bcc crystalline dendritic structure in the in-situ BMG composites since the alloys containing 0 and 5 at % Nb are not composites but monolithic metallic glasses. Nevertheless, the difference in the properties between both alloys with 0 and 5 at % Nb suggests a positive effect of Nb addition on the hydrogen permeation.

[0121] Similar behavior was obtained for samples prepared by vacuum suction casting technique. The hydrogen permeation properties of the in-situ Ti-based BMG composites are superior to those of pure Pd as indicated in FIG. **8**B showing the variation of the product flux.t (where t is the thickness) as a function of the difference of the square root of the pressure. In this plot, the variation is almost linear suggesting that the variation of the hydrogen concentration follows the Sievert's law. In addition, this plot indicates that the hydrogen flux increased as the temperature increased.

[0122] These properties have been reported in FIGS. **8**C and **8**D by showing the variation of the hydrogen permeability as a function of the inverse of temperature. This chart indicates that values of hydrogen permeability for the composites containing more than 10 at % Nb are found between those of Pd and those of pure Nb.

[0123] In FIGS. **8**C and **8**D, the hydrogen permeability of the composites measured at 350° C. and 375° C. are also compared with those of a recently developed Ni—Nb—Zr-based monolithic metallic glass. The values of the hydrogen permeability are found to be more than about 2.5 times larger than those of Pd alloys and more than about 3.5 larger than the currently developed metallic glasses.

[0124] It is also important to notice that the hydrogen permeation properties for samples prepared by suction casting were found to be slightly superior to those prepared from vacuum squeeze casting type. This is believed to result from a slight difference in the structure owing to the difference of cooling rate leading to different volume fraction and morphology of bcc dendritic phase.

[0125] Hydrogen Permeation Tests on In-Situ Ti—Zr—Be—Cu—Ni+Ta BMG Composites

[0126] Hydrogen permeation tests were performed for sample with the composition $(Ti_{45}Zr_{16}Be_{20}Cu_{10}Ni_9)_{95}Ta_5$ prepared by vacuum squeeze casting as described in Example 6. As indicated in FIGS. **8**E and **8**F, the hydrogen permeation properties of this composite containing 5 at % Ta is similar to the properties of the composite formed from the addition of 10 at % Nb.

[0127] The high volume fraction of dendrite phase formed owing to the addition of only 5 at % Ta enabled the high value of the hydrogen permeability.

Exemplary Embodiment 9

[0128] Since constituent elements used in these alloys have good corrosion resistance, it is thus expected that the developed in-situ BMG composites exhibit excellent corrosion properties, too. Ti, Zr and Nb have excellent corrosion resistance in H_2SO_4 solution, Cu is a noble element, Ni is also

known for its good corrosion properties and Be forms BeO, which provide excellent protection again corrosion.

[0129] Corrosion experiments were carried out under 1 M H_2SO_4+2 ppm F^- environment at 80° C. with hydrogen bubbling in order to investigate the resistance of the composite in hydrogen environment. The potentio-dynamic curves obtained under that condition are shown in FIG. **9**A.

[0130] All potentio-dynamic curves are found lower than that of stainless steel and Ti-6Al-4V alloy tested under identical conditions, indicatives of an excellent corrosion resistance of the in-situ Ti-based BMG composites. Furthermore, in contrast to stainless steel and Ti-6Al-4V alloy, the polarization plots for the Ti-based BMG composites do not show active-passive transition behavior. As for the Ti-6Al-4V alloy, the behavior is characterized by a wide passivation plateau followed by transpassive dissolution without any significant increase in current. All the corrosion parameters are given in the Table 5.

[0131] Under H_2 bubbling condition, the alloy with 10 at % Nb exhibits lower passivation current density in comparison other compositions. This may be explained by the high content of Nb in the matrix and the absence of large dendrite which prevents a galvanic effect. As shown in Table 6, the formation of (Ti,Zr,Nb)-rich β-phase particularly in composites containing 15 at % Nb results in a high concentration of Cu in the matrix, which tend to degrade the corrosion resistance.

[0132] The variation of the corrosion current density and passivation current density, shown in FIG. **9**B, demonstrated that although the addition of Nb may lead to the formation of inheterogeneities, a proper alloy design may enable an improvement of the corrosion resistance. Table 5 shows values of the corrosion current density and potential corrosion for tests performed in 1M H_2SO_4+2 ppm F^- at 80° C. with H_2 and air bubbling.

TABLE 5

	H_2 bubbling		air bubbling	
	I_{corr} (A/cm^2)	E_{corr} (V)	I_{corr} (A/cm^2)	E_{corr} (V)
Ti—6Al—4V	9×10^{-4}	−0.76	7.2×10^{-4}	−0.78
$Ti_{45}Zr_{16}Be_{20}Cu_{10}Ni_9$	3.01×10^{-5}	−0.23	4.73×10^{-5}	−0.13
$(Ti_{45}Zr_{16}Be_{20}Cu_{10}Ni_9)_{95}Nb_5$	2.03×10^{-5}	−0.23	1.34×10^{-5}	−0.17
$(Ti_{45}Zr_{16}Be_{20}Cu_{10}Ni_9)_{90}Nb_{10}$	9.14×10^{-6}	−0.19	1.03×10^{-5}	−0.13
$(Ti_{45}Zr_{16}Be_{20}Cu_{10}Ni_9)_{85}Nb_{15}$	8.11×10^{-6}	−0.23	1.39×10^{-5}	−0.17
$Ti_{45}Zr_{14.55}Be_{18.18}Cu_{9.09}Ni_{8.18}Nb_5$	2.53×10^{-5}	−0.26	1.62×10^{-5}	−0.17
$Ti_{45}Zr_{13.09}Be_{16.36}Cu_{8.19}Ni_{7.36}Nb_{10}$	2.29×10^{-5}	−0.25	1.83×10^{-5}	−0.21
$Ti_{45}Zr_{11.64}Be_{14.54}Cu_{7.28}Ni_{5.54}Nb_{15}$	2.13×10^{-5}	−0.27	1.47×10^{-5}	−0.26
$(Ti_{40}Zr_{29}Be_{16}Cu_8Ni_7)_{95}Nb_5$	—	—	4.56×10^{-6}	−0.20
$(Ti_{40}Zr_{29}Be_{16}Cu_8Ni_7)_{97}Ta_3$	—	—	3.42×10^{-6}	−0.28
$(Ti_{45}Zr_{16}Be_{20}Cu_{10}Ni_9)_{80}Nb_{18}Ta_2$	3.92×10^{-6}	−0.27	3.03×10^{-6}	−0.19

[0133] Potentio-static tests were also performed under a constant value of potential of −0.1V for 2 hours. The variation of the current density for the in-situ BMG is shown in FIG. **9**C and is compared with that of Ti-6Al-4V. It may be see that the slope of the current density vs. time decreased as the Nb content increased from 0 to 10 at %, with an absolute value for the composite containing 10 at % Nb lower than any other composition after 2 hours test. However, the slope for the composite formed with 15 at % Nb is extremely large indicating a loss in the corrosion resistance in hydrogen hydrogen environment. These corrosion properties are also superior to those of Ti-6Al-4V alloy. However, the slope for the composite formed with 15 at % Nb is extremely large indicating a loss in the corrosion resistance in hydrogen environment.

[0134] Immersion was also performed in 1M H_2SO_4 at 80° C. for 7 days for the Nb-free (monolithic) Ti-based bulk metallic glass and for the Ti-based BMG composites containing Nb. Results given in Table 6 indicate that the weight loss of the Ti-based BMG composites recorded after 7 days are considerably lower than that of crystalline Ti-6Al-4V demonstrating the superior corrosion resistance of the developed BAMCs. Once again, the best corrosion properties are obtained for the composite containing 10 at % Nb. Table 6 shows weight loss after 7 days immersion in 1M H_2SO_4 at 80° C. measured by change of weight using a micro-balance and calculated from the amount of elements dissolved in the solution.

TABLE 6

	% of weight loss		
Alloy	Weight loss method	Atomic Absorption Spectroscopy (AAS) method	Immersion time
Ti-6Al-4V (crystal)	34.12	37.32	2 days 3 hrs 27 min
$Ti_{45}Zr_{16}Be_{20}Cu_{10}Ni_9$	5.39	4.53	7 days
$(Ti_{45}Zr_{16}Be_{20}Cu_{10}Ni_9)_{95}Nb_5$	2.15	1.82	7 days
$(Ti_{45}Zr_{16}Be_{20}Cu_{10}Ni_9)_{90}Nb_{10}$	1.59	1.33	7 days
$(Ti_{45}Zr_{16}Be_{20}Cu_{10}Ni_9)_{85}Nb_{15}$	1.82	1.73	7 days
$(Ti_{40}Zr_{29}Be_{16}Cu_8Ni_7)_{95}Nb_5$	1.72		7 days
$(Ti_{40}Zr_{29}Be_{16}Cu_8Ni_7)_{97}Ta_3$	0.78	0.88	7 days

[0135] While this invention has been described in connection with what is presently considered to be practical exemplary embodiments, it is to be understood that the invention is not limited to the disclosed embodiments, but, on the contrary, is intended to cover various modifications and equivalent arrangements included within the spirit and scope of the appended claims.

What is claimed is:

1. A Ti-based bulk amorphous matrix composite comprising a composition represented by Formula 1, in at %:

$$Ti_aZr_bBe_cCu_dNi_eM_fI_g \qquad \text{Formula 1}$$

where M is at least one of Nb or Ta, I is an impurity, and a, b, c, d, e, and f vary within the ranges $38 \le a \le 50$, $11 \le b \le 18$, $12 \le c \le 20$, $6 \le d \le 10$, $6 \le e \le 9$, $1 \le f \le 20$ and $0.01 \le g \le 0.5$, with $a+b+c+d+e+f+g=100$.

2. The Ti-based bulk amorphous matrix composite of claim **1**, wherein

the composite has a structure comprising a crystalline phase with a dendritic morphology and of a size varying from about 0.01 μm to about 100 μm in an amorphous matrix.

3. The Ti-based bulk amorphous matrix composite of claim **2**, wherein

elements for a formation of the amorphous matrix are titanium, zirconium, beryllium, copper and nickel.

4. The Ti-based bulk amorphous matrix composite of claim **2**, wherein

elements for a formation of the crystalline phase are titanium, zirconium, and at least one of niobium and tantalum.

5. The Ti-based bulk amorphous matrix composite of claim **2**, wherein

the composition for the formation of the amorphous matrix are defined according to the atomic ratio Ti/Zr less than about 2.8, Ti/Be less than about 2.25, and Ti/(Cu+Ni) less than about 2.37.

6. The Ti-based bulk amorphous matrix composite of claim **5**, wherein

the composition are about 5 at %<Nb<about 20 at % and about 2 at %<Ta<about 8 at %.

7. The Ti-based bulk amorphous matrix composite of claim **1**, wherein

the composite has a mechanical strength of about 1600 MPa to about 2000 MPa at room temperature and a density between about 6.1 g/cm^3 to about 8.0 g/cm^3.

8. The Ti-based bulk amorphous matrix composite of claim **1**, wherein

the composite has a value of hydrogen permeability between about 2×10^{-8} $mmol/m.s.Pa^{0.5}$ to about 6 10^{-8} $mol/m.s.Pa^{0.5}$ at about 350° C., depending on the composition

9. The Ti-based bulk amorphous matrix composite of claim **1**, wherein

the composite has a corrosion current density under a hydrogen environment lower than stainless steel.

10. A method of fabricating a Ti-based bulk amorphous matrix composite comprising:

a vacuum suction casting technique and a vacuum squeeze casting technique,

wherein the composite comprising a composition represented by Formula 1, in at %:

$$Ti_aZr_bBe_cCu_dNi_eM_fI_g \qquad \text{Formula 1}$$

where M is at least one of Nb and Ta, I is an impurity, and a, b, c, d, e, and f vary within the ranges $38\le a\le 50$, $11\le b\le 18$, $12\le c\le 20$, $6\le d\le 10$, $6\le e\le 9$, $1\le f\le 20$ and $0.01\le g\le 0.5$, with $a+b+c+d+e+f+g=100$.

11. The method of claim **10**, further comprising:

annealing at temperature about 0.6Tg to about 0.8Tg, (Tg is the glass transition temperature expressed in Kelvin) for a predetermined time less than 1 hour to release eventual residual stresses.

12. The method of claim **10**, wherein

the composite is deformed under a complex shape in a supercooled liquid region under a neutral and vacuum environment, and the supercooled liquid region, ΔT_x, is a difference between a glass transition temperature, T_g, and a crystallization temperature, T_x.

* * * * *